LICENTIATE THESIS

L

Effects of Grinding Variables on Structural Changes and Energy Conversion during Mechanical Activation Using Line Profile Analysis (LPA)

Parviz Pourghahramani

Effects of Grinding Variables on Structural Changes and Energy Conversion during Mechanical Activation Using Line Profile Analysis (LPA)

Parviz Pourghahramani
Luleå University of Technology
Department of Chemical Engineering and Geosciences
Division of Mineral Processing

Abstract

The mechanical treatment of solids is one of the most common and widely used operations with which man has been concerned from the very beginnings of history of civilization. At the present, mechanical activation has a wide range of application potential. Mechanical activation processes are used to modify the properties of materials, enhance the reactivity of materials and produce advanced materials. When materials are subjected to intensive grinding, the structure and microstructure characters of material change widely. These structural changes determine the reactivity of materials and/or minerals and may play an important role in a proper subsequent process. The use of X-ray diffraction line broadening measurements has been proved to be useful in the characterization of microstructure and structural characteristics.

The objective of this study is to investigate the influence of the milling operation variables on the microstructure and structural changes of natural hematite. The influence of the three variables, mill type, grinding time and media surface, through an experimental design was investigated using different methods of characterization by XRD line profile analysis (LPA).

The results revealed that mechanical activation of hematite brings about great changes in geometrical and microstructural characteristics with increased the grinding intensity, whatever milling methods are applied. The measurements of the BET surface area, granulometric surface area and particle size show a tendency of the particles to form agglomerates during prolonged milling; in particular with grinding under higher media surface. The agglomeration stage of particles appears to be related to the milling operation conditions. The results indicated that the pores of the agglomerates remain accessible for Nitrogen gas, which addresses the formation of relatively weaker (soft) agglomerates. With a first approximation, the vibratory mill yielded the maximum BET specific surface area, accounting for 18.4 m^2/g after 9 hours of milling with higher media surface. The expansions of hematite lattice and volume cell, especially in the initial stages of milling, were identified.

The Williamson-Hall method confirms its merit for a rapid overview of the line broadening effects and possible understanding of the main causes. The anisotropic character of line broadening for deformed hematite as a function of grinding variables was revealed. From the Williamson-Hall plots, it was understood that strain and size contributions exist simultaneously in the milled samples. It was found that the hematite crystal is 'soft' between (024) and other reflections. As seen by the Warren-Averbach method, the planetary mill products yield the smallest crystallites and the maximum root mean square strain (RMSS) (with the exception of the ground sample within one hour and low media surface). The final products contain crystallites sizes between 73.5 and 5.6 nm and its lattice strain (RMSS) at $L=10\ nm, <\varepsilon_{L=10nm}^2>^{1/2}$, varies from 0.06×10^{-3} up to 5.32×10^{-3}, depending on the milling performance.

With a first approximation, the products of the vibratory mill yielded lower X-ray amorphization degree with regard to the grinding time and media surface variables. The approximation of the energy contribution to the long-lived defects demonstrated that the amorphization character is the most important energy carrier in the activated hematite, accounting for more than 93% of overall stored energy in hematite.

For a given stress energy, the activated hematite in the tumbling mill contains the largest excess energy and has in vibratory mill the smallest amount of excess energy. Generally, the vibratory mill brings about less distortion in the hematite than other mills for the same level of stress energy. However, to produce an identical stress energy in different mills, the planetary mill is needed a specific energy input much higher than the other mills.

To investigate the influence of other milling variables in detail, more investigations are recommended, especially as the experiment design and progress in the knowledge nowadays provide possibilities to use advanced methods for the characterization. In our opinion, the investigation of the effect of various defects formed during mechanical activation on the reactivity of the minerals are now only at the beginning of their development. Systematic investigations are recommended to explore what defects are formed under various types of mechanical action in the crystal of the substances of different types and how these defects influence reactivity.

Acknowledgments

List of appended papers

I. Microstructure Characterization of Mechanically Activated Hematite Using XRD Line Broadening

Parviz Pourghahramani and Eric Forssberg

II. Comparative Study of Microstructural Characteristics and Stored Energy of Mechanically Activated Hematite in Different Grinding Environments

Parviz Pourghahramani and Eric Forssberg

III. Changes in the Structure of Hematite by Extended Dry Grinding in Relation to Imposed Stress Energy

Parviz Pourghahramani and Eric Forssberg

IV. Review of applied particle shape descriptors and produced particle shapes in grinding environments. Part I: particle shape descriptors

Parviz Pourghahramani and Eric Forssberg

V. Review of applied particle shape descriptors and produced particle shapes in grinding environments. Part II: the influence of comminution on the particle shape

Parviz Pourghahramani and Eric Forssberg

Contents

1. Introduction

1.1. Historical perspective

Research on mechanical activation is a subfield of mechanochemistry. Therefore, it is appropriate to review the history of general mechanochemistry.

Mechanochemical processes (MCP) use mechanical energy to activate chemical reactions by developing structural changes. However, these are not new process. Mechanically activated processes date back to the early history of humankind, the use of flints to initiate fires (Welham, 2003; Mccormick &Froes, 1998). Following these early uses, the field of mechanochemistry has had a rich history, particularly in Europe, which has led to the use of ball mills for processing a wide range of materials, ranging from minerals to advanced materials.

The first systematic studies concerned with the effects of grinding on properties of substances were attributed to Carey Lea at the end of the nineteenth (Heinicke, 1984; Juhasz and Opoczky, 1990; Takacs, 2004). He reported that the halides of gold, silver, platinum and mercury decomposed to halogen and metal during fine grinding in a mortar. In these publications for the first time, the mechanical energy was pointed out to initiate chemical reactions and local heating is not the only possible mechanism of initiating chemical reaction by mechanical action. Ostwald (1891 and 1919) introduced the mechanochemistry term and Ostwald ripening (small particles more reactive). He regarded the mechanochemistry as a part of physical chemistry like thermochemistry, electrochemistry or photochemistry.

In the 1929, Tamman studied the effect of mechanical energy on metal. He concluded that the grinding increases the dissolution rate of metal and the accumulation of mechanical energy (5-15%) is responsible for this process. In the 1930, it was primarily Fink and latter Bowden and Tabor, who investigated the effects of friction and abrasion on the oxidation reactions of metals and on their composition. They formulated the conception of" hot spots" (Steinike and Hennig, 1992)

According to Huttig (1943), the mechanochemistry includes only the release of lattice bonds without any formation of new substances. The influence of mechanical energy on several reactions and their relations with changes in color was investigated by Peters (1962). The author used the thermodynamic argument to discuss these reactions. Peters added the transformations due to mechanical stress of material which are accompanied by chemical reaction into the mechanochemistry category definition. Gerlach and Gock (1973) used the attrition milling for production of activated chalcopyrite. They stated that the milling greatly increased the dissolution rate of leaching processes.

The first book in Tribochemistry field was published by Heinicke (1984).The definition of Heinicke regarding to mechanochemistry is still widely accepted: *"mecchanochemistry is a branch of chemistry which is concerned with chemical and physico-chemical transformation of substances in all states of aggregation produced by the effect of mechanical energy"*.

The term of mechanical activation was defined by Smekal in the 1942s. According to this author mechanical activation is a process in which the reaction ability of a material increases without changing the material. If the activation causes the changes in composition and structure, it is a mechanochemical reaction. Butjagin consider the mechanical activation as an increase in the reaction ability because of stable changes in solid structure. He considered the

three main effects of mechanical activation on solids including structural disordering, structural relaxation and structural mobility (Balaz, 2000).

Mechanochemistry has become the topic of numerous publications and the significance of this topic is gradually increasing, and nowadays it is an integral part of agenda of any international congress on comminution. Many papers have been published in different journals and conference up to now from different view points in different fields of mechanochemistry subject. Since the chemical effects of mechanical treatment have been investigated in a large number of systems, several publications with regard to mechanical treatment at very recent past published in English should be emphasized; Mechanical Activation of Minerals (Tkacova, 1989), Mechanical Activation of Minerals by Grinding, Pulverizing and Morphology of Particles (Juhasz & Opoczky, 1990), Mechanochemistry of Solid Surfaces (Gutman, 1994), Mechanochemistry of Materials (Gutman, 1998) and Extractive Metallurgy of Activated Minerals (Balaz, 2000).

 Terms like mechanical activation, mechanochemical processing (MCP), mechanical alloying (MA) and mechanical milling (MM) reflects the versatility of these techniques and how they have been employed in different fields (and at different scales) ranging from fundamental physics and advanced material science to traditional mineral processing. There are some disagreements among authors regarding the definitions of aforementioned terms but the most accepted definitions are:

- *Mechanical activation: using mechanical energy to enhance a reaction during subsequent processing.*
- *Mechanochemistry: using mechanical energy to induce a reaction whilst the energy is being input to the system.*
- *Mechanical milling, milling of a pure metal or compound that is in a state of thermodynamic equilibrium at the start of milling.*
- *Mechanical alloying: using mechanical energy to cause (mutual?) solid solution (or dispersion) of elements (or compounds) during energy input. The terms refer especially to the formation of alloys from elemental precursors during processing in a ball mill.*

The main application of mechanical activation of minerals are found within the field of extractive metallurgy, where mechanical activation is used as a pre-treatment step prior to leaching and extraction in order to increase the solubility of the minerals in question. In extractive metallurgy reactivity is measured in terms of dissolution kinetics. It was shown by Zelikman et al. (1975) that mechanical activation of crystalline materials resulted in a decrease in activation energy for dissolution reaction, therefore increasing the rate of leaching. Similar mechanisms are thought to be responsible for increasing the reactivity of activated material with different application such as kinetic of adsorption and catalysis and synthesis.

The effect of mechanical activation has been studied on many ore concentrates in order to build up an appropriate technological flow sheet. Sulphide concentrates with Fe, Cu, Pb, Zn, Ni, Mo, As, Au and Re content were tested in order to utilize the advantage of mechanical activation [Gerlach et al., 1973; Pawlek, 1976; Gock, 1977; Aytekin, 1981; Gerlach, 1982; Daiger and Gerlach, 1982; Daiger and Gerlach, 1983; Gock and Asiam, 1988; Kammel et al., 1987; Balaz et al., 1988, 1998, 2000; Kuzeci et al., 1989; Pawlek et al., 1989; Tkacova et al., 1993; Kusnierova et al., 1993; Amer, 1995, 2002; Kahler et al., 1996; Maurice and Hawk 1998, 1999a, b; Welham, 1997a, b; 2001a, b, c, d; Welham and Llewellyn ,1998; Ficeriova,

2000; Godocikova, 2001; Godocikova et al., 2002a, 2002b; Ficeriova et al., 2002 and Mulak et al., 2002].

The method of mechanical activation has been also used for the concentrates of rutile (Gock and Jacob, 1980), ilmenite (Welham, 1997a, b), volframite (Amer, 2000), zircon (Welham, 2001f), cassiterite (Amer, 2001), tantalite/columbite (Welham, 2001e) and silicates (Juhasz 1974, Puclin et al.1995, Zhang et al. 1997 and Kalinkin et al.2003).

In addition to the application of mechanical activation in mineral processing and extractive metallurgy, mechanical activation is heading for new fields of research such as preparation of alloys, cement and pozzolanic cements, composites, nanocrystalline and amorphous substances, intermetallic compounds and smart material for 21st century.

1.2. Background

1.2.1. Comminution and mechanical activation

The application of treatments in milling devices may be briefly divided into three main categories, including coarse grinding, fine grinding and mechanical activation. The coarse grinding is mainly used in mineral beneficiation and ore dressing to liberate locked minerals. Coarse grinding is rather well explored. It is known that the correlation between the average particle size and intensity or duration of milling may be described satisfactorily. In contrast, the oversimplified idea is invalid for submicron grinding range (Boldyrev et al., 1996, Karagedov and Lyakhov, 2003).

In the case of fine grinding, the size reduction takes paces but its explanation requires a more fundamental knowledge of process physics, especially the physics of mechanical energy relaxation (Austin, 1992). The fine grinding is an intermediate between coarse grinding and mechanical activation and its grinding limit is determined by ductile-brittle transition state if the mechanical energy relaxation in grains of a polycrystal has the same nature as in the particles of powder. However, in description of grinding limit, the material property and mill intensity which depends on mill construction and mode of operation should be kept in mind. For example, if the milling device can not transfer sufficient energy and impacts to powder being ground, the particles cannot be ground, but the size of particles are still larger than ductile-brittle transition (Boldyrev et al., 1996).

The objectives followed by mechanical activation are structural changes not size reduction, although the size reduction also takes place simultaneously during mechanical activation. When the mechanical energy relaxation changes from breakage to ductile (tough), the strain increases drastically in material, from 0.1-0.3 up to 30-100 % (Mclean, 1965). Consequently, the extreme dislocation flows take place and subsequently moving and interacting dislocations develop other types of defects. In other words, changing the grinding process from breakage to plastic deformation causes the structure distortions (Schönert, 1990, Goldberg and Pavlov, 1990). These structural changes determine the reactivity of activated materials (Boldyrev, 1996). The ground material is mechanically activated by increasing of both specific surface energy and elastic strain energy. The activation free energy can be dissipated by different ways of energy transitions. Various relaxation processes can take place such as heating, formation of new surface, aggregation, adsorption, imperfections and chemical reactions. The surface activation can be relaxed as the newly exposed fracture surfaces are becoming active to the extent that agglomeration, or adsorption of environmental

gaseous species and moisture, take place. The bulk activation can be relaxed by fracturing of brittle material or the crystallographic lattice arrangement in polymorphic transformation, mechanical alloying, mechanochemical decomposition or synthesis (of a new chemical compound). The elastic strain energy transforms into elastic energy of lattice defects such as point defects (vacancies), linear defects (dislocations), planer defects (stacking faults or sub-crystallite interfaces) and volumetric (structural disordering). Availability of these processes depends largely on the structural nature of material involved and their kinetics depends much on dissipation process involved (Lin, 1998). It should be noted that the kinetics of activation process or the overall rate of activation process depends on kinetics of grinding process (Boldyrev, 1996).

1.2.2. Physico-chemical changes of mechanically activated material

Grinding may change the physical and chemical properties of the material. Some times the changes can be utilized such as increase of rate and amount of solubility, decrease of processing time and reaction time, increase of surface reactivity and attain better catalytic effects, produce new synthetic materials, improve the sinterability and strain stronger products and production of new alloys and cements. Various processes may take place during mechanical activation of solids depending on stressing condition. According to the published literature (Balaz, 2000; Lin et al., 1975, Fernandez-Bertran, 1999; Heegn, 1987 and 1979; Tkacova, 1989) stress, deformation and fracture initiate changes in solids, their kind and volume are a function of material properties and stress conditions in milling devices and generally the following effects may be observed in the activated solid substances:

- *Disintegration and fracturing, formation of new surfaces, enlargement of surface area, surface aggregation and surface oxidation*
- *Material abrasion and material transitions between solid particles*
- *Plastic deformation and disordering of crystal structure (lattice distortions), the formation of various lattice defects such as point lattice, linear defects, etc, electron defects and amorphization, Consequently increase of dislocation density, lattice strain and crystallite size*
- *Phase transformation in polymorphic materials*
- *Emission of photons, electrons and lattice components*
- *Stimulation of lattice oscillations and local heating of solids*
- *Electrostatic charge-discharge processes*
- *Magnetic properties and susceptibility*
- *Chemical reactions, decomposition, ionic changes, oxidation-reduction, complex and adduct formation, etc.*

Besides, the secondary effects of interaction between the stressed solids and the ambient medium must be taken into account. This interaction with the environment can be on purpose or not.

1.2.3. Relaxation modes in mechanical activation process

The structural relaxation has important effects in the reactivity of solids. There are two types of disorder and instability in activated material. One of these relates to highly excited, short lived defects with the relaxation time of $10^{-7} - 10^{-3} s$, which cause the activation to attain the highest level (Meyer, 1968). The short lived defects decay as soon as they are generated. The same short time is required for destruction of a solid by fracture. These kinds of defects do not influence the reactivity of activated material whose relaxation time is less than the characteristic time of reaction itself (Ljachov, 1994). On the other hand, some long -lived

defects, having a life length from $10^{-3} - 10^{6}\,s$, are generated due to deep imperfections in the activated solid substances. These are very hot and unstable defects. The relaxation of these defects decrease the activation energy considerably, but they never reach the initial state (free defect-level energy) and consequently a residual activity (residual disorder) remains (Meyer, 1968). The influence of these defects has to be a subject of further mechanical activation studies.

The type of stress relaxation depends on external and internal conditions of stressing, i.e. on the magnitude and direction of forces acting, on the stress rate and frequency of loading and the material nature. A variety of process can take place during intensive grinding such as plastic deformation, heat release, fragmentation of particles, chemical reaction and phase transformation. Fig. 1 displays the changes in relaxation modes during mechanical activation.
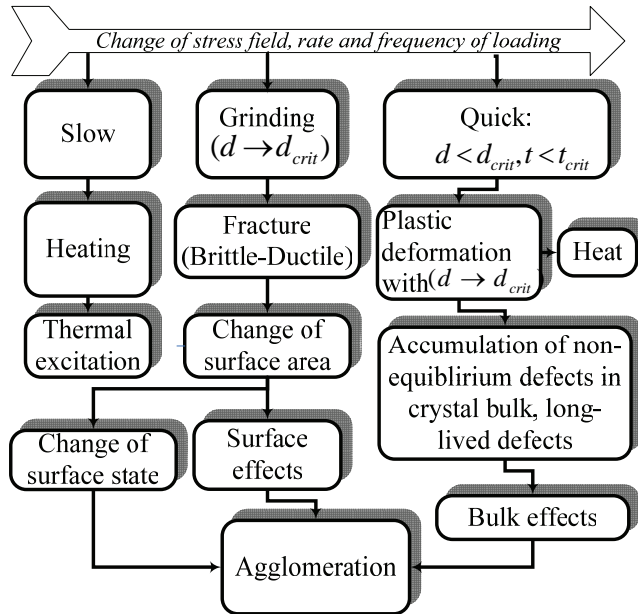
Fig. 1. *Changes in relaxation modes vs. the stress field (Boldyrev, 1986).*

Under the action of cyclic loading, the mechanism of failure changes with the particle size and the structure of the particles undergoing grinding. The brittle fracture is typical for the initial stage of the grinding process when the particles are larger than the critical size. With increasing grinding time (number of loading cycles) the particle size tends to decrease and previous cracks disappear. Defects are accumulated at the surface due to plastic deformation. By analogy with the well known mechanism of plastic fatigue in metals, it may be assumed that the initiation of micro plastic fatigue takes place in regions with high concentration of micro plastic strain (Tkacova, 1989). Depending on the internal and external conditions of stressing the process can be halted at this stage ($d \leq d_{dcri}$) or the cracks can propagate in a multistage energy-intensive process with a partial relaxation, which causes changes in the surface state of the particles formed. Ultimately, if the rate of deformation turns into high level, the former changes may occur when the time during which the pulse acts is less than the critical time required to generate a crack. When a crack can not be formed in both cases

($d < d_{crit}$, $t < t_{crit}$), the increase of dislocation density and other lattice formation due to dislocation motion takes place. The complete relaxation of elastic energy as formation of lattice defects in plastic strain may takes hours, days or even years. Elastic energy that remains in the activated material as defects is the source of excess Gibbs energy and enthalpy.

1.2.4. Mechanical activation, relaxations and energy state

The active mechanical energy that partially is transferred, is stored in the form of lattice defects. In this way the solid systems gain an activated state. The disordering process is equivalent to a decrystallization and an entropy increase, which are reflected and characterized by an increase of volume (decrease of bulk density). The structural disordering implies an increase of both entropy and enthalpy and thus stimulates the crystal properties according to the thermodynamic modification. Fig. 2 displays the relation ship between Gibbs energy and relaxations during mechanical activation processes.
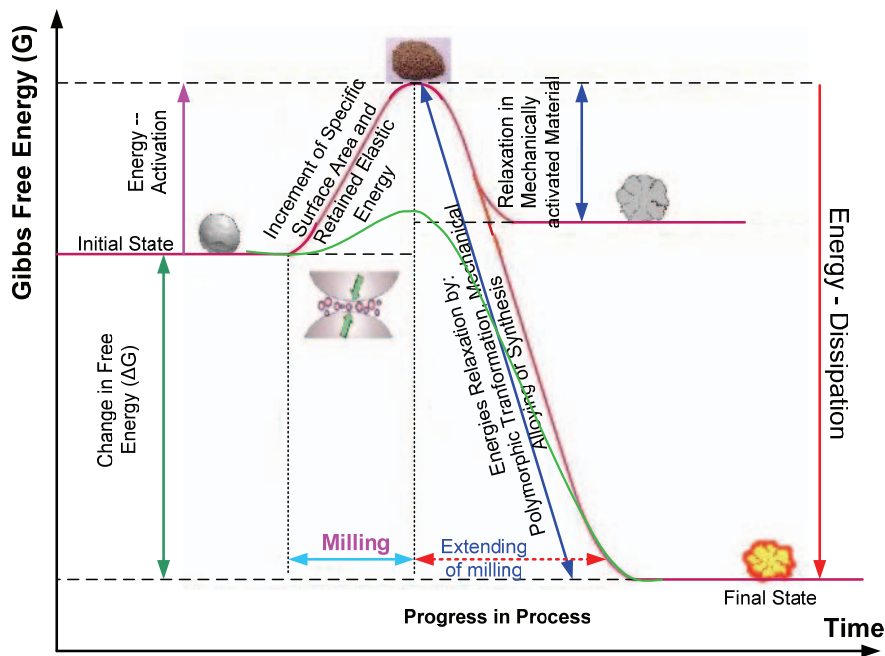
Fig. 2. *Relationships among mechanical activation, relaxation and energy state.*

In the case of comminution, only a small part of approximately 10 per cent of the excess enthalpy of the activated product may account for surface enlarging. The main fraction of the excess enthalpy and modification of properties can mostly be assigned to the development of thermodynamically unstable states in the lattice and not to the reduction of particle size. Since the activated system is unstable, the process of activation is reversible resulting in deactivation, re-crystallization, entropy loss and energy output of system. The reverse process continues to thermodynamically equilibrium but never reaches an ideal structure free of defects. As a result, in the course of mechanical activation of minerals, the relaxation

processes cannot completely decrease Gibbs free energy and some energy remains in the material in the form of lattice defects. A proper subsequent reaction, such as dissolution, can decrease the excess energy level in reactant (activated material) to produce new components with low energy and stable conditions. In the same way, such reaction can take place during mechanical alloying or synthesis with extending of grinding and some process like decomposition or solid solution reactions can occur.

The short-lived defects do not influence the reactivity of activated material whose relaxation time is less than characteristic time of reaction itself (Ljachov, 1994). On the other hand, some long-lived defects, having longer duration of life ranging from $10^{-3} - 10^{6} s$ are important in enhancement of solid reactivity. The relaxations of these structural defects decrease the excess energy considerably but never reach initial state (free defect-level energy) and consequently a residual activity (residual disorder) remain (Meyer, 1968).

1.2.5. Reactivity of mechanically activated solids

Reactivity of solids depends on the changes of Gibbs free energy states during mechanical activation. Huttig (1943) defined the activated solid substances as a thermodynamically and structurally unstable state. According to this author, the activated state of solid substances can be explained in terms of residual Gibbs energy:

$$\Delta G = G_T^* - G_T \qquad (1)$$

where G_T^*, G_T and T are the Gibbs free energy of mechanically activated solid, Gibb free energy of non-activated solid and temperature, respectively. According to the Gibbs-Hemholtz equation, the residual Gibbs free energy between activated and non-activated solid state depend on changes in enthalpy (ΔH) and entropy (ΔS).

$$\Delta G = \Delta H - T\Delta S \qquad (2)$$

The values of ΔS are very small and negligible, if the crystal disordering is low. In contrast, in highly deformed and disordered crystals, it can be significant and will influence the Gibbs free energy.

The excess Gibbs free energy or enthalpy in the activated solid substances is due to the two main components, specific surface area and defect structure. In the case of comminution, only a small fraction, approximately 10 percent, of the excess energy of activated product may account for surface area. In contrast, the excess energy component of defect structure contains almost the remaining fraction of excess energy (Tkacova et al., 1993; Balaz, 2000).

The activation energy for a chemical reaction, E, is a level of energy barrier that initiates a reaction, i.e. the larger the activation energy, the slower the reaction. To progress a reaction, the sufficient Gibbs free energy are necessary to overcome the activation energy. Generally speaking from the thermodynamic view point, what is happening during mechanical activation is the increase of Gibbs free energy and this makes the activated material reach high potential to overcome the activation energy barrier to initiate a reaction. Zelikman et al. (1975) stated that the breaking of bonds in crystalline lattice of minerals bring about a decrease in activation energy (ΔE) and are increase of the rate of leaching

$$\Delta E^* = E - E^*; \qquad K^* = K\exp(\Delta E^* / RT) \qquad (3)$$

where E is the apparent activation energy of the non activated mineral and E^* the apparent activation of disordered mineral; K, R and T stands for the rate constant of leaching for the non-disordered mineral, pre-exponential factor, gas constant and reaction temperature, respectively; K^* is the rate constant of leaching for the disordered mineral. If $E > E^*$, thus, $K^* > K$, i.e., the rate of leaching of an activated mineral is greater than that of an ordered mineral (Balaz et al., 2005).

1.2.6. Energy contribution to the long-lived defect structures

An important part of an analysis of the grinding process is the calculation of the contribution from the long-lived defects to energy content of the activated solid substances. The calculation of total energy contributing to the activated solid is not satisfying in most cases. However, the energy contribution for each defect structure to interpret satisfactorily the grinding process is necessary. The energy of macro state is equal to the sum of energy of the microstates.

$$H = \sum_{i=1}^{m} c_i H_i \tag{4}$$

where $\sum_{i=1}^{m} c_i = 1$ the concentration of lattice elements is c_i is their concentration in the ith energy level and H_i is the enthalpy required to transfer a lattice element to the ith state. In the case of fine grinding and mechanical activation, the detection of the mode of the state of lattice atoms and concentration is difficult. It seems that the following variables are the most suitable for characterizing the state of activated solids (Heegn, 1979; Tkacova, 1989; Tkacova et al., 1993; Tromans and Meech 2001):

1) Relative lattice distortion as a measure for dislocation density (ΔH_d)

2) The formation of new phases such as polymorphic transformation (ΔH_P)

3) The formation of amorphous material (ΔH_A)

4) Specific surface area as a measure for the grain boundary to the surrounding medium (ΔH_S)

For the enthalpy increase of the active solid the following equation is valid:

$$\Delta H_T = \Delta H_d + \Delta H_S + \Delta H_A + \Delta H_p \tag{5}$$

Further defects and especially short-term activated states are also important, but can only be quantified theoretically and experimentally with difficulties. The presented approximation is not intended to further observe these defects.

The quantitative estimate of the increase in molar chemical free energy (increase in stored energy) has been connected theoretically to the dislocation density by Tromans and Meech (2001) according to expression:

$$\Delta H_d = (\rho M_V) \frac{b^2 \mu_S}{4\pi} \ln\left(\frac{2(\rho)^{-1/2}}{b} \right) \tag{6}$$

where M_V, b, μ_S and ρ correspond to the molar volume of mineral, Burger's vector, elastic shear modulus and dislocation density respectively.

The specific surface energy as a measure for the grain boundary to the surrounding medium has been given by expression (Heegn, 1979 and 1987):

$$\Delta H_S = \sigma_S o_S \qquad (7)$$

where σ_S and o_S refer to specific interfacial energy and specific surface respectively.

Energy fraction of newly formed phases (our experiments suggested only amorphization not the formation of other new phases) can be estimated in first approximation by equation (Heegn, 1979 and 1987):

$$\Delta H_A = C_A E_A \qquad (8)$$

C_A and E_A denote the concentration of amorphous phase and molar amorphization energy respectively. Amorphization, which is in fact a highly distorted periodicity of lattice elements, is often compared to a quasi-molten state. In order to calculate the contribution for X-ray amorphous regions, the energy coefficients are substituted by molar enthalpies of fusion (Heegn, 1979 & 1987; Tkacova et al., 1993).

1.3.   The scope of thesis

The overall aim of this work is to test analysis techniques for studies of the influence of operational conditions and milling devices on the induction of microstructural characteristics during mechanical activation on hematite concentrate, subsequently, the conversation of energy into activated hematite. Another goal of project was also to investigate the relationship between stress energy (grinding work) and structure changes in hematite with treating in the mills in stead of individual variables. Three main factors, grinding time, media surface and mill type, have been used in this work for investigation. For quantitative and qualitative characterizations, two methods have been used; Integral breadth method and Warren-Averbach method. In addition, data were collected according to a statistical design at 3 levels for mill type and grinding time and two levels for media surface factors respectively.

2. Experimental

2.1. Materials

The chemical analysis showed that the initial hematite powder contained about 97.91% Fe_2O_3, 0.73% Al_2O_3, 0.73% SiO_2, 0.27% TiO_2, 0.20% MgO, 0.0218% MnO, and 0.088% P_2O_5. Other components such as K_2O, CaO, and $Na2O$ comprise 0.051 %. The X-ray diffraction analysis represented only the hematite diffraction lines. From the size analysis the mean diameter and F_{80} of the starting powder were estimated to around 23 and 80 μm respectively. The fractions of particles smaller than 10 and 1 μm were estimated around 19.14% and 7.8% respectively. The XRD diffraction pattern and size distribution of initial sample are given in paper1.

To exclude the instrumental broadening contribution from the samples, a standard reference sample (SRM 660a), Lanthanum Hexaboride Powder, LaB_6 with reference number SRM660a which proposed by National Institute of Standard and Technology (NIST) of U.S.A was used. The use of standard sample allows a true comparison of results among different laboratories. The typical particle size distribution as determined by Laser Scattering is displayed in Fig. 3. The size of crystallite was in the 2 μm to 5 μm range. The XRD patterns and peak positions using $CuK\alpha$ radiation ($\lambda = 0.15406\,nm$) is given in paper 2.
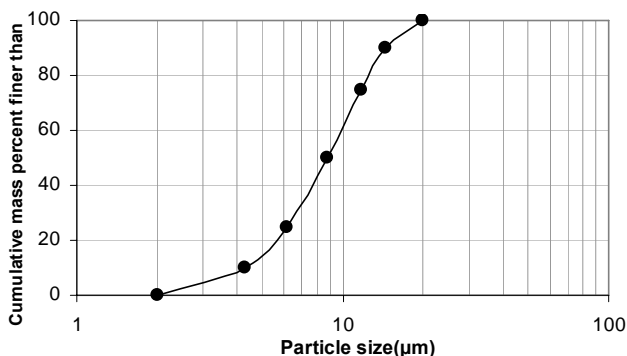
Fig. 3. *Particle size distribution of standard sample (LaB_6).*

2.2. Methods

2.2.1. Data collection (main steps)

Since the detailed data collection is described in the attached papers, we only give here the main steps that were performed for data collections. For data collection, a full factorial experiment design with one qualitative and two quantitative factors were constructed. The qualitative factor, grinding mill, was set at three levels; tumbling, vibratory and planetary mills. The quantitative grinding time factor was leveled at 1, 3 and 9 h. The two levels 1 and 4 m^2 per kg of material were chosen for media surface variable. Dry grinding tests were performed according to the design. The martial temperature and specific energy input were recorded after finishing each experiment run. The material temperature was measured by a

thermometer instantly after stopping the mill. The detail experimental conditions of milling tests are given in papers 2 and 3.

The X-ray diffraction (XRD) patterns were collected using a Siemens D5000 powder diffractometer with Bragg-Brentano geometry equipped with a curved graphite monochromator in the diffracted beam arm and using Cu Kα ($\lambda = 0.154 nm$) radiation. The XRD patterns of samples were recorded in the range $2\theta = 10 - 90°$, using a step size of $0.02°$ and a counting time of 5s per step.

We loaded the recorded XRD patterns into Profile software to calculate the line broadening parameters. This procedure will be discussed in next section completely. After the extraction of line profile parameters, the physically broadened profile obtained by unfolding the instrumental contribution using the standard reference sample (LaB_6). At the next step, the crystallite and strain components must be deconvoluted from physically broadened profile. To achieve this, two methods were used; Integral breadth method (Williamson-Hall) and Warren-Averbach methods. Both methods are discussed in detail in the coming sections.

The particle size distribution of samples was measured by the method of Laser diffraction (CILAS 1064) in the liquid mode. From the Laser diffraction measurements, the mean particle diameter and granulometeric specific surface area were also calculated. The specific surface area of samples was determined by the BET method with the Flow Sorb II 2300 (Micromeretics), from which the equivalent particle diameter, assuming spherical shape for particles, was determined.

After the extraction of microstructure characters and their comparison, the energy contributions of the long-lived defects were evaluated with a first approximation by previously proposed expressions and microstructure characters. Finally, the stress energy (grinding work) has been estimated with regard to the grinding variables.

2.2.2. The source of line breadth

The broadening of diffraction peaks arises mainly due to three factors; instrumental effects, crystallite size and lattice strain. The instrumental effects are due to imperfect focusing, unresolved α_1 and α_2 peaks or including the limited widths of the α_1 and α_2 in cases where they are resolved, wavelength dispersion, flat sample effect and detector resolution. Therefore, the ideal peak shape (with negligible width) becomes broadened due to instrumental effect (Fig. 4). In addition to the instrumental effects, the broadening due to smaller crystallite and lattice strain transform to the measured XRD diffraction patterns. To extract precisely the microstructure characters, the instrumental effect should be removed from XRD diffractions and then the microstrain and crystallite size contributions must be separated from each other.
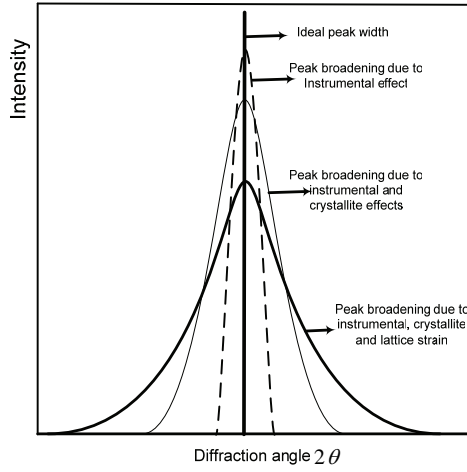
Fig. 4. *The broadening of X-ray diffraction peaks; the different source of broadening are shown (not drawn to scale). The decrease of the line intensity implies the formation of the amorphous phase.*

2.2.3. Profile fitting procedure

In order to characterize the microstructure in terms of defect parameters such as crystallite (domain) sizes and microstrain and to obtain high precise and accurate line position, intensities, widths, and shapes from diffraction spectra, the Profile software was used. The procedures of profile fitting are summarized in Fig. 5. More information can be found in paper1.
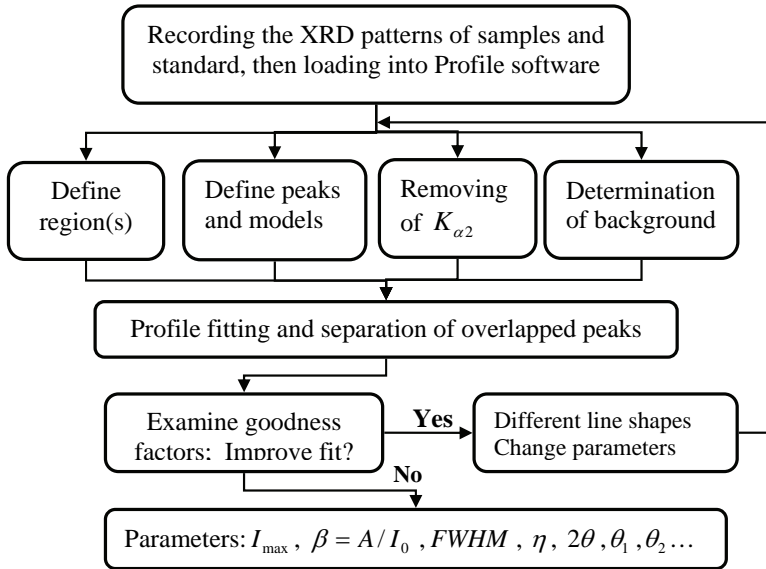
Fig. 5. *The summary of profile fitting procedure.*

It was experimentally verified that the Pseudo-Voigt line shape has high correspondence to the XRD patterns which is an approximation form of Voigt line shape and consists of linear form of Gaussian and Lorentzian line shape function, as follow (Young et al., 1982):

$$I_P(x) = I_P \{\eta C(x) + (1-\eta)G(x)\} \tag{9}$$

where $C(x) = (1+x^2)^{-1}$ and $G(x) = \exp\left[-(\ln 2)x^2\right]$, with $x = (2\theta - 2\theta_0)/FWHM$, η is Cauchy constant (mixing factor) and $2\theta_0$ is the position of the peak maximum. Fig. 6 shows schematically a Cauchy and Gaussian line profile shapes where the tails decay very fast for a Gaussian profile and more slowly for a Lorentzian (Cauchy) profile. The Pseudo –Voigt occupies the intermediate situation of both functions.
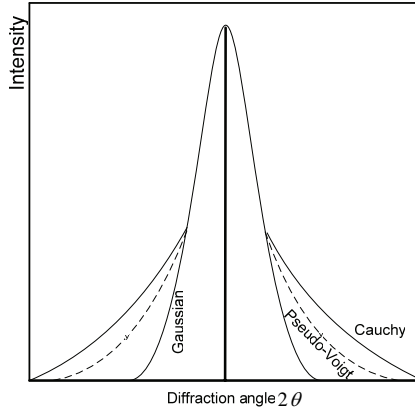
Fig. 6. *Comparison of Cauchy, Gaussian and Pseudo-Voigt line profiles (not drawn to scale).*

The integral breath of the Pseudo-Voigt function is also given by:

$$\beta = \frac{FWHM}{2}\left[(1-\eta)(\pi/\ln 2)^{1/2} + \eta\pi\right] \quad \text{or} \quad \beta = \eta\beta_L + (1-\eta)\beta_G \tag{10}$$

where β_L and β_G is Cauchy and Gaussian broadening components contributing to profile.

Several fitting criteria of the profile shape function to the actual profile were considered and examined. Their definitions are (Siemens AG, 1996a)

$$\text{Reliability factor:} \quad R = 100 \times \sqrt{\frac{\sum w(I_o - I_c)^2}{\sum wI_o^2}} \tag{11}$$

$$\text{Reliability index:} \quad RI = 100 \times \frac{\sum |I_o - I_c|}{\sum I_o} \tag{12}$$

$$\text{Reliability index: } RI = 100 \times \frac{\sum |I_o - I_c|}{\sum I_o} \tag{13}$$

$$\text{Or, a weighted reliability factor: } RW = 100 \times \frac{\sum \sqrt{W} |I_o - I_c|}{\sum \sqrt{w} I_o} \tag{14}$$

$$\text{And theoretical reliability: } TR = 100 \times \sqrt{\frac{\sum w I_o}{\sum w I_o^2}} \tag{15}$$

where w is the weighting factor, I_c corresponds to the calculated intensity and I_o to the observed intensity. In the profile fitting process each of above mentioned factors were refined to a value of <5% for all the studied samples. Fig. 7 exemplifies the Pseudo-Voigt line shapes which are fitted to XRD diffraction patterns of hematite concentrate ground in the vibratory mill for one hour with media surface of $1\,m^2/kg$. More information regarding profile fitting and modeling of standard sample characters can be found in paper1.
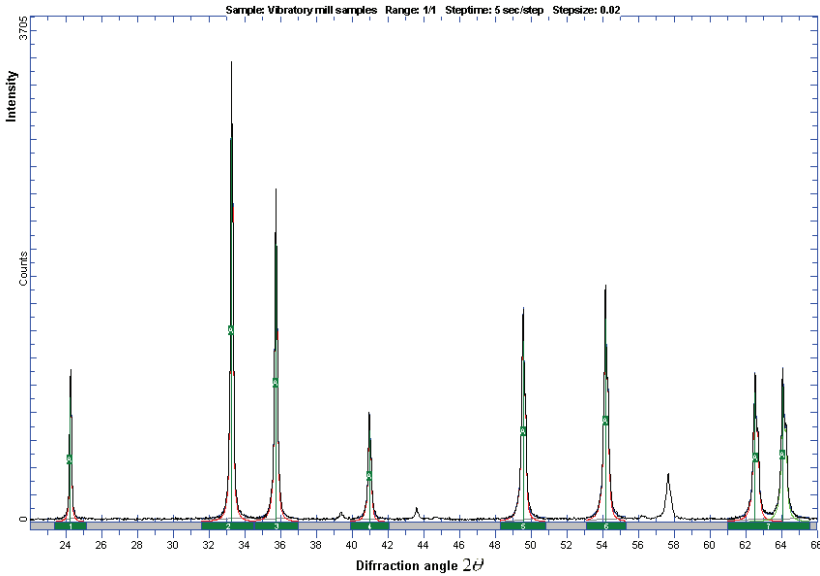
Fig. 7. *Pseudo- Voigt line shape fitted to XRD pattern of hematite activated in the vibratory mill with low media surface for 1 hour*

2.3. Microstructure characterization methods

X-rays diffraction line profile analysis (LPA) is a powerful tool to characterize the behavior of a material powder obtained under high-energy ball milling and prolonged grinding conditions. Origins of the line broadening are numerous. Generally, any lattice imperfection will cause additional diffraction line broadening. Crystallite size is a measure of the size of coherently diffracting domain and is not the same as particle size as whole due to polycrystalline aggregates. Particles could compose (and most often they do) from several or many small crystallites. Crystallite size is a fundamental property of material. Important properties of nanomaterials are dependant to the size of the crystals, but not the size of

particles. The crystallite size depends on both particle size and distortions of material. i.e., not only deceasing of particle size decrease the crystallites but also the plastic deformation increases the defects in material and subsequently lead to smaller crystallites. Extended defects disrupt the atomic arrangement of a crystal. Consequently, the crystallographic ordered domains of the crystal effectively terminate.

Analysis and deconvolution of the peak broadening can give important information regarding microstructure. To analysis peak broadening, two most common parameters are frequently used. One includes full width at half of maximum intensity (*FWHM)* and another is the integral breath and defined as $\beta = A/I_0$, A being the peak area and I_0 the height of the observed line profile. The *FWHM* and β can be related to each other in for specific peak shape. Besides, there are several methods to extract the size of coherent diffracting domains from diffraction peak. Two applied methods in our work are described in the following paragraphs.

2.3.1. The Williamson–Hall integral breath method

Williamson and Hall (1953) assumed that the size and strain profile components have Cauchy shape and proposed a method for deconvoluting size and strain broadening by looking at peak widths as a function of 2θ. The corresponding integral breadths are linearly combined and the integral breadth of the total broadening β_f can be written as (known also as Cauchy-Cauchy or Williamson-Hall plot):

$$\beta_f^* = \frac{\beta_f \cos\theta}{\lambda} = \frac{1}{D_v} + 2\varepsilon d^* \quad ; \quad \frac{2\sin\theta}{\lambda} = \frac{1}{d} = d^* \tag{16}$$

To make a Williamson and Hall plot, a plot of β_f^* (y axis) versus $2d^*$ (x axis) should result in a straight line, and the values for size and strain can then be obtained from the intercept and slope of straight line respectively. Other variants of the Williamson-Hall method exist, adapting Gaussian shaped functions. That can be applied to a Gaussian profile in a similar way (known as Gaussian-Gaussian approximation) which is given in paper1.

2.3.2. The Warren-Averbach method and Stokes deconvolution

The Stokes Fourier deconvolution (Stokes, 1948) method followed by Warren-Averbach analysis of the physically broadened line profile is the least biased approach to analysis of the line broadening (Balzar and Ledbetter 1993 & 1995). Because this method analyze the entire shape of several reflections in the pattern (ideally higher order reflection of the same type i.e. (1 0 0), (2 0 0), (3 0 0). In this method, a Fourier series is fitted for each reflection of interest in samples and standard. Once those results obtained, they used to deconvolute the sample broadening from the instrumental broadening via a Stokes Fourier deconvolution.

2.3.2.1. Stocks deconvolution

A general Fourier series which is periodic in x with a period length *a* can be represented as:

$$f(x) = \sum_{n=-\infty}^{n=+\infty} (A_n \cos 2\pi n \frac{x}{a} + B_n \sin 2\pi n \frac{x}{a}) \tag{17}$$

The index n takes all integral values from $-\infty$ to $+\infty$ and for each value of n there is a cosine coefficient and a sine coefficient.
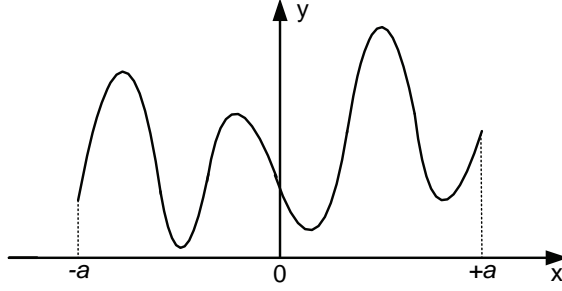
Fig. 8. *Representation of the function y=f(x) which is periodic in x with a period a.*

The coefficient is made up of a real, $C_r(n)$, and imaginary, $C_i(n)$, part and the following expressions give the coefficients:

$$A_n = C_r(n) = \frac{1}{a}\int_{-a/2}^{a/2} f(x)\cos 2\pi n\, x/a\, dx \qquad (18)$$

$$B_n = C_i(n) = \frac{1}{a}\int_{-a/2}^{a/2} f(x)\sin 2\pi n\, x/a\, dx \qquad (19)$$

In the Fourier analysis the line breadth is corrected for instrumental broadening using Stock's correction (1948).
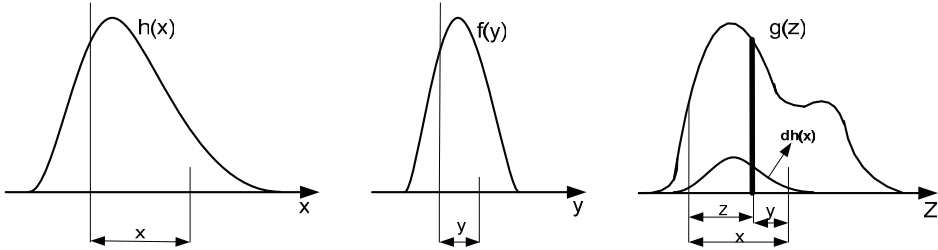
Fig. 9. *Three curves which are involved in the correction for instrumental broadening. where f(y), g(z) and h(x) are the curves corresponding to physical broadening, instrumental broadening and measured broadening respectively (From Warren, 1969).*

According to Stock's approach, the observed distribution of X-ray intensity across a line is related to the distribution due to instrumental and specimen broadening by the expression:

$$h(x) = \int_{-a}^{a} f(y)g(x-y)dy \qquad ; \qquad y = x - z \qquad (20)$$

To obtain the structural parameters in a specimen, the physically broadened profile *f* must be extracted from the observed profile. Knowing $g(z)$ and $h(x)$, the Fourier coefficients of $f(y)$ can be calculated by Fourier analysis. The Fourier components $G(t)$ of the instrumental profiles $g(x)$ are given by:

17

$$G_r(t) = \frac{1}{a} \int_{-a/2}^{a/2} g(z)\cos(2\pi zt/a)dz \qquad (21)$$

$$G_i(t) = \frac{1}{a} \int_{-a/2}^{a/2} g(z)\sin(2\pi zt/a)dz \qquad (22)$$

where t is the harmonic number and the profile is divided into a intervals. A similar expression can be written for $h(x)$. Once those are known, the corresponding sine and cosine Fourier coefficients are calculated by:

$$F_r(t) = \frac{H_r(t)G_r(t) + H_i(t)G_i(t)}{G_r^2 + G_i^2} \qquad (23)$$

$$F_i(t) = \frac{H_i(t)G_r(t) - H_i(t)G_i(t)}{G_r^2 + G_i^2} \qquad (24)$$

The $f(x)$, physically broadened profile, can be calculated from $F_r(t)$ and $F_i(t)$ using the formula:

$$f(x) = \int_0^t F_r(t)\cos(2\pi xt/a)dt + \int_0^t F_i(t)\sin(2\pi xt/a)dt \qquad (25)$$

2.3.2.2. The Warren-Averbach method

The Warren–Averbach derived another definition of domain size: the surface weighted average. The Warren-Averbach method originally was developed for plastically deformed material, but since its introduction it found successful applications to many other materials. The method is described extensively by Warren (1969). Each domain is represented by columns of cells along the a_3 direction normal to the diffracting planes (00l). All variables are expressed as function of column length $L = n|a_3|$, which is assumed to be positive, being distance in real space between a pair of cells along direction of a_3. The distances L and a_3 are calculated, to a good approximation, from the relation:

$$L = n|a_3| \; ; \quad a_3 = \frac{\lambda}{2(\sin\theta_2 - \sin\theta_1)} \qquad (26)$$

L is the Fourier length, n denotes the integer and a_3 is the unit of the Fourier length in the direction of the diffraction vector, g, and the line profile is measured from θ_1 to θ_2 and λ is wavelength of the X-rays.

According to Warren, the distribution of diffracted power can be expressed as a Fourier series. The convolution of the size and strain contributions on the profile in reciprocal space corresponds to the product of the Fourier transforms in real space. The expressions for deconvolution of size and strain components are given in paper1.
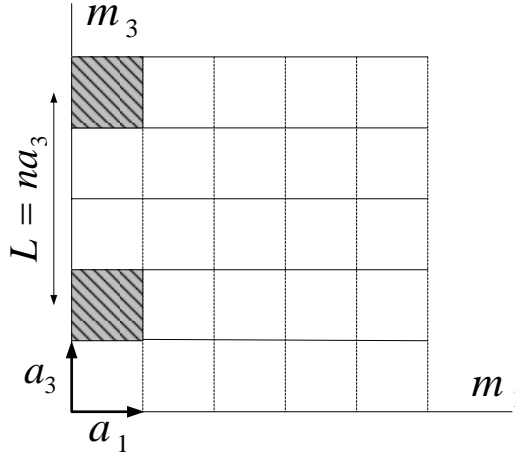
Fig. 10. *Representation of the crystal in terms of column of cells along the a_3 direction. a_1, a_2 and a_3 are the crystal axes. m_1, m_2 and m_3 are integers such that the cell $m_1m_2m_3$ is the one whose origin is displaced from the crystal origin by $m_1a_1 + m_2a_2 + m_3a_3$ (Warren, 1969).*

2.4. Data treatments

Profile fitting procedures were performed with commercial software Profile (Siemens AG, 1996a). This software is used for fitting a line shape to measured XRD patterns in order to extract the line profile parameters. It also allows changing fitting parameters and different line shapes to fit properly line shape for measured XRD diffraction patterns.

The software WIN-CRYSIZE (Siemens AG, 1996b) was applied for extraction of crystallite size, crystallite size distribution, lattice strain and its distribution from diffraction peak broadening using the Warren-Averbach theory. WIN-CRYSIZE works with the fitted profiles from both a sample and a standard measurement. The lattice expansions were evaluated based on the peak positions which resulted from profile fitting.

We used Unit Cell software which is a free software and proposed by Holland and Redfern (1997). It refines cell parameters from powder diffraction data. It uses a non-linear least squares method, which allows the refinement to be carried out on the actual observed data (e.g. two-theta in the case of angle-dispersive monochromatic diffraction, energy in the case of energy-dispersive diffraction). Furthermore, the program incorporates regression diagnostics, particularly deletion diagnostics, to aid in the detection of outliers and influential data which could be deleterious to the regressed results.

3.   Results and discussion

Through the experiments the particle size reduction, newly formed surface area, the changes of XRD diffraction pattern and broadening of the diffraction lines and microstructural characters were measured and estimated. Some important features of the obtained results are given in the following sections. More detail information can be found in the papers 1 to 3 presented in Appendix.

3.1. Particle size and surface area

Mechanical activation of hematite is accompanied with disintegration of the particles and increasing of the surface area. The particle size reduction and surface area measurements are summarized in Table 1 in terms of grinding variables.

Table 1. *The characterization of particle size and surface area.*

Grinding variables			Laser diffraction Method				BET method	
Mill types	Ms (m^2/kg)	Time (h)	d_{50} μm	R_{10}^* %	R_1^* %	SG m^2/g	Surface m^2/g	Size μm
Tumbling mill	1	1	10.8	61.8	19.3	1.1	1.4	0.81
	1	3	5.9	77.3	34.8	2.1	2.6	0.44
	1	9	4.5	83.9	44.3	2.2	4.6	0.25
	4	1	6.7	77.2	37.0	1.6	4.1	0.28
	4	3	4.1	85.1	47.0	2.4	5.3	0.21
	4	9	5.7	79.9	44.5	2.2	6.8	0.17
Vibratory mill	1	1	6.2	75.4	27.9	1.6	1.9	0.61
	1	3	3.9	86.7	45.6	2.1	3.9	0.29
	1	9	3.4	90.0	54.3	2.6	5.2	0.22
	4	1	5.7	79.8	41.6	2.1	4.4	0.26
	4	3	3.4	88.0	53.0	2.5	7.5	0.15
	4	9	5.6	73.6	42.9	2.1	18.4	0.07
Planetary mill	1	1	8.1	69.7	23.5	1.2	2.1	0.54
	1	3	5.0	84.0	42.2	1.8	3.4	0.34
	1	9	4.8	84.7	42.8	1.9	4.4	0.26
	4	1	4.4	85.8	45.7	2.2	5.1	0.22
	4	3	6.0	78.6	44.4	2.3	8.0	0.14
	4	9	6.7	74.0	38.8	2.0	8.8	0.13
initial	--	--	46.6	19.1	7.8	0.4	0.6	1.9**

R^*_{10} and R^*_1 refer to the fraction of particles smaller than 10 and 1 μm respectively.

*SG denotes Granulometric surface area; ** is not very precise.*

There are two stages in the changes of the measured parameters. Most of parameters change sharply in the initial stages of milling and continue to change slightly with progress in milling. In the case of the lower media surface, $Ms= 1$ m^2 per kg of material, prolonged grinding in both tumbling and vibratory mills tends to produce finer particles. This indicates that further size reduction in such mills at the given circumstances is possible. The size reduction with lower media surface is completed within three hours of milling in the planetary. The use of higher media surface provides a rapid size reduction in the initial stage of milling and

tendency of the particles to agglomeration in prolonged milling, which can also be investigated by granulometric surface area. The agglomeration of particles during extended milling was reported for various minerals by Welham and Llewellyn (1998), Welham (2001), Balaz (2000), and Zhang et al. (1996). These suggest that agglomeration phenomena may be a feature of extended dry milling. Grinding of hematite in lower media surface did not show any evidence of the formation of agglomerates with grinding in tumbling and vibratory mills.

 The portion of particles smaller than 10 μm is a character of ultrafine grinding (Balaz, 2000). If the fraction of particles smaller 10 μm being above 50%, the grinding proceed into ultrafine grinding region. Clearly, our ground samples have been affected by ultrafine grinding regime.

The results concerning the BET surface area show that specific surface area increases as the milling time and media surface goes up. The maximum specific surface area in the milling with vibratory, planetary and tumbling mill ranged to 18.4, 8.8 and 6.8 m^2/g respectively. The use of higher media surface produces larger BET surface area whatever milling devices are applied. The vibratory mill produced large surface area in particular in prolonged milling probably due to stressing of particles in shear mode and generation of higher temperature. The comparison of particle size, granulometric surface area and BET surface area results give evidence to the agglomeration of particles in intensive grinding conditions without decreasing of BET surface area, indicating that the agglomerates pores remain accessible for the nitrogen gas and probably grinding process prevails to the aggregation of particle. The effect of media surface appears to be more important than grinding time and mill type variables.

3.2. X-ray diffraction results

The XRD patterns of the mechanically-ground hematite show rapid changes during the grinding process (Fig. 11). The milled and unmilled samples are mainly composed of hematite indicating that hematite did not undergo a reaction or phase transformation during mechanical activation. As the milling time and media surface increased the peaks became weaker and broader suggesting refinement of the crystallites and increasing the lattice strain within powder whatever milling methods are used. Both plastic deformation of the structure and disintegration cause the broadening of X-ray diffraction lines. The structural disorder due to increasing abundance of X-ray amorphous material is manifested by decreases in the intensity of diffraction lines. Clearly, there are significant changes in the crystalline structure due to the extended milling and increasing of media surface. The peaks become broader and weaker with increasing of the milling intensity. With a first approximation, it was concluded that the planetary mill causes broader and weaker peaks than tumbling and vibratory mills. The alteration in the XRD diffraction patterns for hematite powder because of milling was reported by many authors (Zdujic et al., 1999; Stewart et al., 2003; Tokumitsu, 1997). It must be emphasized that the literature data diverge to a large extent and there are large differences in the literature with respect to, for instance, the characteristics of the starting powder, mill type, grinding variable and operation conditions and etc. The observed general trend is consistent with each other although the quantitative comparisons are not much reliable.
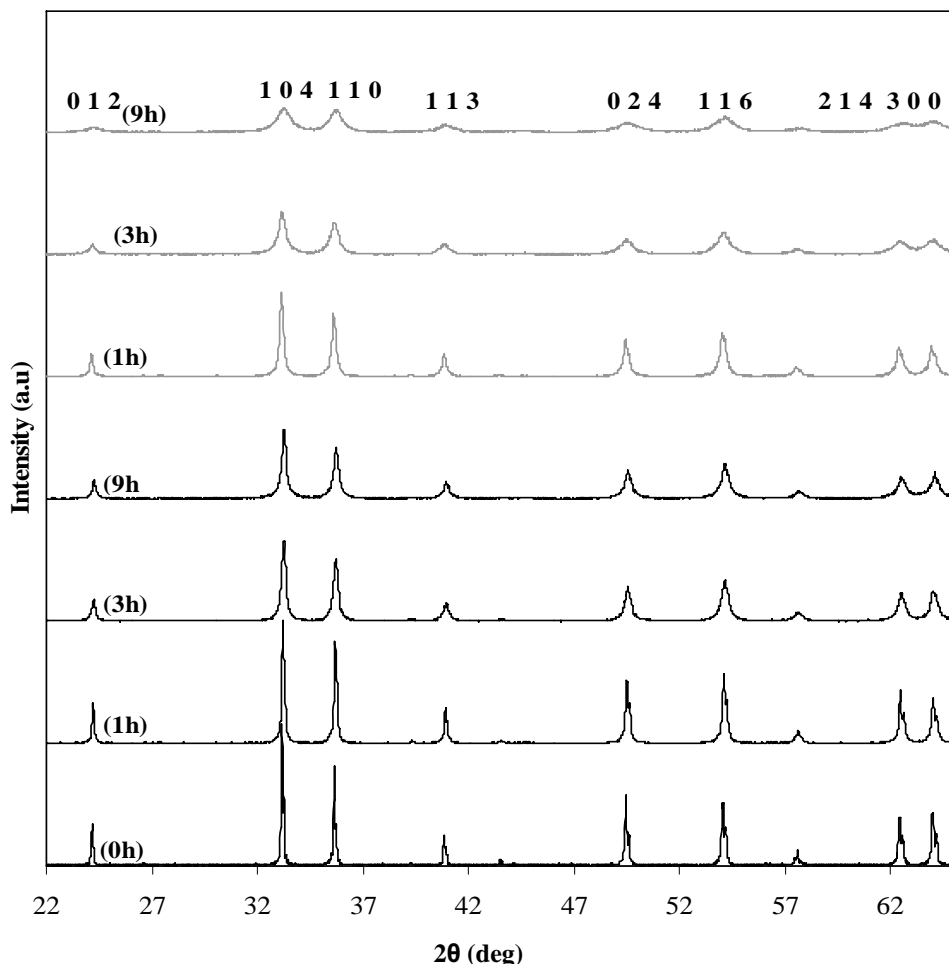
Fig. 11. *The X-ray diffraction patterns of activated hematite as function of the grinding time and media surface for planetary mill. The solid line and grey line refer to X-ray spectra obtained using media surface 1 and 4 m^2 per kg of hematite respectively.*

3.2.1. X-ray amorphization degree

For a quantitative comparison, the average relative intensity and X-ray Amorphization degree, which are estimated based on the intensity and background of the eight most intensive reflections with comparing to those of starting sample, are determined from XRD diffraction lines. The influence of the media surface and grinding time are evident from Fig.12 an13. The planetary mill products yield the weakest peaks and subsequently the least relative intensity. There is a marginally difference between tumbling mill and vibratory mill. A well correspondence can be observed between the amorphization degree and relative intensity. The lower relative intensity, the more amorphization. The maximum and minimum fraction of amorphous phase in the case of lower media surface created during grinding in the planetary and vibratory mills, accounting for 72 and 58 % respectively and there is small differences between tumbling and planetary mill products. In the case of higher media surface, with a first

approximation, the planetary mill produced more X-ray amorphous material, after 9 hours of milling 85 percent of the initial hematite was converted into amorphous phase.
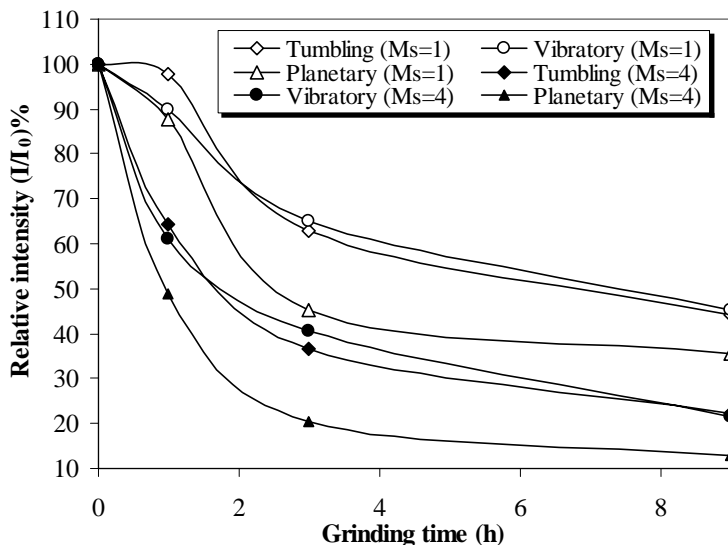
Fig. 12. *Changes in the relative intensity of XRD diffraction patterns. The average values calculated by taking into account of the eight most intensive reflection peaks.*
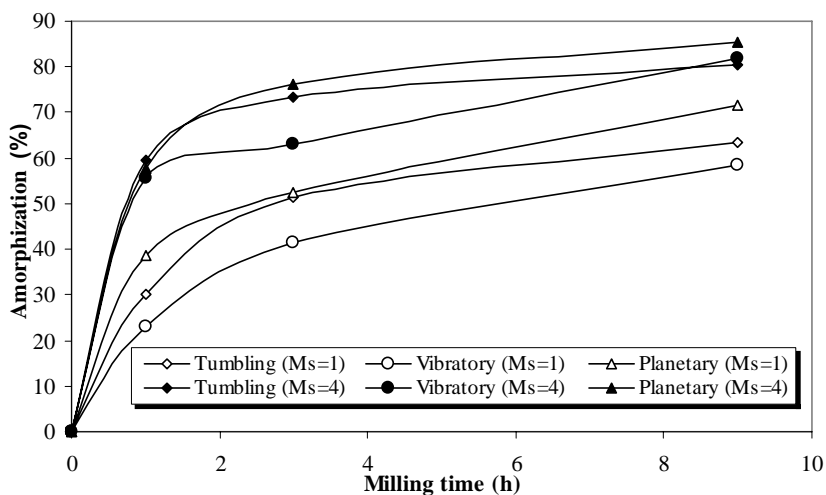
Fig. 13. *The changes in the amorphization degree of material vs. grinding variables. The average values calculated by taking into account of the eight most intensive reflection peaks.*

As said, the planetary mill favors the production of great amorphous material whatever media surface level are used. It should be noted that the amorphization increases sharply in the initial stages of milling and continues to increase steadily. The amorphization degree for activated gibbsite (Kitamura and Senna, 2001), sulphide minerals (Balaz, 200) have been investigated vs. grinding time. Our data trend agrees with their findings. The intensive milling seems to

alter drastically the symmetry of activated material and subsequently the formation of amorphous phase. Since higher media surface (higher ball to powder weight ratio) impose higher impact energy to the particles being ground lead to the formation of great amorphous material.

3.2.2 . Comparison of line breadths

The XRD measurements of the hematite powders showed that the XRD lines become substantially broadened upon ball milling (Fig. 14). This broadening can be ascribed to crystallite-size reduction and introduction of lattice microstrain as shown in the next sections. From Fig. 14, it can be further observed that planetary mill brings about much broader peaks and it is expected to yield smaller crystallite size and higher microstrain.
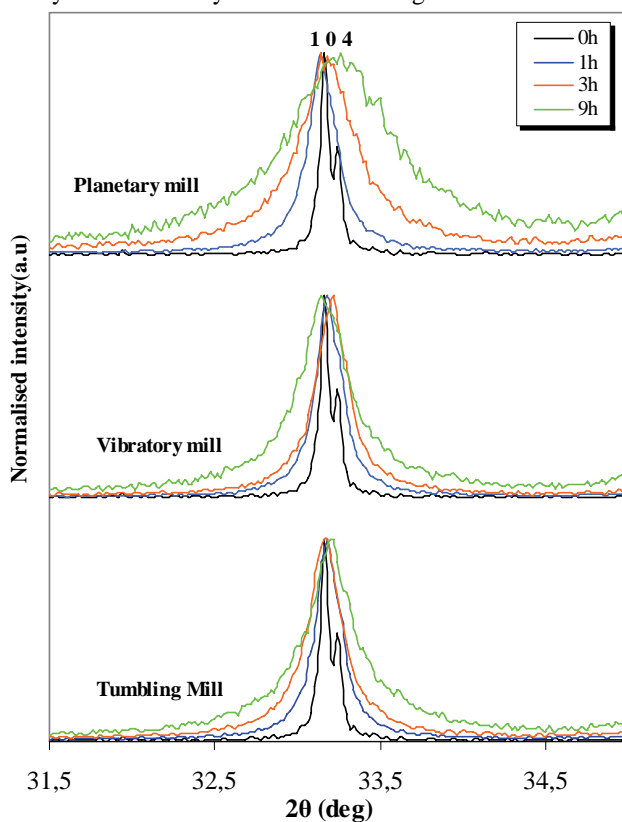
Fig. 14. *The comparison of the broadening of the (104) reflection for different grinding times and higher media surface in mills. The intensity normalized to maximum intensity of (104) reflection.*

The quantitative comparison of line breadths (FWHM) is depicted in Fig. 15 for samples with different grinding variables. The physical broadening was calculated according to Halder Halder-Wagner (1966) approximation.
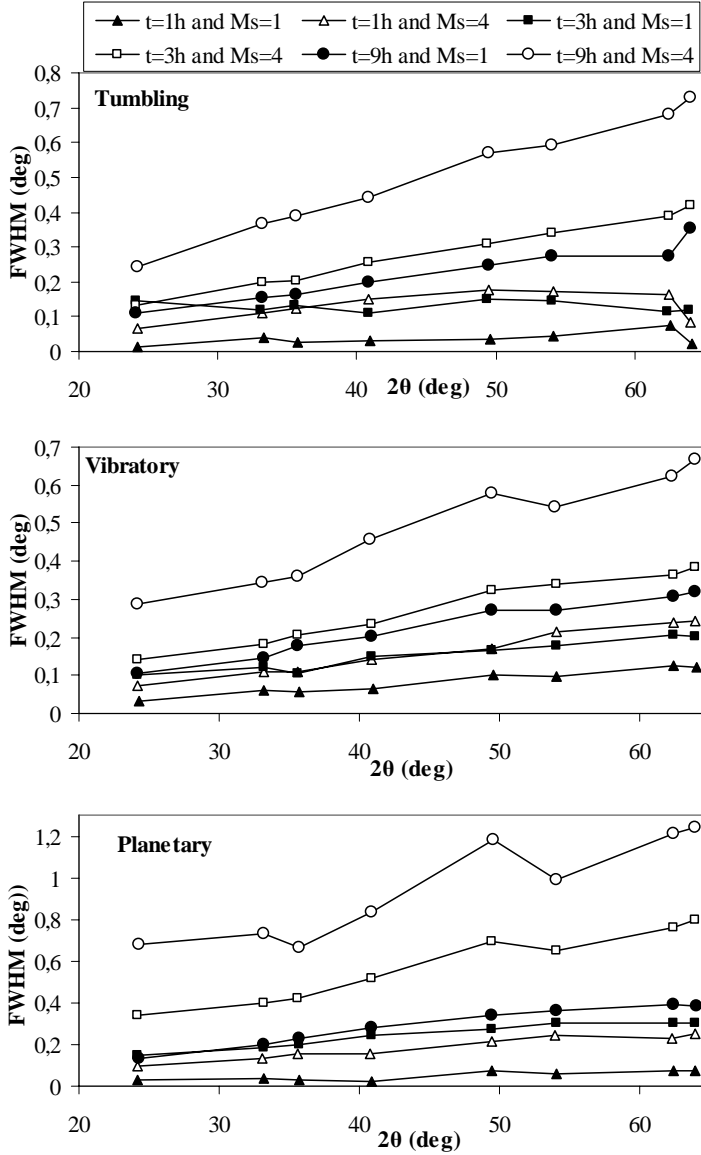
Fig. 15. *Change in the physical FWHM for activated samples in different grinding times and media surface for three mills.*

From Fig. 15, it can be observed that the planetary mill brings about the maximum broadening of reflection peaks. The broadening for the samples milled with the tumbling and vibratory mills differs marginally, the vibratory mill products shows slightly larger broadening than the products of tumbling mill. For example, after 9 hours of milling with the lower media surface for the reflection (014), FWHM= 0.229 deg with planetary mill, FWHM=0.179 deg with the vibratory mill and FWHM=0.162 deg with tumbling mill were

obtained. These indicate the changes in crystallite size and strain domain in different milling environments. These characters will be discussed in the next section.

3.3. Resolving the size and strain components

Through the experiments, two methods of the Williamson-Hall plot and Warren-Averbach, approach, were used to deconvolute the strain and domain size components. Simple qualitative information regarding the nature of the coherently diffracting domain, i.e., morphology, size and strain information, prior to any detailed analysis may be obtained on the basis of the Williamson-Hall plot. In addition, the Warren-Averbach method based on Fourier analysis, which can precisely determine microstructure characters (Balzar, 1999), was used for [012] direction.

3.3.1. Integral breadth method (Williamson-Hall plots)

As discussed in papers 1 and 2, from the integral breadth method, the anisotropic character of line broadening for deformed hematite and changes in the trend of microstructural characteristics as a function of milling condition can be revealed. The Williamson-Hall plots suggested that strain and size components contribute to line broadening simultaneously in the milled samples. It was concluded that there is difference in the elastic moduli of single crystal hematite existing between (024) and other crystallographic directions and the hematite lattice is 'soft' between the (024) and the others crystallographic directions. The scatter of the β_f^{*2} values indicates that the crystallite shape differs from a spherical one. The Williamson–Hall plots are given in papers 1 and 2.

3.3.2. The results of Warren-Averbach method

The variation of crystallite size and root mean square strain (RMSS), $<\varepsilon^2_{L=10nm}>^{1/2}$, in direction [012] as functions of grinding variables are summarized in Table 2. Since the integral breadth method reveals the anisotropy contribution to the line broadening, the Warren-Averbach method is an unbiased method to evaluate the microstructure characters.

Table 2. *The microstructural characteristics in [012] direction using the Warren-Averbach method for activated hematite in different environments.* D_S *and* $<\varepsilon^2_{L=10nm}>^{1/2}$ *indicate the surface weighted crystallite size and root mean square strain at L=10 nm respectively.*

Parameters		$Ms = 1 m^2 / kg$		$Ms = 4 m^2 / kg$	
Milling type	Time(h)	$D_S (nm)$	$<\varepsilon^2_{L=10nm}>^{1/2} \times (10^{-3})$	$D_S (nm)$	$<\varepsilon^2_{L=10nm}>^{1/2}$ (10
	1	54.16	0.062	44.4	2.236
Tumbling mill	3	42.6	1.52	25.0	2.84
	9	27.3	2.25	17.3	4.44
	1	73.5	1.75	36.4	1.84
Vibratory mill	3	43.5	2.08	23.7	2.79
	9	29.6	2.58	12.2	3.95
	1	66.7	1.25	28.1	1.94
Planetary mill	3	20.5	2.03	11.6	4.44
	9	16.5	3.011	5.6	5.32
Initial hematite*	0	199.1	n.d.(0)		

*Calculated using single peak method.

From Table 2, it is clear that the surface weighted crystallite size in direction [012] decreases and the microstrain values increases as the milling time and media surface increase. The planetary mill brought about more reduction of domain size and increasing of microstrain than vibratory and tumbling mills in the intensive grinding condition. In the earlier stages of milling, the crystallite size declines rapidly to the nanometer range. Obviously, both the refinement rate and ultimate grain crystallite size depend on type of mill used, the milling intensity and the overall milling temperature. Variations in the ball media surface have a more important influence on the crystallite refinement; the larger media surface the faster is the reduction of grain size. The ground sample within one hour in planetary mill with lower media doesn't follow the changes in microstructure characters among mills which can probably be ascribed to the higher powder to ball weight ratio and subsequently hindering of ball motion during the milling process. On the other hand, the results relating to tumbling and vibratory mill products show some slight differences between size and strain components when the media surface changes in milling process. Obviously, grinding of hematite with lower media surface in vibratory mill resulted in larger crystallite size and higher strain than grinding in tumbling mill. Besides, the products of the tumbling mill have slightly larger crystallites and higher strain values than of those in the vibratory mill, when hematite is subjected to grinding with higher media surface. This may be related to the changes in stressing manner of particles in milling process especially in vibratory mill. Perhaps, when grinding with lower media surface proceed to higher media surface, the dominant type of stress changes from compressive and impact change to shear and or attrition. These changes can facilitate the size reduction and breakage in fine and ultrafine range. The results regarding to the strain and crystallite size are in line with observations of Bid et al. (2001) and Sahu et al. (2003), however, our results regarding crystallite sizes and strain in direction [012] show some differences. This can be related to the initial material characteristics and milling conditions. Bide et al. and Sahu et al. used planetary mills with high angular velocity.

The Warren-Averbach method also gives some valuable information regarding the crystallite size and strain distribution in terms of crystal length (column length) from which some qualitative results and conclusions about homogeneity, the new phase formation and disordering of material can be drawn. These results are thoroughly discussed in paper 2.

3.4. The variation of lattice parameters

The calculated lattice parameters and unit volume cell for the activated samples with lower media surface in different milling machines are shown in Fig. 16 as a function of milling time. It is seen that the unit cell parameters and unit cell volume increased with activation time. This suggests the lattice and volume expansion of hematite during mechanical activation process. The confidence level of data at 95% is also given in Fig. 16. There are some significant differences among different millings for a lattice and unit cell volume characters in specific grinding times, but it doesn't stand with higher media surface. The results concerning to higher media surface level is given in paper 2.

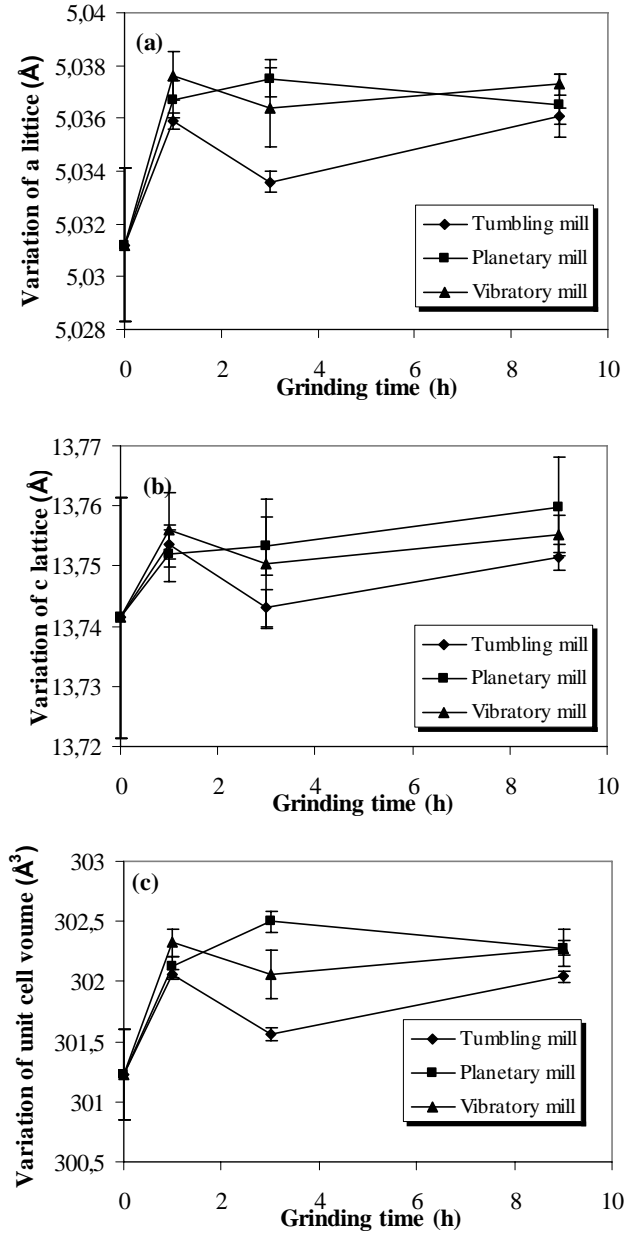**Fig. 16.** *Variation of lattice parameter and unit cell volume for mille sample in different milling devices using lower media surface level (Ms=1 m² / kg).*

3.5. The relationship between stress energy and structure changes

During mechanical activation, mechanical energy is partially transferred to the particles being ground. The stored energy relaxes by forming lattice defect and enlarging the surface area.

Input energy during milling was recorded by an energy meter. An approximate evaluation of the stress energy has been made on basis of an analysis of the forces acting for the predominant mode of stress in various grinding mills using the equations proposed by Heegn (1986). It should be kept in mind that these equations are derived on basis of the periodic – impulsive character of energy transfer during grinding. This approach is only a mental abstraction that describes an idealized case, in which the material being ground is uniformly distributed throughout the mill and spatial conditions of interactions between particles and grinding bodies, as well as between the members of the particulate assembly, don't vary in the course of grinding. The advantage of this simplified approach is that it allows to estimate the efficiency with which the energy is converted to grinding work. The used equations summarized in paper 3 take into account the number of impulses and the rate of stress, which can be estimated from the known characteristics of the mill performance. The number of impulses in ball, vibration and planetary mill is determined by the number of rotations and by the grinding time. The stress energy with regard to the grinding variables is determined to explore the changes of hematite structure vs. grinding variables. The stress energy takes into account the grinding variables simultaneously.

Fig. 17 shows the relationship between stress energy and surface area in different mills. It can be seen that the production of unit surface area in the vibratory mill needs more energy than other mills. It is obvious that the rate of new surface formation depends on both applied stress energy and the types of mills. The BET surface area shows an increasing trend, especially at lower levels of stress energy. The BET surface area continues to increase during the intensive grinding stages when hematite is subjected to the milling in tumbling and vibratory mills. On the other hand, the BET surface area of the ground samples in the vibratory mill increases sharply at higher level of stress energy. With growing stress energy, the products of planetary mill produce marginally higher specific surface area than the products of tumbling mill as opposed to the initial stage of milling bearing lower intensity. Thus, the agglomeration at different stages disturbs the trend of BET surface area changes in terms of stress energy.
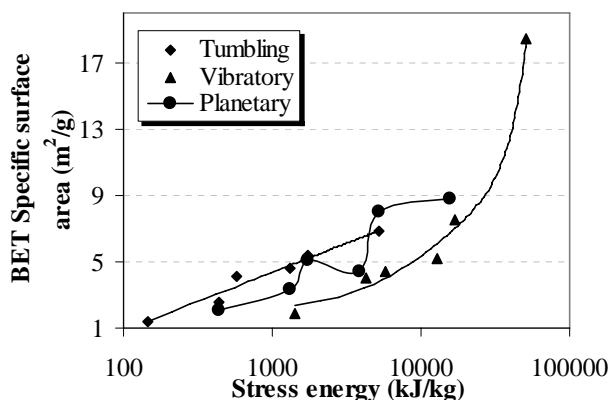
Fig. 17. *Change in specific surface area in different mills as a function of stress energy.*

The content of the amorphous phase is determined with regard to the reduction of diffraction intensities and their background. The results are displayed in Fig. 18 for different mills in terms of stress energy. The amorphization degree increased to 80, 82 and 86% by grinding in the tumbling, vibratory and planetary mills, respectively, after releasing 5230, 51300 and

15600 kJ/kg of energy. These results indicate that much more energy is needed in the vibratory mill and planetary mill to produce the same amorphization degree as tumbling mill. The increase of X-ray amorphous phase due to intensive milling was reported for calcite, quartz and magnesite (Heegn, 1986), sulphide minerals (Balaz, 2000). The amorphization is in fact a highly distorted periodicity of lattice elements, and it is often characterized as a short range order in contrast to the long order of a fully crystalline structure.
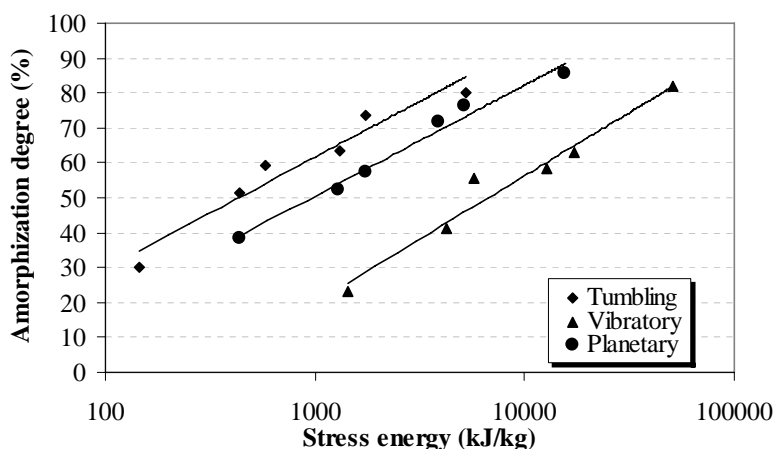
Fig. 18. *The content of X-ray amorphous phase for different milling environments as a function of stress energy.*

The changes in the surface weighted crystallite size and root mean square strain (RMSS) are shown in Fig. 19. With a first approximation, we can draw a conclusion that the largest crystallites are resulted from the milling in the vibratory mill for a given stress energy. With planetary, tumbling and vibratory mills, the hematite crystallites refined maximum up to the values of 5.6, 17.3 and 13.5 nm, respectively, after receiving the stress energy levels to the values of 15600, 5230 and 51300 kJ/kg during grinding in mills. Generally, more severe decrease of crystallites can be seen for hematite mechanically activated in the planetary mill regardless of stress energy.
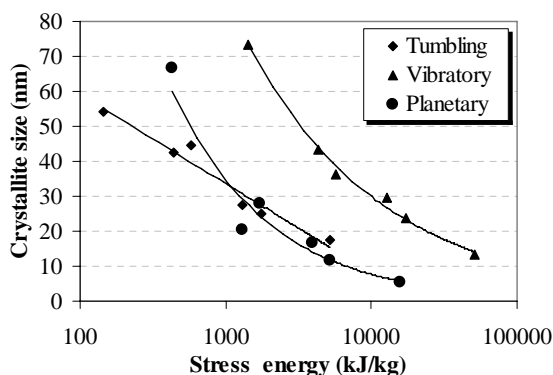
Fig. 19. *The variations of the surface weighted crystallite size in [012] direction with milling in different mills as a function of stress energy.*

The root mean square strain values, $< \varepsilon^2_{L=10nm} >^{1/2}$, for activated hematite in mills are displayed in Fig. 20. At lower levels of stress energy, there is only a small difference between the mills in deformation of hematite lattice, while with growing the grinding intensity the difference becomes large. The distinguish difference among mills starts after releasing more than 1700 kJ/kg of energy and the magnitude of differences maintain to increase as the stress energy intensify. After releasing 5230, 51300 and 15600 kJ/kg, respectively, in tumbling, vibratory and planetary mills the microstrain $< \varepsilon^2_{L=10nm} >^{1/2}$ exceeds 4.4×10^{-3}, 3.9×10^{-3} and 5.3×10^{-3}.
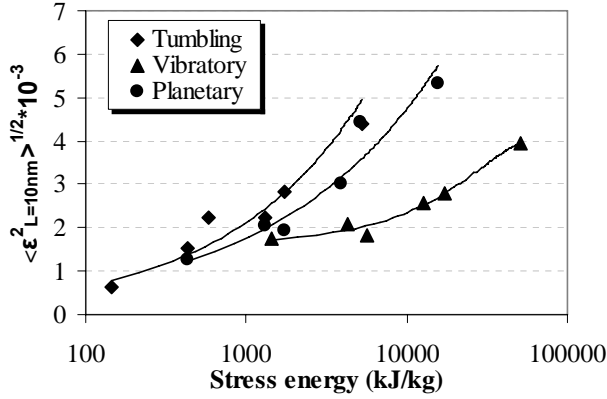
Fig. 20. *Variations of the lattice strain ($< \varepsilon^2_{L=10nm} >^{1/2}$) values in different grinding machines vs. stress energy.*

3.6. The comparison of input energy, stress energy and stored energy

A comparison of mills can be seen in Fig. 21 for our operation conditions. The different classification of mills can also be seen. Higher grinding energies are released in vibratory mill. The planetary mill is placed in the medium position and the ball mill (tumbling mill) at a low level of grinding energy input. Besides, only a small fraction of energy input affects the particles being ground. This relation is linear. The planetary mill needs more input energy than other mills to achieve an identical grinding energy (stress energy). Grinding in the vibratory mill need the smallest amount energy input to achieve the same stress energy as tumbling and/or vibratory mills. This is in relation to the capacity and scale of mills.
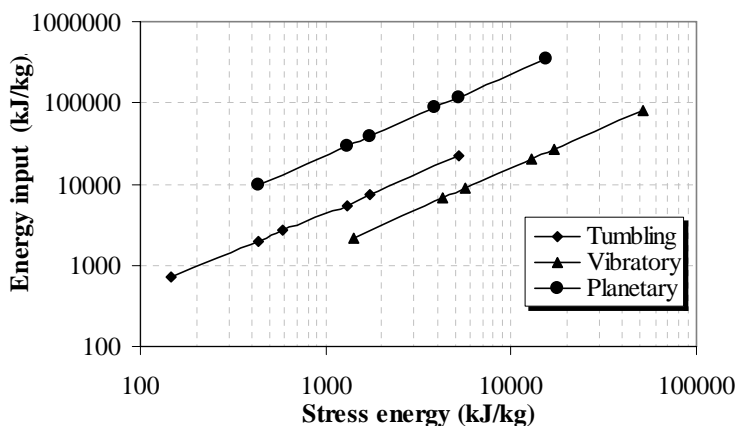
Fig. 21. *Stress energy vs. energy input in milling operation conditions.*

The stored energy (excess enthalpy) on basis of long lived defects and stress energy are compared in Fig. 22. An increasing trend between excess energy and stress energy can be observed, i.e., the higher specific energy, the more excess energy is stored in hematite. According to Fig. 22, a distinguished difference can be observed among mills. For a given stress energy level, the activated hematite in the tumbling mill contains the maximum excess enthalpy and in the vibratory mill has the minimum excess energy. For example, to achieve a excess energy in hematite by mechanical treatment about 60 kJ/mole, the required stress energies in tumbling, planetary and vibratory are around 1300, 2800, 17000 kJ/kg respectively. It should be reminded that the X-ray amorphization is the most important energy carrier during mechanical activation (about 93-98% of total stored energy).
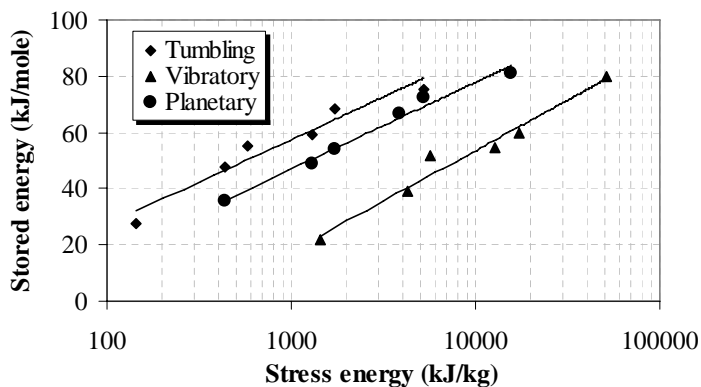
Fig. 22. *The comparison of stress energy and excess energy stored in activated hematite for different mills.*

Although theses considerations are based on a very simple model, they will be helpful for better understanding of the influence of different mills and operating parameters on grinding results and mechanical activation and induction of microstructure characters in hematite.

4. Conclusions

The results presented in this thesis show that the techniques developed and used in this study are well suited for the investigation of the influence of grinding parameters on the structure and properties of the milled material as well as on the milling energy values. The use of X-ray diffraction line broadening measurements has been proved to be useful in the analysis of the stress, degree of amorphization, defect structure and stored energy of milled material. Further detailed conclusions from the investigation of the influence of grinding variables on the activation of hematite are:

- The size reduction in the planetary mill is completed earlier than the other mills. Agglomerates during dry grinding are formed rapidly in planetary mill rather than the other mills, in particular for higher media surface.
- The vibratory mill produced larger specific surface area and smaller particles than other mills, in particular in the later stages of milling. The maximum surface area reached 18.4 m^2/g after 9 hours of milling with higher media surface in the vibratory mill. For a given grinding time and media surface level, tumbling mill produced the smallest specific surface area.
- As the milling time and media surface increase, the line broadening increases and integral intensity decreases. The lattice and unit cell volume of hematite expanded during mechanical activation.
- From the Williamson-Hall plots, it was understood that strain and size contributions exist simultaneously in the milled samples. The Williamson-Hall and Scherrer relations revealed the anisotropic character of line broadening. It was concluded that hematite lattice is 'soft' between the (024) and the others crystallographic directions.
- The use of higher media surface and prolonged grinding lead to higher specific surface area, X-ray amorphous material, physical broadening, microstrain, dislocation density, stored energy and smaller crystallites whatever milling types and methods are applied.
- The Warren-Averbach method revealed that planetary mill products have smaller crystallites and higher microstrain than the products of tumbling and vibratory mill with the exception for the samples activated for 1 hour with low media surface. The final products contain crystallites between 73.5 and 5.6 nm and the lattice strain (RMSS) at $L=10\ nm, <\varepsilon_{L=10nm}^2>^{1/2}$, varies from 0.06×10^{-3} up to 5.3×10^{-3} depending on the milling performance.
- The crystallite size and strain distribution for [012] direction suggested a homogeneous activation of hematite concentrate with main single crystallite group at high-intensive milling operation and non-homogeneous activation in low intensity milling accompanying at least two main crystallite groups.
- It is also verified that the amorphous material is the most important energy carrier in the activated material. The amorphous material contains between 93 and 98% of total stored energy (excess enthalpy).
- For a given stress energy, the vibratory mill brings about the lowest BET surface area, the minimum reduction of the XRD diffraction intensities and their broadening, the largest crystallites, the lowest lattice strain and the least defect concentration among the used mills.
- The activated hematite in the tumbling mill accounted for the highest levels of the excess energy and the product of vibratory mill gave the minimum excess energy for a identical stress energy. However, in the planetary mill much more input energy is needed to attain an identical stored energy value compared to the other mills.

5. Further research

- Further experiments and research are recommended to explore the effect of other grinding variables such as amplitude, mill diameter, mill speed, frequency, grinding media density, acceleration, grinding atmosphere, mode of grinding (wet and dry) and etc through an experimental design which provide some advantageous to the conventional methods.
- More investigations are necessary to conduct based on stress energy or a proper intensity definition in different mills to provide a way to compare different mills and different variables. The correlation and modeling with the first item provide a way to understand which variables explain grinding process and generation of microstructure characters.
- The Warren-Averbach methods are recommended for microstructure characterization with integral breadth method. However, the other characterization methods such as Double-Voigt method and in particular Rietveld analysis when different phases exist are promising and should be tested.
- In our opinion, the investigation of the effect of various defects formed during mechanical activation on the reactivity of the minerals are now only at the beginning of their development. Systematic investigations are recommended to explore what defects are formed under various types of mechanical action in the crystal of the substances of different types and how these defects influence reactivity.
- Reactivity tests based on desired applications for the activated hematite are necessary to find the influence of the mechanical activation and microstructure parameters refinement. In addition to the correlation between the reaction kinetics and microstructure characters, the influence of the individual microstructure parameters must be investigated.
- Statistical analyses are recommended to investigate the significance level and importance of the grinding variables and prediction of response variables by grinding variables.
- Systematic studies are recommended to investigate that whether achieving the same stress energy by varying other grinding variables like frequency, acceleration, speed and so on have similar influence on the structural changes or not.

References

Amer, A.M., 1995. Investigation of the direct hydrometallurgical processing of mechanically activated complex sulphide ore, Akarem area, Egypt. Hydrometallurgy 38, 225– 234.

Amer, A.M., 2000. Investigation of the direct hydrometallurgical processing of mechanically activated low-grade volframite concentrate. Hydrometallurgy 58, 251–259.

Amer, A.M., 2001. Kinetics of acid pressure leaching of mechanically activated cassiterite concentrate. Erzmetall 54, 446– 449.

Amer, A.M., 2002. Alkaline pressure leaching of mechanically activated Rosetta ilmenite concentrate. Hydrometallurgy 67, 125-133.

Austin, L.G., 1992. Some topics for research on fine grinding. In: Lecture in Harrogate Meeting IFPRI.

Aytekin, Y., 1981. Wet chemical extraction of metals from bulk concentrates of nonferrous ores. Aufbereitungs-Technik 22, 62– 71.

Balaz, P., 2000. Extractive Metallurgy of Activated minerals. Elsevier, Amesterdam

Balaz, P., 2003. Mechanical activation in hydrometallurgy. International Journal of Mineral Processing 72, 341-354

Balaz, P., Alacova, A., Achimovicova, M., Ficeriova, J., Godocikova, E., 2005. Mechanochemistry in hydrometallurgy of sulphide minerals. Hydrometallurgy 77, 9-17.

Balaz, P., Ficeriova, J., Boldizarovz, E., Haber, E., Jelen, S., Kammel, R., 2000. Thiosulphate leaching of gold from a mechanochemically pretreated complex sulphide concentrate. In: Massaci, P., (Ed.), Proc. of the XXI. Int. Miner. Proc. Congress Rome, Vol. A. Elsevier, Amsterdam, pp. A6-74–A6-81.

Balaz, P., Huhn, H.J., Tkacova, K., Heegn, H., 1988. Laugungsverhalten und physiko-chemische Eigenschaften von in unterschiedlichen mu¨hlen vorbehandelten chalkopyrit. Erzmetall 41, 325– 331.

Balaz, P., Stevulova, N., Kammel, R., Malmstrom, R., 1998. Extraction of Ni, Cu and Co from mechanically activated pentlandite concentrate. Metall 10–11, 620–623.

Balzar, D., 1999, Voigt-Function Model in Diffraction Line-Broadening Analysis, in *Defect and Microstructure Analysis from Diffraction*, edited by R.L. Snyder, H.J. Bunge, and J. Fiala, International Union of Crystallography Monographs on Crystallography No. 10 (Oxford University Press, New York, 1999), pp. 94-126.

Balzar, D., Ledbetter, H., 1993. Crystal Structure and Compressibility of 3:2 Mullite. *American Mineralogist* 78, 1192-1196.

Balzar, D., Ledbetter, H., 1995. Accurate Modeling of Size and Strain Broadening in the Rietveld Refinement: the "Double-Voigt" Approach. *Advances in X-ray Analysis* 38, 397-404.

Bid, S., Banerjee, A., Kumar, S., Pradhan, S. K., De, U., Banerjee, D., 2001. Nanophse iron oxides by ball-mill grinding and their Mössbauer characterization. Journal of Alloys and Compounds 326, 292-297.

Boldyrev, V.V., 1986. Mechanochemistry of inorganic solids. Proc. Indian natn. Sci. Acad. 52A, 400-417.

Boldyrev, V.V., Pavlov, S.V., Goldberg, E.L., 1996. Interrelation between fine grinding and mechanical activation. International Journal of Mineral Processing 44-45,181-185.

Daiger, K., Gerlach, J., 1982. On the kinetics of direct leaching of sulphide ores. Erzmetall 35, 609–611.

Daiger, K., Gerlach, J., 1983. U¨ ber den Katalytischen Effekt der Schwingmahlung auf die

Lo¨sungsgeschwindigkeit bei der direkten Laugung sulfidischer Erze des Kupferkiestypus. Erzmetall 36, 82–87.

Fernandez-Bertan, J., 1999. Mechanochemistry: an overview. Pure Applied chemistry 71, 4, 581-586.

Ficeriova, J., 2000. Possibilities of mechanical activation at intensification of non-cyanide leaching of gold bearing concentrate. PhD thesis, Institute of Geotechnics of Slovak Academy of Sciences, Kosice. In Slovak.

Ficeriova, J., Balaz, P., Boldizarova, E., Jelen, S., 2002. Thiosulphate leaching of gold from a mechanically activated Cu Pb Zn concentrate. Hydrometallurgy 67, 37–43.

Gerlach, J. K., Gock, E., Ghosh, S.H., 1973. Activation and leaching of chalcopyrite concentrates by diluted H2SO4 solutions. In: Evans, D.I., Schoemaker, R.S. (Eds.), Proc. 2nd Int. Symp. On Hydrometallurgy. Metall. Soc. AIME, Chicago, pp. 87–94.

Gerlach, J., 1982. Untersuchungen zur direkten Laugung komplexer sulfidischer Erze. Metall 36, 518– 523.

Gock, E., 1977. The Influence of Solid State Reactions in Vibratory Mill on leachability of Sulphidic Raw Materials. Habilitationsschrift, TU Berlin. In German.

Gock, E., Asiam, E., 1988. Gewinnung von Edelmetalen aus Kohlenstoffhaltigen Arsenopyritkonzentraten nach mechanischer Aktivierung. In: Tkacova K. (Ed.), Proc. Vth Int. Symp. ''Theoretical and theoretical Aspects of Comminution and Mechanical Activation''. Institute of Mining, Slovak Academy of Sciences, Kosice pp. 60– 65.

Gock, E., Jacob, K.-H., 1980. Direct dissolution of rutile with sulphuric acid. Erzmetall 33, 308– 314.

Godocıkova, E., 2001. Chloride leaching of mechanically activated complex CuPbZn concentrate. PhD thesis, Institute of Geotechnics of Sovak Academy of Sciences, Kosice. In Slovak.

Godocıkova, E., Balaz, P., Boldizarova, E., 2002b. Structural and temperature sensitivity of the chloride leaching of copper, lead and zinc from a mechanically activated complex sulphide. Hydrometallurgy 65, 83–93

Goldberg, E.L. and Pavlov, S.V., 1990. Conceptual grinding-activation model. In: Proceedings of Second World Congress Particle Technology, Society of Powder Technology, Kyoto, pp. 507–515.

Gutman, E.M., 1994, Mechanochemistry of Solid Surfaces. World Scientific, Singapore

Gutman, E.M., 1998. Mechanochemistry of Materials. Cambridge International Science Publishing, Cambridge

Halder, N.C., Wagner, C.N.J., 1966. Separation of particle size and lattice strain in integral breath measurements. Acta Crystallography 20, 312-313.

Heegn, H., 1979. Effect of fine grinding on structure and energy content of solids, in: Proc.of 6th POWRECH, Birmingham, pp. 61-69

Heegn, H., 1986. Concerning some fundamentals of fine grinding. In: Leschonski, K., Editor, 1986. *Proc. 1st World Congress on Particle Technology, Part II. Comminution*, Nürnberger Messe und Austellungsgesellschaft, Nürnberg, pp. 63–67.

Heegn, H., 1987. Model describing the resistance against structural changes and the hardness of crystalline solids. Crystal Research Technology 22, 9, 1193-1203

Heinicke, G., 1984. "Tribochemistry". Academie-Verlag, Berlin.

Holland, T.J.B., Redfern, S.A.T., 1997. Unit cell refinement from powder diffraction data: the use of regression diagnostics. Mineralogical Magazine 61: 65-77.

Huttig, G.F., 1943. Zwischenzutände bei Reaktionen in Festen Zustand und ihre Bedeutung fur die Katalyse. In: Handbuch der Katalyse IV, Springer Verlag, Wien, pp. 318-331

Juhasz, A.Z., 1974. Mechanochemical activation of silicate minerals by dry fine grinding. Aufbereitungs-Technik 10, 558-562

Juhasz, A. Z., & Opocki, L., 1990. Mechanical Activation of Minerals by Grinding, Pulverizing and Morphology of Particles. Ellis Horwood, London.

Kahler, J., Friedrich, I., Gock, E., 1996. Processing of molybdenite concentrate containing rhenium without exhaust gas generation. Erzmetall 49, 415– 425.

Kalinkin, A.m., Kalinkina, E.V., and Makarov, V.N., 2003. Mechanical activation of natural titanite and its influence on the mineral decomposition. International Journal of Mineral Processing 69, 143-155

Kammel, R., Pawlek, F., Simon, M., Li, X., 1987. Oxidizing leaching of sphalerite under atmospheric pressure. Metall 41,158– 161.

Karagedov, G.R., Lyakhov, N.Z., 2003. Mechanochemical grinding of inorganic oxides. Kona 21, 76-86.

Kitamura, M., Senna, M., 2001. Electrorelogical properties of mechanically activated gibbsite. Inorganic Materials 3, 563-567

Kusnierova, M., Sepelak, V., Briancin, J., 1993. Effects of biodegradation and mechanical activation on gold recovery by thiourea leaching. JOM, December, 54– 56.

Kuzeci, E., Li, X., Kammel, R., 1989. Untersuchungen zur sauren Laugung von sulfidischem Nickelkonzentrat. Metall 43, 434– 439.

Lin, I.J., 1998. Implications of fine grinding in mineral processing; mechanochemical approach. Journal of Thermal Analysis52, 453-361.

Lin, I.J., Nadiv, S., and Grodzian, J.M., 1975. Changes in the state of solids and mechanochemical reactions in prolonged comminution processes. Materials Science Engineering 7, 4.

Ljachov, N., 1994. Mechanical activation from the viewpoint of kinetic reaction mechanisms, in: Proc. Ist Int. Conf. On mechanochemistry "In CoMe 93" (Tkacova. K ed.), Vol.1, Kosice, 1993, Cambridge interscience publishing, Cambridge, 1994, pp.59-65.

Lucks, I., Lamparter, P., Mittemeijer, E.J., 2004. An evaluation of methods of diffraction-line broadening analysis applied to ball-milled molybdenum. Journal of Applied Crystallography 37, 300-311.

Maurice, D., Hawk, J.A., 1998. Ferric chloride leaching of a mechanically activated chalcopyrite. Hydrometallurgy 49, 103-124

Maurice, D., Hawk, J.A., 1999a. Ferric chloride leaching of a mechanically activated Pentlandite-chalcopyrite concentrate. Hydrometallurgy 52, 289-312.

Maurice, D., Hawk, J.A, 1999b. Simultaneous autogenousl grinding and ferric chloride leaching of chalcopyrite. Hydrometallurgy 51, 371-377.

Mccormick, P.G., and Froes, F.H., 1998. The fundamentals of mechanochemical processing. Wilson Applied Science and technology abstracts 50,11, pp-61-65

Mclean, D., 1965. Mechanical Properties of Metals. Metallurgia, Moscow.

Meyer, K., 1968. Physikalisch-chemische Kristallographie. VEB Deutscher Verlag Fur Grundstoffindustrie Leipzig, pp 302-320.

Mulak, W., Balaz, P., Chojnacka, M., 2002. Chemical and morphological changes of millerite by mechanical activation. International Journal of Mineral Processing 66, 233– 240.

Ostwald, W., 1891. Lehrbuch der Allgemeinen Chemie. Bd.2 Stöchiometrie (Engelmann, Leipzig, 1163.

Ostwald, W., 1919. Handbuch der Allgemeinen Chemie. Akademische Verlagsgesellschaft1, Leipzig.

Pawlek, F., 1976. The influence of grain size and mineralogical composition on the leachability of copper concentrates. In: Yannopoulos, J.C., Agarwall, J.C. (Eds.), Proc. Int. Symp. ''Extractive Metallurgy of Copper'', vol. II. Metall. Soc. AIME, Las Vegas,

pp. 690– 705.

Pawlek, F., Kheiri, M.J., Kammel, R., 1989. Optimierung der Feinstmahlung mit einer Ruˆhrwerkskugelmuˆhle gezeigt am Beispiel eines Zinkonzentrates. Metall 43, 838– 842.

Peters, K., 1962, Mechanochemische Reaktionen, in Proc. I. Europäischen Symp."Zerkleinern" (Rumpf. H, ed.) Weinheim, Frankfurt. p78-98

Puclin, T., Kaczmarek, W.A., Ninham, B.W., 1995. Mechanochemical processing of $ZrSiO_4$. Materials chemistry and Physics 40, 73-81

Sahu, P., De, M., Zdujic, M., 2003. Microstructural characterization of the evolved phases of ball-milled $\alpha - Fe_2O_3$ powder in air and oxygen atmosphere by Rietveld analysis. Material Chemistry and Physics 82, 864-876.

Schönert, K., 1990. Physical and technical aspects of very and micro fine grinding. In: Proceedings of Second World Congress Particle Technology, Society of Powder Technology, Kyoto, pp. 257–271.

Siemens AG, 1996a. Diffrac plus, profile Fitting Manual program

Siemens AG, 1996b. WIN-CRYSIZE 3, Crysttallite size and microstrain manual.

Steinike, U., and Hennig. H. P., 1992. Mechanically induced reactivity of solids, Kona 10, 15-23

Stewart, S.J., Borzi. R.A., Cabanillas, E.D., Punte, G., Mercader, R.C., 2003. Effects of milling-induced disorder on the lattice parameters and magnetic properties of hematite. Journal of Magnetism and Magnetic Material 260, 447-454.

Stokes, A.R., 1948. A numerical Fourier –analysis method for the correction of widths and shapes of lines on X-ray powder photographs. Proc. phys. Soc, London 61, 382-391.

Takacs, L., 2004. M.carey Lea, the first mechanochemist. Journal of Material Science 39, 4987-4993

Tkacova, K., 1989. Mechanical Activation of Minerals. Elsevier, Amesterdam

Tkacova, K., Balaz, P., Misura, B., Vigdergauz, V.E., Canturija. 1993. Selective leaching of zinc from mechanically activated complex Cu–Pb–Zn concentrate. Hydrometallurgy 33, 291– 300.

Tokumitsu, K., 1997. Reduction of metal oxides by mechanical alloying method. Solid State Ionics 101-103, 25-31

Tromans, D., Meech, J.A., 2001. Enhanced dissolution of minerals: stored energy, amorphism and mechanical activation. Mineral Engineering 14, 11, 1359-1377

Warren, B.E., 1969. X-ray diffraction. Addison-Wesley, New York

Welham, N.J., 1997a. The effect of extended milling on minerals. Canadian Institute of Metallurgy Bulletin 90, 64– 68.

Welham, N.J., 1997b. Enhancement of the dissolution of ilmenite (FeTiO3) by extended milling. Transactions of Institution of Mining and Metallurgy C106, 141– 144.

Welham, N.J., 2001a. Enhanced dissolution of tantalite/columbite following milling. International Journal of Mineral Processing 61,145-154

Welham, N.J., 2001b. Effect of extended grinding on the dissolution of a Ta/Nb concentrate. Canadian Metallurgical Quarterly 40, 143– 154.

Welham, N.J., 2001c. Mechanochemical processing of enargite (Cu_3AsS_4). Hydrometallurgy 62, 165-173.

Welham, N.J., 2001d. Mechanochemical processing of gold-bearing sulphides. Minerals Engineering 14, 341– 347.

Welham, N.J., 2001e. Enhanced dissolution of tantalite and columbite following milling. International Journal of Mineral Processing 61, 145– 154.

Welham, N.J., 2001f. Enhancing zircon (ZrSiO4) dissolution by ambient temperature

processing. Proceedings - Australasian Institute of Mining and Metallurgy 305, 1– 3.

Welham, N.J., 2003. Plenary lecture on mechanical activation at the 4th INCOME conference in Braunschweig, Germany.

Welham, N.J., Llewellyn, D.J., 1998. Mechanical enhancement of the dissolution of ilmenite. Mineral Engineering 11, No 9, 827-841

Williamson, G.K., Hall, W.H., 1953. X- ray line broadening from field aluminium and wolfram. Acta Metallurgy 1, 22-31.

Young, R.A., Wiles, D.B., 1982. Profile shape function in Rietveld refinements. Journal of Applied Crystallography 15, 430-438.

Zdujic, M., Jovalekic, C., Karanovic, L.J., Mitric, M., 1999. The ball milling induced transformation of $\alpha - Fe_2o_3$ powder in air and oxygen atmosphere. Material Science Engineering A 262, 204-213.

Zelikman, A.N., Voldman, G.M., Beljajevskaja, L.V., 1975. Theory of hydrometallurgical processes. Metallurgija, Moscow, In Russian.

Zhang, Q., Kasai, E., Saito, F., 1996. Mechanochemical changes in gypsum when dry ground with hydrated minerals. Powder Technology 87, 67-71.

Zhang, Q., Sugiyama, K., and Saito, F., 1997. Enhancement of acid extraction of magnesium and silicon from serpentine by mechanochemical treatment. Hydrometallurgy 45, 323-331.

Appended papers

Paper I

Microstructure Characterization of Mechanically Activated Hematite Using XRD Line Broadening

Parviz Pourghahramani and Eric Forssberg

Microstructure characterization of mechanically activated hematite using XRD line broadening

Parviz Pourghahramani *, Eric Forssberg

Division of Mineral Processing, Luleå University of Technology, Luleå, Sweden

Abstract

The effect of dry milling in a vibratory mill on the structural changes and microstructural characteristics of hematite using different methods was investigated. We have described the line profile analysis (LPA) to extract the size of coherently diffracting domains and the lattice strain of activated hematite in a vibratory mill. The Warren–Averbach and Williamson–Hall methods were used as the main tools for characterization. The changes in the particle size, surface area and new phase formation of hematite concentrate were also investigated. It was concluded that the breakage and agglomeration of particles take place mainly at lower and higher levels of specific energy input, respectively. The pores in agglomerates remain accessible for the nitrogen gas. Milling of hematite increased specific surface area up to 18.4 m^2/g. The hematite milled under various levels of specific energy input did not undergo a significant reaction or phase transformation during milling. The Williamson–Hall method confirms its merit for a rapid overview of the line broadening effects and possible understanding of the main causes. The anisotropic character of line broadening for deformed hematite as a function of specific energy input was revealed. Higher level of specific energy input favors the generation of small crystallite size, higher microstrain, BET surface area, amorphization and line breadth. The Warren–Averbach method suggested that the nanocrystalline hematite with grain sizes of 73.5–12.2 nm was formed by mechanical treatment using different milling intensities in the vibratory mill. The root mean square strain (RMSS) at $L = 10$ nm varies between 1.7×10^{-3} and 4.0×10^{-3} depending on the level of energy input. Limits in the applicability of Williamson–Hall method and reliability of the results are discussed in detail.
© 2006 Elsevier B.V. All rights reserved.

Keywords: microstructure; mechanical activation; grinding; line profile analysis; vibratory mill

1. Introduction

Mechanical activation (MA), a narrow field of the Mechanochemistry (MC) applied for the activation of chemical reaction by mechanical energy, has been used in mineral processing to produce finely ground particles, increased surface area and improved chemical reactivity of milled materials. The process involves prolonged grinding and is reported to cause a variety of processes to take place such as generation of a large new surface, formation of dislocations and point defects in the crystalline structure, phase transformations in polymorphic materials, chemical reactions, decomposition, ionic exchange, and oxidation and reduction reactions.

Mechanical activation increases the free energy of the particulate material systems by addition of both

* Corresponding author. Tel.: +46 920 491313; fax: +46 92097364.
  E-mail address: Parviz.Pourghahramani@ltu.se
  (P. Pourghahramani).

ARTICLE IN PRESS

2 *P. Pourghahramani, E. Forssberg / Int. J. Miner. Process. xx (2006) xxx–xxx*

surface free energy and volumetric elastic strain energy. Therefore, the ground material is activated and gained free energy can be relaxed through different modes of energy transitions (Lin, 1998). Decreasing the particle size during mechanical activation beyond its initial size leads to changes in relaxation from brittle fracture to ductile fracture. These changes are accompanied with rises in strain. As a result, the dislocation flows take place in the particles. Consequently, it leads to the growth of structure distortion. Those structural changes determine the reactivity (Boldyrev et al., 1996). With the development of research in mechanical activation of solids, it has been known that activation increases defect concentration and subsequently the reactivity of the solids (Balaz, 2000; Tkacova, 1989; Zoltan Juhasz, 1998). The characterization of structural changes is important in the course of mechanical activation.

Peak shape analysis, known as line profile analysis (LPA), is used to obtain information from the material structure. X-ray diffraction line profile analysis is an adopted technique, powerful tool and non-destructive method, to characterize the behavior of milled powder under various high-energy ball milling conditions. The X-ray diffraction patterns recorded from an activated material show broadening due to imperfections in the crystal structure. Structural line broadening is usually subdivided into crystallite size and microstrain broadening. Consequently, we can acquire information from microstrain, crystallite size and dislocation generated during intensive-milling condition. The X-ray line broadening analysis has been used widely to characterize the microstructure of materials. However, the use of this technique requires careful experimentation, sample preparation and calculation. Two basic methods of line profile analysis have been used: deconvolution and convolution methods (Balzar, 1999).

A number of attempts have been made to characterize the behavior of mechanically activated sulfide minerals. The influence of mechanical activation on the dissolution and leaching behavior of a large number of sulfide minerals and the principles of extracting of metals from sulfide minerals were studied; the whole process was described by Balaz (2000). Moreover, the chemical and morphological changes of millerite (Mulak et al., 2002) and leaching behavior of pentlandite–chalcopyrite concentrate (Maurice and Hawk, 1999) have been investigated. Extensive studies have been made on the structural changes of hematite especially on the polymorphic transformation of α-Fe_2O_3 to Fe_3O_4 and γ-F_2O_3 during mechanochemical treatment of α-Fe_2O_3. Kosmac and Courtney (1992) reported the transformation (reduction) of α-Fe_2O_3 to Fe_3O_4 and subsequently to FeO phase

Table 1
Experimental milling conditions

Parameter	Value
Media filling (%)	70
Milling time (h)	1 3 9
Ball to powder weight ratio	16.92 : 1, 67.68 : 1
Speed (RPM)	1000
Amplitude (mm)	8
Media apparent density (g/cm^3)	4.875
Amplitude (mm)	8
Temperature of material (°C)	48–105

either in argon or air atmosphere. The complete transformation of α-Fe_2O_3 to Fe_3O_4 by ball milling under vacuum or in argon atmosphere is possible; while in air the transformation is very slow or does not occur (Kaczmarek and Ninham, 1994). It was demonstrated that the transformation of α-Fe_2O_3 to Fe_3O_4 greatly depends on the manner in which milling was performed. Frequent opening of the mill door suppresses the transformation, while closing the door of the mill, the complete transformation of α-Fe_2O_3 to Fe_3O_4 takes place. The oxygen atmosphere delays the transformation process (Zdujic et al., 1998, 1999).

Most of the aforementioned treatments were made in planetary mills or in shaker mills such as SPEX mills on commercial hematite powder, wherein small amounts of commercial hematite powders in the order 10 g were examined. The goal of this work is to study the influence of milling operation conditions in terms of specific energy input on the structural changes of hematite concentrate with large powder weight (1959.4 and 490 g) and line broadening technique, which has not been studied yet. Quantitative and qualitative characterizations of the microstructural features of activated hematite as a function of specific energy input using integral breath methods and Fourier analysis are discussed in detail.

2. Experimental

The dry grinding tests were carried out in a vibratory ball mill with dimensions of $L320 \times \phi185$ mm. Steel balls with different sizes from 6 to 22.2 mm with total media surface of 1.9594 m^2 were used as grinding media. Milling experiments were made in air atmosphere under closed milling condition, i.e., the door of mill was kept closed during the milling process periods. The temperature was measured by a thermometer immediately after stopping the mill. The energy consumed by the mill was measured during grinding test by an electrical meter called a Micro VIP (Elcontrol Co. Italy).

ARTICLE IN PRESS

P. Pourghahramani, E. Forssberg / Int. J. Miner. Process. xx (2006) xxx–xxx

3

The samples were sealed into plastic tubes and kept in a freezer for further measurements. The grinding conditions are summarized in Table 1.

The particle size distribution of samples was measured by the laser diffraction method (CILAS 1064) in the liquid mode. From the laser diffraction measurements, the mean particle diameter and granulometric specific surface area were calculated. The specific surface area of the samples was determined by the BET method with the Flow Sorb II 2300 (Micromeretics Co. Ltd., USA), from which the equivalent particle diameter assuming spherical shape for particles was determined. The density of the starting material was calculated by using a Pycnometer (Micromeretics Co. Ltd., USA).

The X-ray diffraction (XRD) patterns were collected using a Siemens D5000 powder diffractometer with Bragg–Brentano geometry equipped with a curved graphite monochromator in diffracted beam arm and using Cu Kα radiation (Siemens, Germany). The XRD patterns of samples were recorded in the range $2\theta = 10$–$90°$ using a step size of $0.02°$ and a counting time of 5 s per step. Similarly, the X-ray diffraction pattern of the standard sample powder LaB$_6$, a standard proposed by the National Institute of Standards and Technology of USA, was obtained. The standard sample profile was used to remove the instrumental broadening effects from the observed profile broadening.

3. Materials

The chemical analysis showed that initial hematite powder contained about 97.91% Fe$_2$O$_3$, 0.73% Al$_2$O$_3$, 0.73% SiO$_2$, 0.26% TiO$_2$, 0.20% MgO, 0.022% MnO, and 0.088% P$_2$O$_5$. Other components such as K$_2$O, CaO and Na$_2$O comprise 0.051%. The X-ray diffraction analysis represented only the hematite diffraction lines. From the size analysis, the mean diameter and F_{80} of the starting powder were estimated around 23 and 80 μm, respectively. The BET measurements gave a specific surface area of 0.59 m^2 g^{-1}. The density of the starting material was calculated about 5240 kg/m^3.

4. Profile fitting procedure

In order to characterize the microstructure in terms of defect parameters such as crystallite (domain) sizes and microstrain, the parameters of line positions, intensities, widths, and shapes must be obtained from X-ray diffraction spectra. For this purpose, the Profile software (Siemens, 1996) was used. The $K_{\alpha 2}$ component was removed from the recorded XRD patterns with the assumption that $K_{\alpha 2}$ intensity is half of the $K_{\alpha 1}$ intensity.

The background was subtracted from the measured profiles. Each goodness factor was refined to a value of <5% for all used reflections of the studied samples.

For profile analysis, the eight most intensive reflection peaks (012), (104), (110), (113), (024), (116), (214) and (300) were selected. The overlapped peaks were carefully separated by using the Profile software. The profile fitting procedure was performed without smoothing of the XRD patterns to avoid introducing any bias in calculations. For each adjusted line profile, the following parameters were obtained:

(1) The maximum height of the peak (I_{max}).
(2) The integral breadth of line profile, ($\beta = A/I_{max}$, where A is the peak area).
(3) The full-width at half of maximum (FWHM).
(4) The mixing factor (η) of Lorentzian and Gaussian functions.
(5) The peak position (2θ).

5. Microstructure characterization (theoretical background)

Deviation from the ideal crystallinity such as finite crystallite size, strain (at the atomic level) and extended defects (stacking faults and dislocations) leads to broadening of the diffraction lines. Crystallite size is a measure of the size of coherently diffracting domains and is not generally the same as particle size due to polycrystalline aggregates. Strain is defined as change in length per unit length and is measured as the change in d spacing of a strained sample compared to the unstrained state.

According to Scherrer (1918), the apparent crystallite size can be obtained:

$$D_V = \frac{K\lambda}{\text{FWHM}}\cos\theta \qquad (1)$$

where K is a constant close to unity, θ is the Bragg angle of the (h k l) reflection and λ is wavelength of X-rays used. D_V is a volume-weighted quantity. Wilson (1963) used integral breadth β instead of FWHM in Eq. (1).

The dependence of strain ε to line broadening is defined as (Stokes and Wilson, 1944):

$$\varepsilon = \frac{\beta}{4}\cot\theta = \frac{\beta}{4\tan\theta}. \qquad (2)$$

When the XRD patterns are adjusted to a combination of Cauchy and Gaussian line shapes, the Halder and

Wagner (1966) approximation is better suited for obtaining the physical broadening:

$$\beta_f \cong (\beta_h^2 - \beta_g^2)/\beta_h \tag{3}$$

where terms β_g, β_h and β_f refer to the integral breadths of the instrumental, observed and measured (physical) profiles, respectively.

5.1. The Williamson–Hall integral breadth method

Williamson and Hall (1953) proposed a method for resolving size and strain broadening. Williamson–Hall plots can be applied to a Gaussian profile (Santra et al., 2002).

$$\beta_f^{*2} = \left(\frac{\beta_f \cos\theta}{\lambda}\right)^2 = \frac{1}{D_v^2} + 4\varepsilon^2 d^{*2} \tag{4}$$

A plot of β_f^{*2} against $4d^{*2}$ gives a straight line. From the intercept and slope of line crystallite size and strain can be calculated.

5.2. The Warren–Averbach Fourier method

According to Warren (1969), each diffraction domain is represented by columns of cells along the a_3 direction normal to the diffracting planes (00l):

$$L = n|a_3|, \qquad a_3 = \frac{\lambda}{2(\sin\theta_2 - \sin\theta_1)} \tag{5}$$

where n denotes the integer and a_3 is the unit of the Fourier length in the direction of the diffraction vector. The line profile is measured from θ_1 to θ_2.

It has been shown that the cosine Fourier coefficients A_L of the profile are the products of the size coefficients A_L^S and distortion coefficients A_L^D:

$$A_L = A_L^S \cdot A_L^D \Rightarrow \ln A_L = \ln A_L^S + \ln A_L^D \tag{6}$$

$$A_L^D = \exp(-2\pi L^2 d^* <\varepsilon_L^2>) \tag{7}$$

$$\begin{aligned}\ln A_L &= \ln A_L^S - 2\pi^2 L^2 d^{*2} <\varepsilon_L^2> \Rightarrow \ln A_L \\ &= \ln A_L^S - 2\pi^2 L^2 <\varepsilon_L^2>/d^2\end{aligned} \tag{8}$$

where $<\varepsilon_L^2>$ is the mean-squared strain for the correlation distance L and d is the interplanar spacing of the reflecting planes (Balzar, 1999; Santra et al., 2002). The separation of distortion and size coefficients can be made by preparing proper plots according to above-mentioned equations.

6. Results and discussions

6.1. Particle size and surface area

The BET specific surface area and granulometric surface area are compared in Fig. 1. The BET surface area increases during the grinding process. Higher levels of specific energy input favor the production of great surface area. The specific surface area increases up to 31 times after consuming the energy of 22 kWh/kg by the mill. The generation rate of surface area at lower level of energy input is larger than the higher level of energy input. This can be ascribed to the fact that the breakage rate at initial stages of comminution is great and continues to decrease with progress in milling. The granulometric surface area increases rapidly at earlier stages of milling and continues to decrease steadily when energy
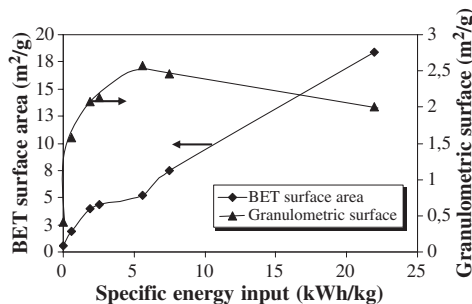

Fig. 1. Change in the BET specific surface area and granulometric surface area with specific energy input. Hereafter 0 kWh/kg refers to the initial sample.

ARTICLE IN PRESS

P. Pourghahramani, E. Forssberg / Int. J. Miner. Process. xx (2006) xxx–xxx 5

input exceeds 5.5 kWh/kg as opposed to the BET surface area. This addresses the agglomeration of the particles during extend dry grinding.

This is in agreement with observations of Tkacova (1989) for oxide minerals. A similar trend was observed for sulfide minerals (Balaz, 2000) with short grinding times. This addresses the influence of milling conditions and mineral type on the formation of agglomerates and beginning stage of agglomeration. In addition, the agglomeration of particles in most previous studies was manifested by a decrease in the BET surface area. As with hematite, it seems that the agglomerate pores remain accessible for the nitrogen gas.

From the BET measurements, the particle size was determined via surface area by using well known equation:

$$d_{av} = 6/\sigma S \qquad (9)$$

where d_{av} is the equivalent spherical particle diameter (μm), σ is the density (g/cm^3) and S is the specific surface area (m^2/g). Fig. 2 shows change in the BET particle size and mean diameter (d_{50}) of the particles in samples. The particles produced in intensive grinding are finer than of those obtained in the initial stages of milling. The mean BET particle size decreases as the specific energy input increases. The particle size decreased remarkably in the initial stage of milling after consuming the energy of 0.6 kWh/kg by the mill. By extending energy input in milling up to 5.5 kWh/kg, the particle size declines very slightly. A small increase in d_{50} (mean diameter) after intensive grinding is an indication of agglomeration which is inevitable in the finest grinding regime. For a given energy input, the mean particle size of hematite obtained from the laser diffraction method are larger than the sphere-equivalent diameter of those determined from the BET specific surface area. This also implies that pore agglomerates of primary particles are produced during intensive milling.

A comparison of particle size, BET surface area and granulometric surface indicates that the particle pores remain accessible in agglomerates and the nitrogen gas can penetrate the pore space of particles. As a result, the BET method determined higher specific surface area and yielded small particles in contradiction with the particle size measurements from the laser diffraction method. The agglomeration of particles during extended milling was reported for various minerals by Balaz (2000), Welham (2001), Welham and Llewellyn (1998), and Zhang et al. (1996). These results suggest that agglomeration phenomena may be a feature of extended dry milling.

6.2. X-ray diffraction

The starting sample and ground hematite are indexed in a hexagonal (trigonal) symmetry (R-3c space group). The X-ray patterns of the milled samples only show the Bragg reflections of hematite (Fig. 3), suggesting that the starting material did not undergo significant reactions during milling and after milling. The XRD method studies do not show phases below 2 wt.%. This agrees with the observations of Kaczmarek and Ninham (1994) and Stewart et al. (2003). However, our observations disagree with the findings of Kosmac and Courtney (1992) and Zdujic et al. (1998). They reported a transformation of α-Fe$_2$O$_3$ to Fe$_3$O$_4$ during ball milling in a planetary mill. In our opinion, the reason for this contradiction is the grinding condition and probably the source of starting material. Zdujic et al. (1998, 1999) made comprehensive studies to discuss the published results of the hematite transformation to Fe$_3$O$_4$ and subsequently to FeO. They stated that the transfer of sufficient energy to the particles is necessary to change the stability state of α-Fe$_2$O$_3$ to Fe$_3$O$_4$ and subsequently to FeO.

From the XRD patterns, it can be further observed that the resolution of $K_{\alpha 1}$ from $K_{\alpha 2}$ even at high Bragg angles vanished owing to structure symmetry reduction. With increased specific energy input, a continuous broadening of the diffraction peaks and decreased
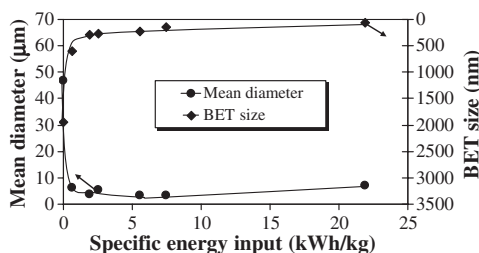
Fig. 2. Effect of specific energy input on the mean particle diameter (d_{50}) and BET particle size.

ARTICLE IN PRESS

6   P. Pourghahramani, E. Forssberg / Int. J. Miner. Process. xx (2006) xxx–xxx
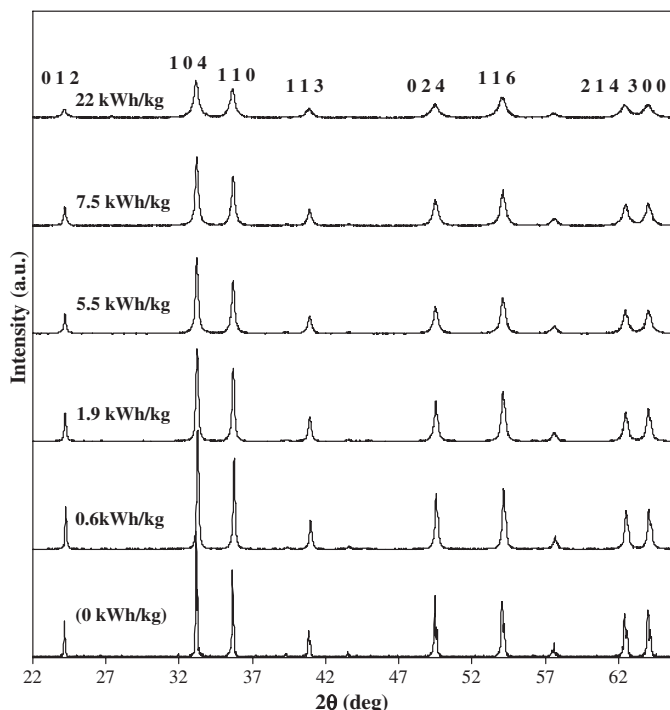
Fig. 3. XRD patterns of activated hematite as a function of specific energy input.

intensity of diffraction peaks were observed. These observations indicate an increase in the degree of lattice disorder and a decrease in the crystallite size; reducing the symmetry of the unit cell until some fraction of the material becomes amorphous. Comparing the XRD patterns indicates that the maximum line broadening and minimum reflection intensity were obtained from the hematite sample ground at a higher level of energy input.

The structural disorder due to increasing the abundance of X-ray amorphous material is manifested by decreases in the integral intensity of diffraction lines.

The factional amorphization is defined as (Ohlberg and Strickler, 1962):

$$A = 100 - X = 100 - \left(\frac{U_0}{I_0} \times \frac{I_x}{U_x} \times 100 \right) \qquad (10)$$

where U_0 and U_x refer to the background of non-activated sample and activated sample while I_0 and I_x are integral intensities of diffraction lines of non-activated sample and activated sample. A and X denote the degree of amorphization and the degree of crystallinity, respectively. The results are shown in Fig. 4. The X-ray
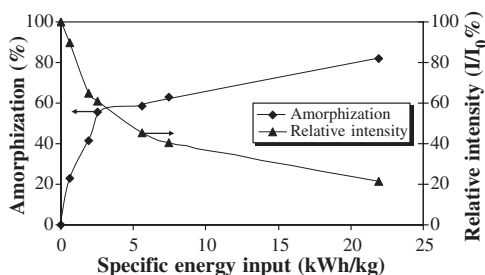
Fig. 4. Change in the X-ray amorphization degree and average relative intensity (I/I_0) of ground hematite with specific energy input.

ARTICLE IN PRESS

P. Pourghahramani, E. Forssberg / Int. J. Miner. Process. xx (2006) xxx–xxx   7

amorphization degree increased and the reflection intensity decreased rapidly in the earlier stages of milling. The amorphization degree reached almost 80% after consuming the energy of 22 kWh/kg energy by the mill. The curve trend indicates that the long-range ordering of hematite was lost rapidly at the early stages of grinding.

The changes in average integral breadth values $\bar{\beta}$ from the eight most intensive reflection peaks and for (014) reflection in terms of energy input are shown in Fig. 5. As grinding intensity increases, the line breadths increase for both (014) reflection and the eight most intensive reflection peaks, which is in agreement with the observations of Stewart et al. (2003). This suggests that all the hematite lattice faces are distorted.

The lattice parameters were refined in Hexagonal system by regression diagnostics method using Unitcell software (Holland and Redfern, 1997). The regression diagnostics are numbers, calculated during the regression, which supply valuable information on the influence of each observation the least squares result and on the estimated parameters. The initial hematite yields the value of lattice parameters ($a = 5.0312$ Å, $c = 13.7414$ Å and $V = 301.2291$ Å^3) displaying very slight variations to the values given in the mineralogy database (Mineral database, 2005) ($a = 5.0317$ Å, $c = 13.737$ Å and $V = 301.20$ Å^3). The changes in the lattice parameters a-parameter and c-parameter for samples were calculated and displayed in Fig. 6. Generally, we observed a unit cell expansion and an increase of the lattice parameters in comparison to the starting material. There are not any significant differences in the expansion of lattice parameters among the milled samples at different levels of energy input.

6.3. Microstructure characterizations

For microstructure characterization, two methods are applied: the integral breadth and Warren–Averbach methods. The results are discussed in the following paragraphs.

6.3.1. The integral breadth method

The integral breadths β_f of the physically broadened X-ray diffraction lines were separated into the two components (broadening resulting from small crystallite size and induced lattice strain) by the Williamson–Hall method. The Williamson–Hall plots for milled samples are illustrated in Fig. 7 according to Eq. (4). The plots for the first and second orders of the (012) reflection, [012] direction; and all intensive reflection peaks were made. The correlation coefficients for plots were between 0.90 and 0.96, indicating a strong relationship between β_f^{*2} and d^{*2}.

According to Fig. 7, there is no doubt that mechanical activation results in severe broadening of diffraction lines. A systematic deviation was observed relative to the line connecting the orders of (012) and (024) reflections, all data points lie below it. The differences between all reflections and direction [012] for lower level of energy input are negligible. The deviation increases as the milling intensity goes up. This could be due to difference of the elastic moduli of single crystal hematite existing between (024) and other crystallographic directions (Borner and Eckert, 1997; Vives et al., 2004). The scatter of β_f^{*2} values indicates that the crystallite shape differs from a spherical one. From Fig. 7, it can be observed that the physical broadening of the samples milled with higher grinding intensity is much larger than of the samples milled with less intensive milling. From the curves trend, it is apparent that strain increases with rising the specific energy input level and crystallite size decreases due to much higher impact and stress on the powder particles. Similar trends were observed for iron powder milled in a planetary ball mill with different disk speeds (Vives et al., 2004). Lucks et al. (2004) observed that the broadening of molybdenum
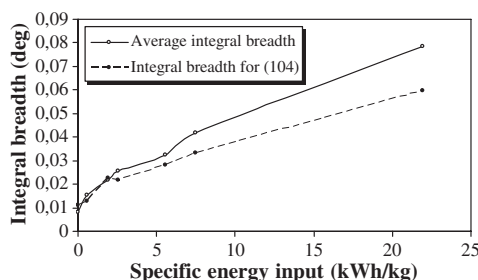
Fig. 5. Change in the physical integral breadth for reflection (104) and average physical integral breadth for the eight most intensive reflection peaks as a function of specific energy input.

ARTICLE IN PRESS

8   *P. Pourghahramani, E. Forssberg / Int. J. Miner. Process. xx (2006) xxx–xxx*
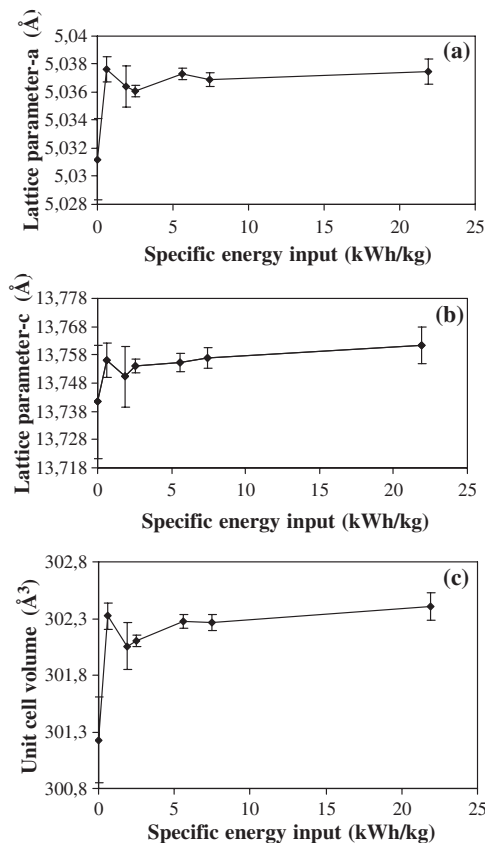
Fig. 6. Variation of lattice parameters of *a* (a), *c* (b) and unit cell volume (c) with specific energy input. The confidence level of measurements at 95% is included.

samples milled with an attritor mill is much larger than the broadening of samples milled with a planetary mill. The observed trend agrees with our observations with regard to the intensity of milling conditions. The production of material with specific microstructural

characteristics using the appropriate milling type and conditions seems promising. The Warren–Averbach method shows higher sensitivity in the calculation of crystallite size, i.e., a very small change in line slope causes dramatic changes in the values of the crystallite
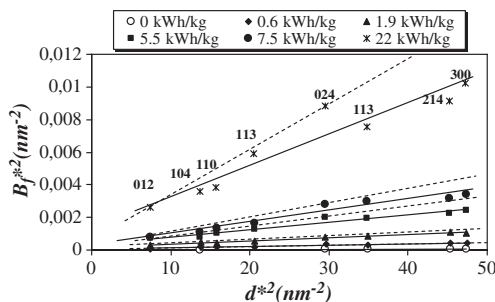
Fig. 7. Williamson–Hall plots for hematite samples milled with different specific energy input. Dashed and solid lines correspond to the first and second order of (012) reflections and to all reflection peaks, respectively.

ARTICLE IN PRESS

P. Pourghahramani, E. Forssberg / Int. J. Miner. Process. xx (2006) xxx–xxx 9
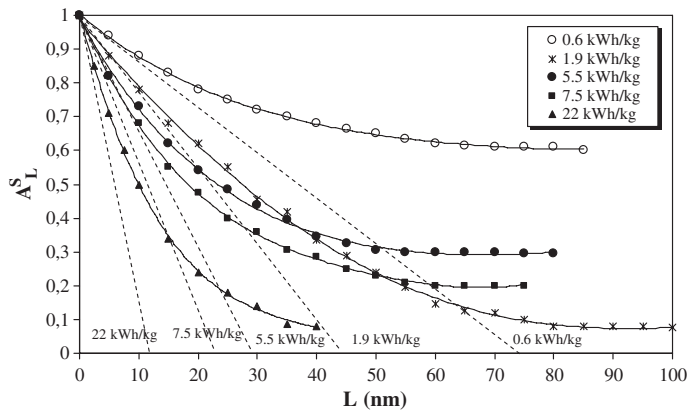
Fig. 8. Change of initial slope of A_L^S for samples milled with different specific energy input.

size. The strain and crystallite size values obtained from the slope and intercept of each straight line are compared with the results of other methods in Section 6.3.3.

6.3.2. The Warren–Averbach analysis

Since the milled samples represented the anisotropy behavior in broadening (according to the Williamson–Hall plot), the precise extraction of the crystallite size and strain for particular direction using the Warren–Averbach analysis is possible. The Warren–Averbach analysis was applied for [012] direction and the results are discussed in the following paragraphs.

6.3.2.1. Crystallite size and strain results.
We calculated the A_L^S coefficients as a function of Fourier length

for line profile of milled samples in different levels of specific energy input (Fig. 8). The A_L^S levels off with increasing L whatever specific energy input was applied. From the intercept of the initial slope on the L-axis (dashed line), the surface weighted crystallite size values were extracted. The use of intensive grinding produces small crystallites. This may be related to intensive line defects, which disrupt the particles and consequently result in small crystallites.

The Warren–Averbach analysis also provides the distribution of RMSS (root mean square strain) as a function of Fourier length. A typical plot of $<\varepsilon_L^2>$ as a function of L shows a monotonically decreasing curve for increasing L values as shown in Fig. 9. It is obvious that intensive milling leads to higher microstrain in particular at small L. A hematite sample, however,
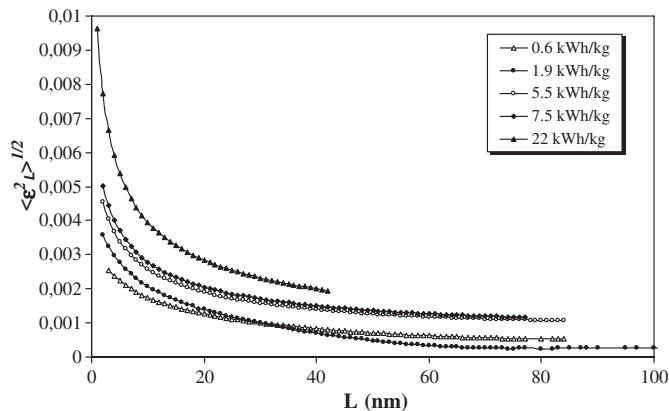
Fig. 9. The RMSS strain obtained using Warren–Averbach method for milled samples with various specific energy input.

ARTICLE IN PRESS

10   P. Pourghahramani, E. Forssberg / Int. J. Miner. Process. xx (2006) xxx–xxx
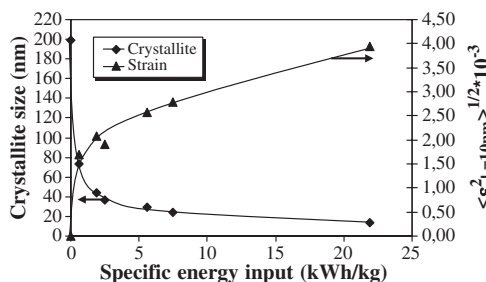
Fig. 10. Variation of surface weighted crystallite size and root mean square strain (RMSS) with specific energy input. The RMSS strain for initial sample assumed to be negligible. The crystallite size for the initial sample is calculated using single peak method.

milled with the specific energy input of 1.9 kWh/kg shows smaller microstrain in higher column length and A_L^S in comparison to that of hematite ground with 0.6 kWh/kg. This may be related to uncertainties in background estimation due to overlapping peaks (measurement accuracy) and/or non-uniform activation. Some uncertainty always exist in all the methods, inasmuch as the task is to determine the tails, which are either hidden or marked by an adjacent overlapping profile or distorted by a non-level background. This may occur when the sample contains an amorphous fraction that can give broad bumps in diffraction pattern which extend over several Bragg reflections. The $<\varepsilon_L^2>^{1/2}$ plot as a function of the L contains more information than a single value at an arbitrary L value. The degree of disorder in samples from the observed trend in $<\varepsilon_L^2>^{1/2}$ versus L plot can be indicated. The lattice disorder can be attributed to the crystalline distortions. This arises from the fluctuations in the interplanar distances and presence of the dislocations in samples which result in a Gaussian distribution of the microstrain (Dong Lin and Gong Duh, 1997).

The normally quoted values for strains are the local values, i.e., at $L=0$. However, the microstrain at $L=0$, $<\varepsilon^2>_{L=0}^{1/2}$ can not be directly determined by using the Warren–Averbach method. The experimental A_L^D functions are often affected by errors, in particular due to the truncation in the Fourier transformation of the diffraction lines (Lucks et al., 2004). Thus, we decided to calculate the strain at $L=10$ nm. The crystallite size and lattice strain are displayed in Fig. 10. The microstrain, $<\varepsilon_L^2>^{1/2}$ at $L=10$ nm increases up to 4.0×10^{-3} after consuming the energy of 22 kWh/kg by the mill. The results regarding the strain and crystallite size are in line with observations of Bid et al. (2001) and Sahu et al. (2003); however, our results regarding crystallite sizes and strains in direction [012] are larger and smaller, respectively, than their observations. This can be related

to the initial material characteristics and milling conditions. Bide et al. and Sahu et al. used planetary mills with high angular velocity. This implies that the ability of energy transfer in a vibratory mill, at least in our grinding conditions, is not as high as when using a planetary mill.

6.3.2.2. The crystallite size distribution characteristics. Another advantage in using the Warren–Averbach method rather than any other method to calculate microstructural characteristics is its ability to give information on the distribution of crystallite size (column length). It is known that the relationship between D_V and D_S depends on the distribution of crystallite size. The differences between D_V and D_S increase as the distribution of crystallite size becomes broader.

The crystallite size (column length) distribution characteristics are summarized in Table 2. At the first glance, the maximum relative frequency for ground samples appears at small L and the maximum relative frequency of column length increases as the intensity of milling grows except the ground sample with 1.9 kWh/kg specific energy input. The investigation of the left and right width values (Lfwhm and Rwhm) corresponding to column length distribution indicates that the distribution functions also follow the lognormal distribution form. The lognormal probability distribution of crystallite size during intensive milling conditions was reported by several authors for different materials: zirconia powders (Dong Lin and Gong Duh, 1997), α-Al_2O_3 prepared by combustion technique (Santra et al., 2002), ball-milled molybdenum (Lucks et al., 2004) and milled iron powders (Vives et al., 2004).

Grinding up to 1.9 kWh/kg energy input resulted in two maxima, suggesting two main crystallite size groups exist in the milled samples. This could be related to the fact that the powder distribution around grinding media affected the energy and stress transferring quantity to the particles being ground due to existing coarser particles.

ARTICLE IN PRESS

P. Pourghahramani, E. Forssberg / Int. J. Miner. Process. xx (2006) xxx–xxx

11

Table 2
Maximum of relative frequency (R.F) of column length and size distribution widths of crystallite size resulting from the Warren–Averbach approach in direction [012]

Specific energy input (kWh/kg)	*L* (nm)	R.F (%)	Lfwhm (nm)	Rfwhm (nm)	fwhm (nm)
0.6	11.4 (65)	2.1 (1.4)	9.6	22.3	31.9
1.9	42.5 (9)	1.7 (1.3)	41.0	25.5	66.5
2.5	10.1	2.6	8.6	19.2	27.8
5.5	7.3	3.1	6.3	16.3	22.6
7.5	6.2	4.0	5.3	13.5	18.8
22	3.7	6.8	3.2	8.7	11.9

Terms Lfwhm, Rfwhm and fwhm correspond to the width of crystallite length distribution at left and right, respectively. Term fwhm is the overall widths of distributions. The values in parentheses denote the second maxima.

With less intensity of grinding, the coarse particles prevent the media from coming into contact with finer particles. Fragmentation of the coarsest particles results in the establishment of a uniform contact between the grinding media and particles being ground. Having this in mind, the existence of two main crystallite size groups can be either attributed to the new phase formation and/or changes of the materials being ground. However, in our investigation we did not observe any phase transformation or new phase formation according to the XRD patterns. In our opinion, less intensive stressing of powders resulted in a wide range crystallite sizes. According to Table 2, as the intensity of milling increases, the widths of crystallite size distributions (fwhm) decline except the sample ground with 1.9 kWh/kg of energy input. As it is expected, the column length distribution becomes sharper, when hematite is subjected to severe

grinding; therefore, we can conclude that the intensive grinding brings about the homogeneous activation of hematite.

6.3.3. The comparison of results

In order to make a rapid comparison, we used Scherrer equation with a first approximation to calculate the crystallite size and strain values. This also confirmed the extremely anisotropic character of crystallite size and strain, i.e., each reflection peaks yielded different crystallite size and strain values. We compared the average values obtained from Scherrer equation using the eight most intensive reflections (with integral breadth), Williamson–Hall by taking all the diffractions and Warren–Averbach method for the [012] direction in Fig. 11 as a function of specific energy input. The crystallite sizes decrease and strain values increase
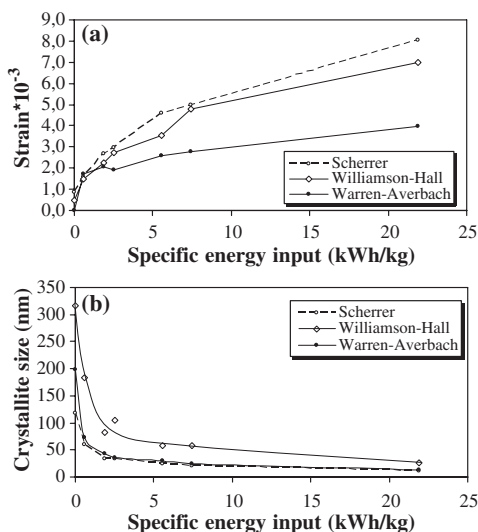

Fig. 11. Variation of crystallite size and strain obtained using different methods with specific energy input.

ARTICLE IN PRESS

12   *P. Pourghahramani, E. Forssberg / Int. J. Miner. Process. xx (2006) xxx–xxx*

drastically as the specific energy input grows. Among all of the methods, the Scherrer equation gives the smallest crystallites and the highest values of the strain. The largest crystallites and lowest strain were obtained using Williamson–Hall and Warren–Averbach methods for $L = 10$ nm, respectively.

The quantitative analysis of size and strain without considering the underlying assumptions is impossible. The Scherrer equation only addresses the line broadening that is entirely caused by size effect or strain effect. This is not valid in case of mechanical activation. The broadening is subdivided into the two components by Williamson–Hall plots and Warren–Averbach method. It should be noted that the Warren–Averbach method does not necessarily assume a gauss strain distribution or that mean square strain is independent of distance L. However, the Warren–Averbach analysis becomes exact in the case of the Gaussian distribution of ε_L for each L. The strain value ε obtained from the Williamson–Hall plots expresses only the maximum value for the strain (Balzar, 1999). In the case of pure-gauss strain broadening, the RMSS is independent of L and the relationship between $<\varepsilon_L^2>^{1/2}$ and ε, strain resulting from integral method, is given by Balzar (1999), Halder and Wagner (1966), and Keijser et al. (1983) follows as:

$$<\varepsilon_0^2>^{1/2} = <\varepsilon_{L=0}^2>^{1/2} = (2/\pi)^{1/2}\varepsilon \qquad (11)$$

However, there is no clear connection between RMSS and ε; if the strain broadened contains a Cauchy component. A rough estimate was given by Balzar (1999) when the Gauss and Cauchy extremes of the strain broadened Voigt profile exist:

$$0.5 \leq \varepsilon/<\varepsilon_L^2>^{1/2} \leq 2. \qquad (12)$$

If D_V and D_S denote the volume weighted parameter and the surface weighted value, respectively, the relationship between D_V and D_S has been given by Balzar (1999) and Lucks et al. (2004):

$$1.31 \leq \frac{D_V}{D_S} \leq 2 \quad \text{for a Voigt size–broadened profile} \qquad (13)$$

$$\frac{D_V}{D_S} \geq r \quad \text{otherwise (Alternative methods)} \qquad (14)$$

r ranges typically between 1 and 3.

Our findings regarding the strain resulting from the integral breadth are in good agreement with the Warren–Averbach analysis. The crystallite size values obtained from the integral breadths, however, represent a rough correspondence to those obtained from the Warren–Averbach analysis, indicating the sensitivity of crystallite size rather than strain due to Pseudo–Voigt line shape fitting. The obtained results are in line with Santra's (2002) observation. Scardi et al. (2004) stated that the reliability of results in integral breadth methods vanishes for some reasons. For example, the crystallites> in polycrystalline material have different sizes and shapes and these affect the width and shapes of all diffraction line profiles. The size distribution and shape for simple polyhedra can be decoupled in principle; but this separation is impossible using the integral breadths. Besides, the line profiles produced by dispersed small crystallites (e.g., according to a Lognormal or Gamma distributions) are non-Voigtian and Eq. (4) is not appropriate. Thus, the integral breadth methods are utilized best when trying to identify trends in the change of microstructure by comparing samples belonging to a series of experiments.

7. Conclusions

The following conclusions based on the experimental results presented in the article can be made:

1. The agglomeration of particles during mechanical activation occurs after consuming the energy of 5.5 kWh/kg by the mill and the agglomerate pores are accessible for the nitrogen gas. Milling of hematite increased surface area up to 18.4 m^2/g after energy consumption of 22 kWh/kg.
2. As the specific energy input increased, the line broadening increases and integral intensity decreased. The lattice parameters and unit cell volume of hematite expanded during mechanical activation. The activated hematite did not undergo significant chemical reaction.
3. The Williamson–Hall plots suggested that strain and size contributions in line broadening exist simultaneously in the milled samples and anisotropic character of line broadening is revealed in products. It was pointed out that the hematite lattice is 'soft' between the (024) and the other crystallographic directions.
4. All the methods display the same trend, rapid decrease of the coherently diffracting domain size and increase of the strain state. Williamson–Hall and Scherrer relations have to be employed only in the

ARTICLE IN PRESS

P. Pourghahramani, E. Forssberg / Int. J. Miner. Process. xx (2006) xxx–xxx 13

first qualitative approximation, more accurate results are obtained using the Warren–Averbach method in direction [012].

5. From the Warren–Averbach method the crystallite sizes were estimated between 73.5 and 12.2 nm depending on the intensity of grinding. The root mean square strain (RMSS) for activated samples exceeds 4.0×10^{-3} for the maximum intensity of grinding. Finally, intensive grinding brings about homogeneous activation of hematite.

Nomenclature

A	Peak area
A_L	Fourier coefficients
A_L^D	Distortion components in the Fourier coefficient
A_L^S	The size components in the Fourier coefficient
a_3	The unit of the Fourier length in direction of the diffraction vector
b	Burgers vector
D_S	Surface-weighted crystallite size
D_V	Volume-weighted crystallite size
d	Interplanar spacing
d_{av}	The equivalent spherical particle diameter
FWHM	Full width at half-maximum of profile
$(h\,k\,l)$	Miller indices
I	Intensity
K	Scherrer constant
L	na_3, column length (distance between two cells in a real space) orthogonal to diffracting planes
RMSS	Root mean square strain
S	Specific surface area
$d*$	$2\sin\theta/\lambda = /d = d*$, variable in the reciprocal space
β	Integral breadth
β_f	The integral breadth of the physically broadened profile
β_g	The integral breadth of the instrumentally broadened profile
β_h	The integral breadth of the observed broadened profile
$\beta*$	$\beta\cos\theta/\lambda$, integral breadth in the units of $d*$ (nm^{-1})
$<\varepsilon_L^2>$	Mean square strain, orthogonal to diffracting planes, averaged over the distance L
ε	Apparent strain
η	Mixing factor of a Pseudo-Voigt function
θ	Bragg angle
λ	X ray wavelength
σ	Density
LPA	Line profile analysis
XRD	X ray diffraction
Å	Angstrom unit (10^{-11} m)

References

Balaz, P., 2000. Extractive Metallurgy of Activated Minerals. Elsevier, Amesterdam.

Balzar, D., 1999. Voigt-function model in diffraction line-broadening analysis. In: Snyder, R.L., H.J. (Eds.), Defect and Microstructure Analysis from Diffraction, pp. 94–126.

Bid, S., Banerjee, A., Kumar, S., Pradhan, S.K., De, U., Banerjee, D., 2001. Nanophase iron oxides by ball-mill grinding and their Mössbauer characterization. J. Alloys Compd. 326, 292–297.

Boldyrev, V.V., Pavlov, S.V., Goldberg, E.L., 1996. Interrelation between fine grinding and mechanical activation. Int. J. Miner. Process. 44–45, 181–185.

Borner, I., Eckert, J., 1997. Nanostructure formation and steady-state grain size of ball-milled iron powders. Mater. Sci. Eng., A Struct. Mater.: Prop. Microstruct. Process. 226–228, 541–545.

Dong Lin, J., Gong Duh, J., 1997. The use of X-ray line profile analysis to investigate crystallite size and microstrain for zircon powders. J. Mater. Sci. 32, 5779–5790.

Halder, N.C., Wagner, C.N.J., 1966. Separation of particle size and lattice strain in integral breadth measurements. Acta Crystallogr. 20, 312–313.

Holland, T.J.B., Redfern, S.A.T., 1997. Unit cell refinement from powder diffraction data; the use of regression diagnostics. Mineral. Mag. 61, 65–77.

Kaczmarek, W.A., Ninham, B.W., 1994. Preparation of Fe_3O_4 and γ-Fe_2O_3 powders by magnetomechanical activation of hematite. IEEE Trans. Magn. 30 (2), 732–734.

Keijser, TH., DE, H., Mittemeijer, E.J., Rozendaal, C.F., 1983. The determination of crystallite-size and lattice-strain parameters in conjunction with the profile-refinement method for determination of crystal structures. J. Appl. Crystallogr. 16, 309–316.

Kosmac, T., Courtney, T.H., 1992. Milling and mechanical alloying of inorganic nonmetallics. J. Mater. Res. 7 (6), 1519–1525.

Lin, J.I., 1998. Implications of fine grinding in mineral processing; mechanochemical approach. J. Therm. Anal. Calorim. 52, 453–461.

Lucks, I., Lamparter, P., Mittemeijer, E.J., 2004. An evaluation of methods of diffraction-line broadening analysis applied to ball-milled molybdenum. J. Appl. Crystallogr. 37, 300–311.

Maurice, D., Hawk, J.A., 1999. Ferric chloride leaching of a mechanically activated Pentlandite–Chalcopyrite concentrate. Hydrometallurgy 52, 289–312.

Mineral database, 2005. http://webmineral.com/data/hematite.shtml.

Mulak, W., Balaz, P., Chojnacka, M., 2002. Chemical and morphological changes of millerite by mechanical activation. Int. J. Miner. Process. 66, 233–240.

Ohlberg, S.M., Strickler, D.W., 1962. Determination of percent crystallinity of partly devitrified glass by X-ray diffraction. J. Am. Ceram. Soc. 45, 170–171.

Sahu, P., De, M., Zdujic, M., 2003. Microstructural characterization of the evolved phases of ball-milled α-Fe_2O_3 powder in air and oxygen atmosphere by Rietveld analysis. Mater. Chem. Phys. 82, 864–876.

Santra, K., Chatterjee, P., Sen Gupta, S.P., 2002. Voigt modeling of size–strain analysis: application to α-Al_2O_3 prepared by combustion technique. Bull. Mater. Sci. 25 (3), 251–257.

ARTICLE IN PRESS

14 *P. Pourghahramani, E. Forssberg / Int. J. Miner. Process. xx (2006) xxx–xxx*

Scardi, P., Leoni, M., Delhez, R., 2004. Line broadening analysis using integral breadth methods: a critical review. J. Appl. Crystallogr. 37, 381–390.

Scherrer, P., 1918. Bestimmung der Grösse und der inneren Structure von Kollooidteilchen mittels Röntgenstrahlung. Nachr. Ges. Wiss. Gött. 2, 98–100.

Siemens, A.G., 1996. Diffrac Plus Profile Fitting Manual Program. 1-1-5-26.

Stewart, S.J., Borzi, R.A., Cabanillas, E.D., Punte, G., Mercader, R.C., 2003. Effects of milling-induced disorder on the lattice parameters and magnetic properties of hematite. J. Magn. Magn. Mater. 260, 447–454.

Stokes, A.R., Wilson, A.J.C., 1944. The diffraction of X-rays by distorted crystal aggregates — I. Proc. Phys. Soc. Lond. 56, 174.

Tkacova, K., 1989. Mechanical Activation of Minerals. Elsevier, Amesterdam.

Vives, S., Gaffet, E., Meunier, C., 2004. X-ray diffraction line profile analysis of Iron ball milled powders. Mater. Sci. Eng., A Struct. Mater.: Prop. Microstruct. Process. 366, 229–238.

Warren, B.E., 1969. X-Ray Diffraction. Addison-Wesley, New York.

Welham, N.J., 2001. Enhanced dissolution of tantalite/columbite following milling. Int. J. Miner. Process. 61, 145–154.

Welham, N.J., Llewellyn, D.J., 1998. Mechanical enhancement of the dissolution of ilmenite. Miner. Eng. 11 (9), 827–841.

Williamson, G.K., Hall, W.H., 1953. X-ray line broadening from field aluminum and wolfram. Acta Metall. 1, 22–31.

Wilson, A.J.C., 1963. Mathematical Theory of X-Ray Powder Diffractometry. Philips Technical Library, Centrex publishing company, Eindhoven, Netherland, pp. 21–53.

Zdujic, M., Jovalekic, C., Karanovic, L.J., Mitric, M., Poleti, D., Skala, D., 1998. Mechanochemical treatment of α-Fe_2O_3 powder in air and atmosphere. Mater. Sci. Eng., A Struct. Mater.: Prop. Microstruct. Process. 245, 109–117.

Zdujic, M., Jovalekic, C., Karanovic, L.J., Mitric, M., 1999. The ball milling induced transformation of α-Fe_2O_3 powder in air and oxygen atmosphere. Mater. Sci. Eng., A Struct. Mater.: Prop. Microstruct. Process. 262, 204–213.

Zhang, Q., Kasai, E., Saito, F., 1996. Mechanochemical changes in gypsum when dry ground with hydrated minerals. Powder Technol. 87, 67–71.

Zoltan Juhasz, A., 1998. Aspects of mechanochemical activation in terms of comminution theory. Colloids Surf., A Physicochem. Eng. Asp. 141, 449–462.

Paper II

Comparative Study of Microstructural Characteristics and Stored Energy of Mechanically Activated Hematite in Different Grinding Environments

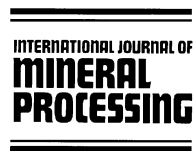**Parviz Pourghahramani and Eric Forssberg**

Comparative study of microstructural characteristics and stored energy of mechanically activated hematite in different grinding environments

Parviz Pourghahramani *, Eric Forssberg

Division of Mineral Processing, Luleå University of Technology, Luleå, Sweden

Abstract

Hematite concentrate was mechanically treated using different milling machines and experimental conditions in air atmosphere. The changes in phase constitution, particles size, specific surface area, lattice parameters and X-ray amorphous phase fraction of activated hematite were determined. It was found that the agglomeration of the particles take place during extended milling with accessible pores for Nitrogen gas. The higher media surface brought about the largest specific surface area whatever milling devices used. After 9 h of grinding with higher media surface, the maximum and minimum specific surface area resulted from the grinding in the tumbling and vibratory mills, accounting for 6.83 m^2/g and 18.42 m^2/g, respectively. For the same grinding condition, tumbling mill produced the lowest X-ray amorphous phase. The maximum X-ray amorphous material estimated around 85% from the grinding in the planetary mill with higher media surface for 9 h of milling.

Structural changes were followed by XRD line broadening analysis (LPA) using the integral breadth method and Warren–Averbach approach. From the Williamson–Hall plots, it was understood that strain and size contributions exist simultaneously in the milled samples. Besides, the physical broadening increases as milling time and media surface increase regardless of milling types. Besides, it was found that hematite crystal is 'soft' between (024) and other crystallographic directions.

From the Warren–Averbach approach, it was observed that the higher grinding media surface and prolonged milling favor the generation of small crystallite, higher microstrain, limited crystallite length and subsequently uniform activation of hematite. After 9 h of milling with higher media surface in tumbling, vibratory and planetary mills, the surface weighted crystallite size reached 17.3, 12.2 and 5.6 nm respectively. The maximum lattice strain, $<\varepsilon_{L=10\ nm}^2>^{1/2}$, in the grinding with tumbling, vibratory and planetary mills was found about 4.44×10^{-3}, 3.95×10^{-3} and 5.23×10^{-3}, respectively. The maximum dislocation density accounted for 46.3×10^{14} m/m^3 in the planetary milling with higher media surface after 9 h of milling. The evaluation of energy contributions of structural defects suggested that the energy contribution of the amorphization was dominant and amounted to 92–98% of the overall stored energy in hematite, depending on milling conditions. Finally, for a given stress energy, the products of tumbling mill represent higher reactivity potential.
© 2006 Elsevier B.V. All rights reserved.

Keywords: grinding methods; mechanical activation; line broadening analysis; microstructure; structural changes

1. Introduction

The applications of treatment of minerals in milling devices are numerous and can roughly be divided into

three categories: coarse grinding, fine grinding and mechanical activation. The most important goal in coarse grinding is size reduction. In contrast, the objective of mechanical activation is the changes in the structure, tension state and chemical composition and reactivity (Zoltan Juhasz, 1998), although the size reduction takes place primarily by mechanical activation. The fine grinding limit is determined by ductile–brittle transition state (Boldyrev et al., 1996). The direct correlation between size reduction and milling intensity becomes absolutely unreliable and invalid in the case of mechanical activation (Karagedov and Lyakhov, 2003).

The active mechanical energy is partially transferred to the particles, e.g. by the impact of solid particles or by induction of tensile and compressive forces in powder mass. The influence of mechanical energy on solids includes a multitude of elementary physicochemical micro- and macro-processes. The mechanical energy leads to changes of the material structure, to the occurrence of structural defects such as changes of the surface, lattice distortion and conversion of long range order to short range order. Therefore, the free energy or chemical potential gained and the composition can change during the mechanical activation. In this way, the solid systems reach an activated state (Balaz, 2000; Tkacova, 1989).

The activation ability of milling equipment is controlled by the frequency of impacts and the modes of stress influence the nature of structural changes. Generally, it has been established that with shear and pressure stresses structural changes are concentrated at regions near the surface and decrease with increasing distance from the surface. With impact stresses the size of the primary crystallite become smaller in the whole volume and the disturbances start at the corners and borders (Tkacova et al., 1993). Based on a geometrical model for defect distribution, mills were divided into two groups of jet mill and disintegrator and mills with loose media by Bernhardt and Heegn (1978). It was concluded that in the former group, the mechanical energy imparted to individual particles during impact. In contrast, in mills with loose media, the particles are stressed in a material bed.

The influence of the density of milling media on mechanical activation of inorganic oxides was investigated by Karagedov and Lyakhov (2003). Dry grinding was found to be more effective than wet milling in the dissolution of Tantalite despite the generation of large specific surface in wet milling (Welham, 2001). It was reported that the crystallite size decreased exponentially and the strain increased with increasing activation time during the mechanical activation of ilmenite (Welham and Llewellyn, 1998). A comparative study of the

influence of attritor, ball and vibratory mills on the reactivity of Sulfide minerals was carried out by Balaz et al. (1988). γ-Fe_2O_3 samples ground with smaller amplitude in a vibratory mill showed higher reactivity (Senna, 1983).

The aim of the present paper is to investigate the influence of different experimental conditions and activation devices on hematite concentrate. The first part of this paper discusses the mechanical activation of hematite concentrate in different activation mills with various grinding variables. The second part is assigned to the characterization of microstructural characteristics of the activated hematite using integral breadth and Warren–Averbach approach in order to distinguish the influence of different milling devices and experimental conditions on the generation of microstructural characteristics and their contributions to the stored energy.

2. Experimental

The changes brought about by different milling devices during the mechanical activation of hematite concentrate were investigated using three types of ball mills; vibratory, planetary and tumbling mills. The milling was carried out by different sizes of steel media from 6 mm to 22.2 mm. A statistical design for three levels of grinding methods, three levels of milling time (1, 3 and 9 h) and two levels of media surface (1 and 4 m^2/kg of hematite) was used. Experiments were performed in dry mode (without any additives) and batch scale grinding. All experiments were performed in air atmosphere. Each experiment was carried out independently and in closed condition. During milling, the temperature of the material was measured by a thermometer immediately after stopping the mill. Obtained powders were sealed into plastic tubes and kept in a freezer for further experiments and measurements. The experimental milling conditions are displayed in Table 1.

The particle size distribution of the samples was measured by Laser diffraction (CILAS 1064) in the liquid mode. The mean particle diameter and granulometeric surface area based on particle size distribution were calculated. The specific surface area of the samples was determined by the BET method with the Flow Sorb II 2300 (Micromeretics). Samples were degassed by heating at 220 °C for 90 min immediately prior to measurements.

The X-ray diffraction (XRD) patterns were collected by a Siemens D5000 powder diffractometer with Bragg–Brentano geometry equipped with a curved graphite monochromator in the diffracted beam arm and using Cu Kα radiation (λ=0.15406). The XRD patterns of the samples were recorded in the range

ARTICLE IN PRESS

P. Pourghahramani, E. Forssberg / Int. J. Miner. Process. xx (2006) xxx–xxx

3

Table 1
Experimental milling conditions and mill types

Milling conditions	Tumbling milling	Vibratory milling	Planetary milling
Specific input energy (kWh/kg)	0.1996–6.221	0.6–21.92	5.286–190.52
Media filling (%)	38.9	70	23.4
Media surface (m²/kg)	1, 4	1, 4	1, 4
Milling time (h)	1, 3, 9	1, 3, 9	1, 3, 9
Ball to powder weight ratio	16.77:1, 67:1	16.92:1, 67.68:1	19.1:1, 76.34:1
Speed (rpm)	60	1000	100 (axle), 200 (drum)
Amplitude (mm)	–	8	–
Media apparent density (g/cm³)	4.875	4.875	4.875
Amplitude (mm)	–	8	–
$L \times \phi$ mm	275 × 245	320 × 185	87 × 115
Temperature of material (°C)	24–38	48–105	39–68

$2\theta = 10°–90°$, using a step size of 0.02° and a counting time of 5 s/step.

To characterize the microstructural characteristics encountered during the mechanical activation of specimens, the line broadening analysis was applied. The broadening analysis is accompanied with difficulties in the case of overlapped peaks. This can make the line broadening analysis more difficult. Special care was exercised in the scanning of samples and on the profile fitting procedures. The eight most intensive reflection peaks of the samples were used in the line broadening analysis. The Profile software supplied by Bruker/Socabin was used in the profile fitting procedures and in the extraction of the parameters. An example of profile fitting and separation of overlapped peaks is displayed in Fig. 1. The obtained X-ray diffraction patterns were
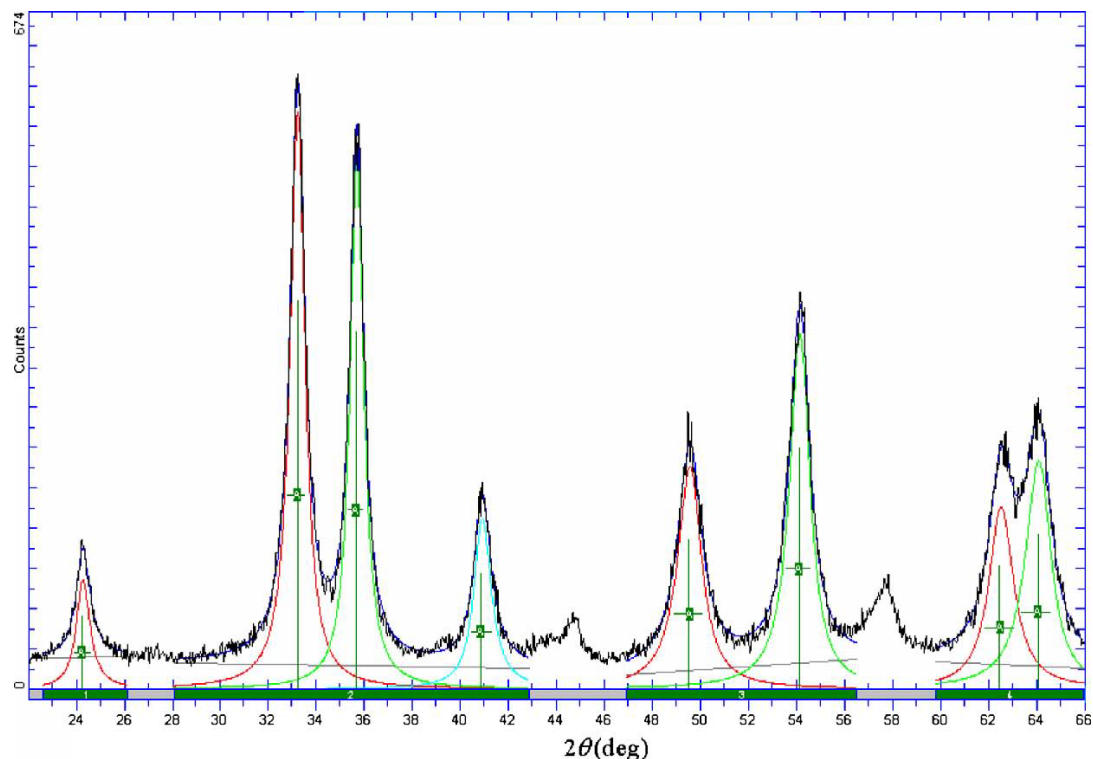
Fig. 1. An example of profile fitting in which the Pseudo–Voigt function is fitted to the Hematite samples ground for 9 h with media surface of 4 m²/kg in a planetary mill.

ARTICLE IN PRESS

4   *P. Pourghahramani, E. Forssberg / Int. J. Miner. Process. xx (2006) xxx–xxx*
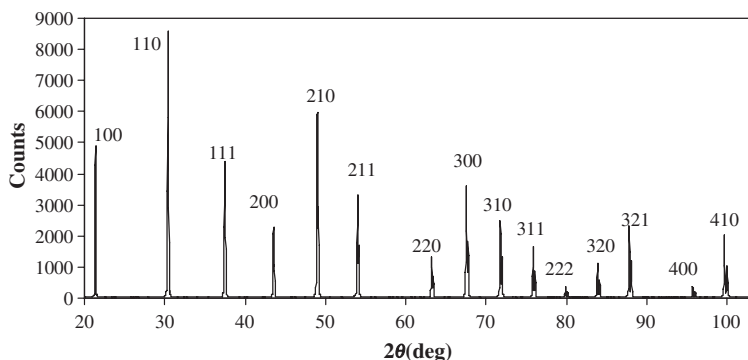
Fig. 2. Standard LaB$_6$ (SRM660a) diffraction patterns.

fitted to Pseudo–Voigt line shape function, which is a linear combination of Cauchy and Gaussian functions. For each adjusted line profile, the following parameters were obtained: (1) the maximum intensity of peaks (I_{max}), (2) the full-width at half of its maximum intensity (FWHM), (3) integral breath (β), (4) the mixing factor (η), and (5) peak position (2θ).

The same procedure was applied for the standard sample, LaB$_6$(SRM 660a), proposed by the National Institute of Standards and Technology (NIST) of the U.S.A. to obtain the instrumentally broadened profile. This profile was used to subtract the instrumental contribution from the measured profiles. The standard sample shows very narrow peaks and provides a good approximation from the instrumental effects (Fig. 2). Since the Kα_2 component in the XRD patterns increases the line broadening and introduces asymmetry into profile, the Kα_2 component was removed from the XRD patterns of standard and specimens.

The physical broadening due to strain and crystallite size was obtained according to the Halder and Wagner approximation (1966). This gives reasonable approximation when the line profile is adjusted to a combination of Lorentzian and Gaussian functions. To extract the microstructure characters, two conventional methods, integral breadth and Warren–Averbach methods, were used. The profile fitting procedure and principles of the methods were discussed in detail in previous work (Pourghahramani and Forssberg, in press).

3. Material

The high-purity hematite concentrate containing about 97.91% Fe$_2$O$_3$ was supplied by the LKAB (Luossavaara Kiirunavaara Aktiebolag) Company in Sweden. The XRD pattern of hematite concentrate (hereafter referred to as initial hematite) only showed the hematite reflection peaks (Fig. 3). The chemical analysis

Fig. 3. The XRD patterns of initial Hematite.

ARTICLE IN PRESS

P. Pourghahramani, E. Forssberg / Int. J. Miner. Process. xx (2006) xxx–xxx

5

Table 2
The chemical analysis of the initial Hematite (%)

Fe_2O_3	Al_2O_3	SiO_2	TiO_2	MgO	MnO	P_2O_5	Other elements
97.91	0.73	0.73	0.27	0.20	0.022	0.088	0.051

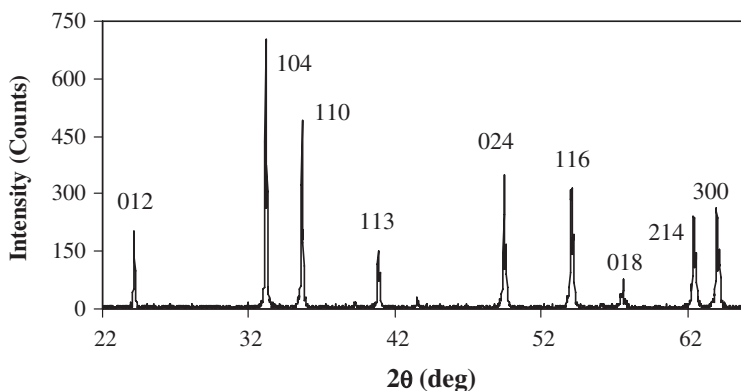of initial hematite is also given in Table 2. From the BET measurement the specific surface area was estimated about 0.59 m^2/g. The mean diameter, F_{80} and density of starting hematite were calculated to around 23, 80 μm and 5240 kg/m^3, respectively.

4. Results and discussions

4.1. Particle size and surface area

The effects of the milling on the particle size distributions are summarized in Fig. 4. The initial hematite has relatively wide distribution in comparison to the milled samples. The gap differences between the curves imply that the rate of breakage in the earlier stages of milling is higher than the later stages of grinding. As the milling progresses, the breakage rate decreases whatever methods and experimental condition are applied.

However, there are some differences among the particle size distributions resulted in different grinding methods and operational conditions. In the case of the lower media surface, Ms = 1 m^2/kg of material, prolonged grinding in both tumbling and vibratory mills tends to produce finer particles. This indicates that further size reduction in such mills at the given circumstances is possible. In the planetary mill with the same media surface, there were no differences between the particles size distributions obtained from 3 and 9 h of milling, i.e., the further size reduction is impossible. Regarding the higher media surface (Ms = 4 m^2/kg of material), it is evident that the grinding up to 3 h in tumbling and vibratory mills favors the formation of finer particles. The further size reduction is impossible if the milling time exceeds 1 h in planetary mill with large media surface. Further milling in the planetary mill causes the particle size distributions move marginally toward large sizes due to agglomeration phenomena. The planetary milling tends to agglomerate particles sooner than both tumbling and vibratory mills. The higher media surface leads to faster production of finer particles and as a consequence to the agglomeration of particles. The agglomeration could be expected to continue with the extended milling, in particular in vibratory and tumbling mills. The agglomeration of particles were reported previously by many authors for

various minerals (Balaz et al., 1996; Welham, 2001; Welham and Llewellyn, 1998; Zhang et al., 1996) almost in the prolonged milling and intensive milling conditions, suggesting that this may be a feature of extended intensive dry milling.

The specific surface area of the samples after different milling times is illustrated in Fig. 5. The most obvious feature in the figure is that the higher media surface brought about higher specific surface area whatever milling methods were applied. Furthermore, the specific surface area in the initial stages of grinding increases rather sharply and continues to rise gradually except the hematite sample ground in vibratory mill with large media surface, which continues to increase sharply. This may be related to the ability of vibratory milling in size reduction because of applying mainly shear stress on the particles being ground. The maximum specific surface areas in the milling with vibratory, planetary and tumbling mill are 18.42, 8.82 and 6.83 m^2/g, respectively.

The granulometric surface areas of the activated samples are compared in Fig. 6. With progress in the milling, the granulometric surface area shows increasing trend in the case of lower media surface. The increasing trend for vibratory mill is clear even up to 9 h of milling and its value exceed 2.58 m^2/g, which is the maximum granulometric surface area. It stands only up to 3 h of milling for tumbling and planetary mills and continues to increase very slightly. Regarding the higher media surface level, the granulometric surface increases rather slightly than lower media surface at the initial stages of milling and continues to decrease as grinding time extends. The decreasing trend of the granulometric surface implies the formation of agglomerates among particles without decreasing the specific surface area. The decreasing rate of granulometric surface area indicates that the agglomeration rate in the planetary milling is higher than the other mills.

The decrease of the BET specific surface area during mechanical activation previously was reported for many minerals: gypsum (Zhang et al., 1996), chalcopyrite (Tkacova and Balaz, 1996), ilmenite (Welham and Llewellyn, 1998), tantalite (Welham, 2001), and feldspar (Cruz Sanchez et al., 2004). But our measurements do not agree with such trends. This is because the magnitude of the BET specific surface area depends on the morphology of the absorbent, or more precisely on the size of its internal pores and cracks, and on the shape and curvature of the external surface. It seems that the internal surface of aggregates remains accessible to the molecules of nitrogen gas. Thus, the nitrogen gas can penetrate the pores in agglomerated particles and

ARTICLE IN PRESS

6   *P. Pourghahramani, E. Forssberg / Int. J. Miner. Process. xx (2006) xxx–xxx*
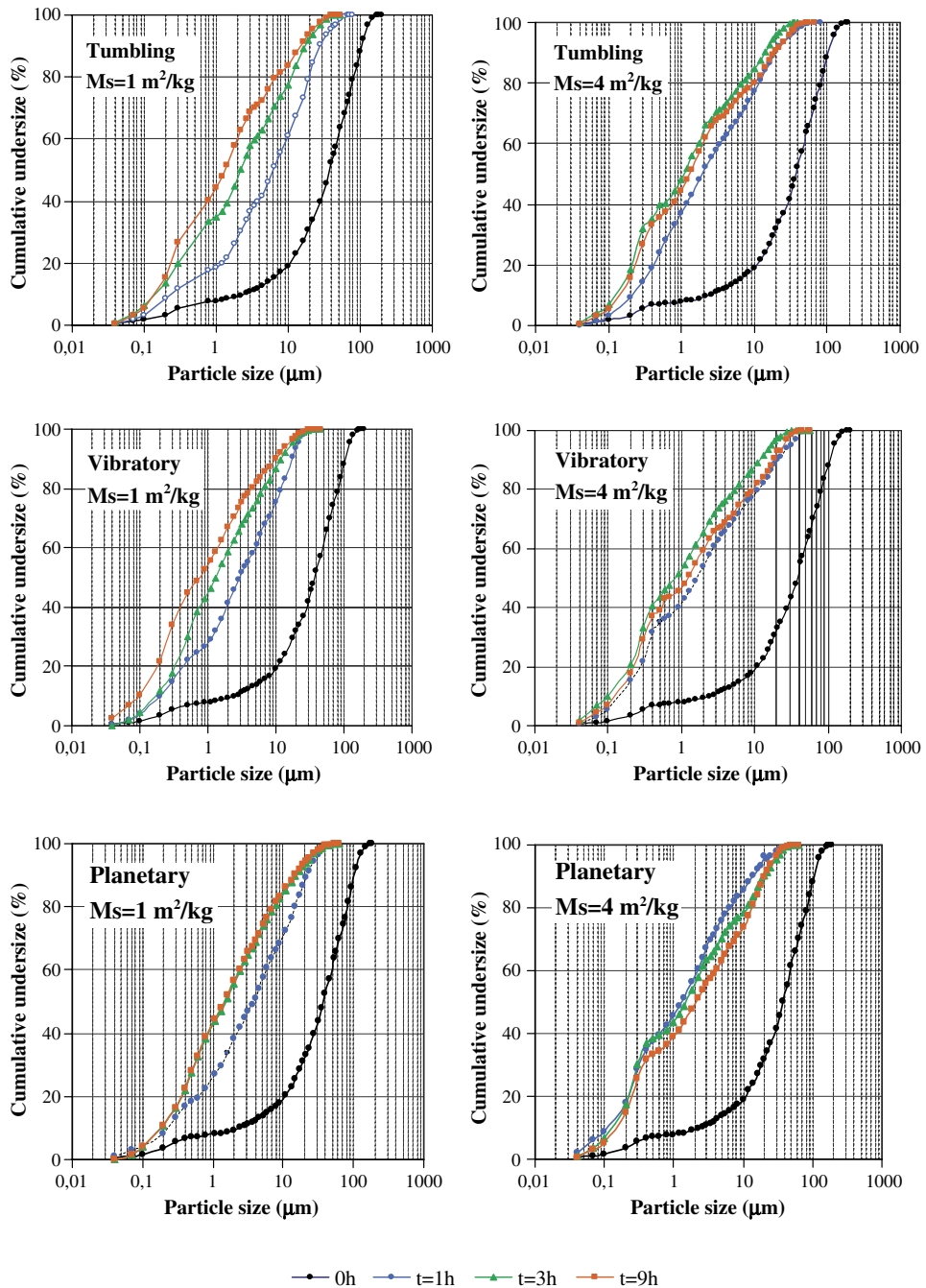
Fig. 4. Particle size distributions of activated Hematite concentrate using different milling devices and operational conditions along with the size distribution of initial Hematite.

ARTICLE IN PRESS

P. Pourghahramani, E. Forssberg / Int. J. Miner. Process. xx (2006) xxx–xxx

7
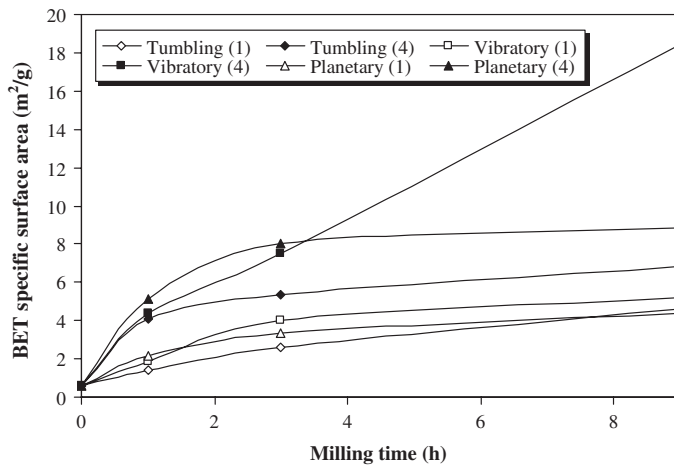
Fig. 5. The changes in the specific surface area of Hematite ground in three mills with two levels of media surface. The numbers in parentheses indicate the level of media surface in terms of m^2/kg.

displays higher BET specific surface area in spite of the agglomeration of particles but the granulometric surface values are markedly affected by the presence of the finest size fractions.

According to the obtained results, the higher media surface variable appears to be more effective in rapid production of smaller particles, increasing the BET surface area and the rate of agglomeration (a mean for reducing the specific surface energy of the particulate system). These could be related to the fact that the use of higher media surface accompanied with the higher impact force because of higher ball to powder weight ratio (see Table 1). Consequently, the number of collisions per unit time increases and more energy transfers to the particles being ground. Besides,

increasing of the milling time increases the number of pulses and subsequently more energy transfers to the particles being ground. Regarding milling types, although the planetary mill have large ability in the transferring energy to the particle, it seems that shear stressing mode and attrition of particles in the vibratory mill and generation of higher temperature up to 105 °C assist the size reduction process and consequently the generation of large specific surface area.

4.2. X-ray diffraction analysis

4.2.1. XRD patterns

The collected XRD patterns of the hematite concentrate are summarized in Fig. 7 for 1 and 9 h grinding
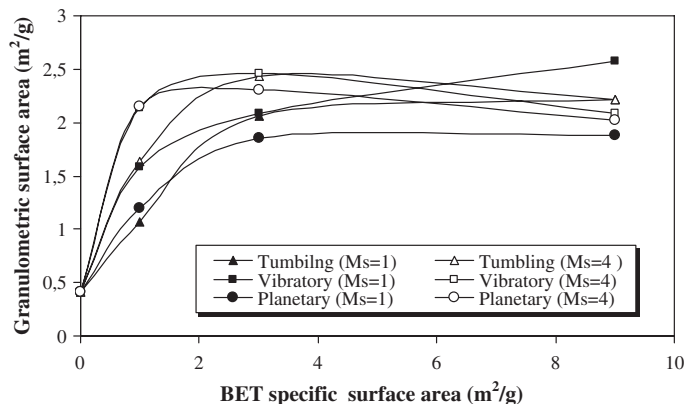
Fig. 6. The changes of granulometric surface area vs. grinding times for different mills.

ARTICLE IN PRESS

8   *P. Pourghahramani, E. Forssberg / Int. J. Miner. Process. xx (2006) xxx–xxx*
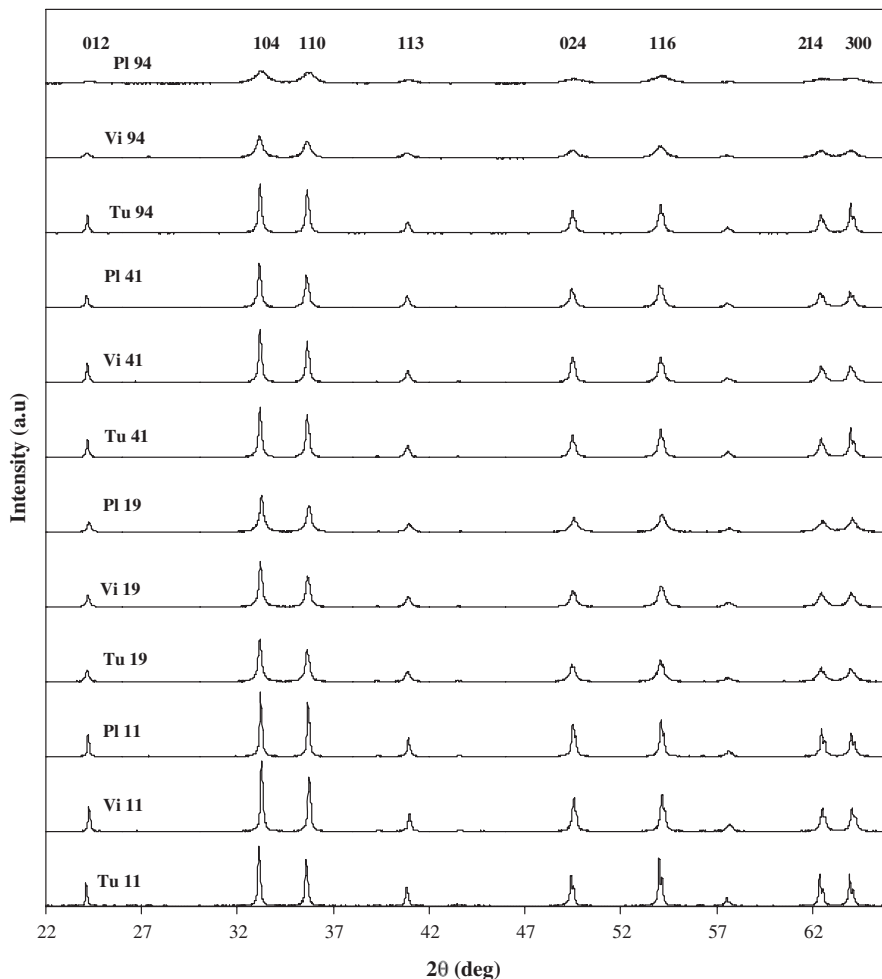
Fig. 7. The X-ray diffraction patterns of activated Hematite as function of the grinding time and media surface for mills. Tu, Vi and Pl refer to tumbling, vibratory and planetary mills, respectively. The first and second numbers after the terms denote the media surface (m^2/kg) and grinding time (h), respectively.

times in mills. XRD patterns show only hematite reflection peaks, indicating that initial hematite did not undergo significant reactions during the milling. The XRD studies do not show phases below 2 wt.%. Our observations agree with the observations of Kaczmarek and Ninham (1994) and Stewart et al. (2003). However, our observation disagrees with the findings of Kosmac and Courtney (1992) and Zdujic et al. (1998). They reported the transformation of α-Fe_2O_3 to Fe_3O_4 during ball milling in a planetary mill. Zdujic et al. made comprehensive studies to discuss the published results of the hematite transformation to Fe_3O_4 and subsequently to FeO. They stated that transferring of

sufficient energy to the particles is necessary to change the stability state of α-Fe_2O_3 to Fe_3O_4 and subsequently to FeO thermodynamically. It is evident that our milling conditions could not change the stability of hematite.

According to Fig. 7, a continuous broadening of the diffraction peaks, due to disintegration and plastic deformation of particles, is evident with increasing milling time and media surface regardless of milling types. In addition, the structural disorder due to formation of the amorphous material is manifested by decreases in the integral intensity of diffraction lines. With increasing of the milling time and media surface the intensity of diffraction line decreased, suggesting the

ARTICLE IN PRESS

P. Pourghahramani, E. Forssberg / Int. J. Miner. Process. xx (2006) xxx–xxx 9

production of more X-ray amorphous material. Rapid changes in line breadths and integral intensities for the samples milled in planetary mill were observed as the milling time increases.

For a quantitative comparison, the physical broadening (FWHM) for different grinding variables are depicted in Fig. 8. It can be observed that the planetary brings about the maximum broadening of reflection peaks. The broadening for the samples milled with the tumbling mill and vibratory mill differs marginally; the vibratory mill products show slightly larger broadening than the products of tumbling mill. For example, after 9 h of milling with the lower media surface for the reflection (014), FWHM=0.229° with planetary mill, FWHM=0.179° with vibratory mill and FWHM= 0.162° with tumbling mill were obtained.
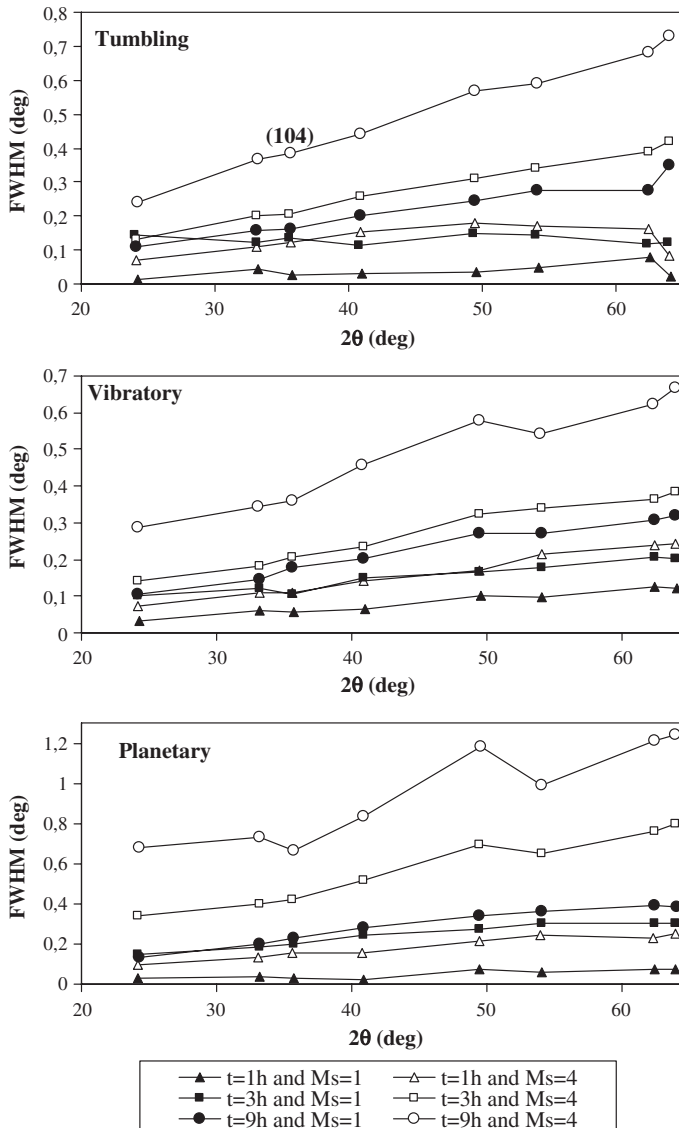

Fig. 8. The changes of physical FWHM for activated samples in different grinding times and media surface for three mills. Depending on the milling, the pronounced broadening occurs as a result of crystallite size reduction and increase of lattice strain.

ARTICLE IN PRESS

10   P. Pourghahramani, E. Forssberg / Int. J. Miner. Process. xx (2006) xxx–xxx

4.2.2. The amorphization degree

The content of X-ray amorphous phase was determined by equation proposed by Ohlberg and Strickler (1962). In our calculations, the eight most intensive reflection peaks were used. It is assumed that the amorphous phase in the initial powder is negligible. The portion of X-ray amorphous phase on average is shown in Fig. 9. It is clear that the amorphization increases with increasing of the milling time and media surface. The amorphization climbs rapidly at the initial stages of milling and continues to increase gradually with progress in milling regardless of milling types. The maximum and minimum fractions of amorphous phase in the case of lower media surface created during grinding in the planetary and tumbling mills, accounting for 71.7% and 58.3%, respectively. In the case of higher media surface, with a first approximation, the planetary mill produces more X-ray amorphous material, after 9 h of milling, 85% of the initial hematite was converted into amorphous phase. The values 81.7% and 80.3% in the same condition are estimated for vibratory and tumbling mills, respectively.

4.2.3. The changes in lattice characters

The lattice parameters were refined in Hexagonal system by regression diagnostics method and using Unitcell software (Holland and Redfern, 1997). The regression diagnostics are numbers, calculated during the regression, which supply valuable information on the influence of each observation on the least squares result and on the estimated parameters. The initial hematite yields the value of lattice parameters ($a=5.0312$ Å, $c=13.7414$ Å and $V=301.2291$ Å^3) displaying very slight variations to the values given in

the mineralogy database (Mineral database, 2005) ($a=5.0317$ Å, $c=13.737$ Å and $V=301.20$ Å^3). The calculated lattice parameters a and c and unit cell volume for the activated samples as a function of milling time for different activation mills in the case of higher media surface level are shown in Fig. 10. It is seen that both unit cell parameters increased drastically at short time of activation and continue to increase gradually. This implies an expansion of hematite cell with an elongation of both a and c axis length during activation. The changes of unit cell volume in tumbling mill have a significant difference with vibratory and planetary mills in the grinding up to 1 h of milling. This also holds marginally for the planetary mill for 3 h of milling. Similar plots were constructed for the lower media surface but they did not carry more information and they have not been reported in the present paper.

4.3. Microstructural analysis

To obtain the microstructural characteristics, two methods including the simplified integral breadth and Warren–Averbach approach were used. The obtained results are discussed in the next sections.

4.3.1. Integral breadth method

The first step in analyzing line broadening is to ascertain the nature of any structural imperfections present. This can be achieved from the Williamson–Hall plots. The Williamson–Hall plots are illustrated in Figs. 11 and 12 for all activated samples using different mill types. The correlation coefficients were estimated between 0.8 and 0.97 depending on the sample. This indicates relatively a strong relationship between β_f^{*2} and d^{*2}.
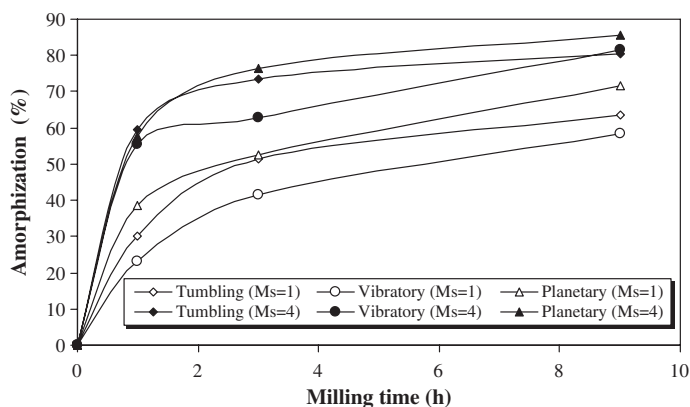

Fig. 9. Variation of amorphization with the time of mechanical activation and media surface in different milling devices. The values in parentheses refer to the level of media surface in terms of m^2/kg of material.

ARTICLE IN PRESS

P. Pourghahramani, E. Forssberg / Int. J. Miner. Process. xx (2006) xxx–xxx 11
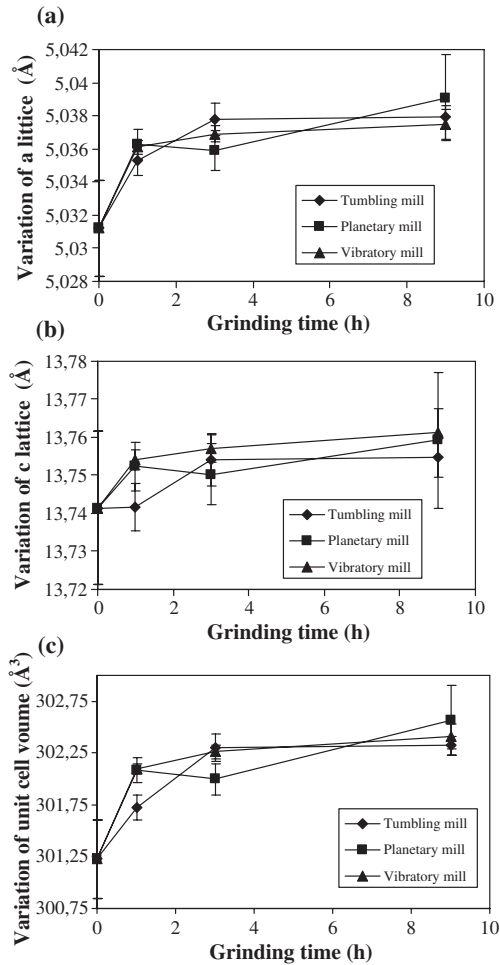
(a)

(b)

(c)

Fig. 10. The variation of lattice parameters with grinding time: (a) variation of a lattice parameter; (b) c lattice parameter; (c) the unit cell volume for higher media surface level (Ms = 4 m²/kg).

From the Williamson–Hall plots, lines for all intensive reflections and [012] direction have non-zero and different slopes and intercepts. This suggests that the strain and size contributions exist simultaneously in the milled samples. The increase of physical broadening vs. grinding time and media surface indicates that intensive milling extends great defects and deformations in materials. The scatter of the β_f^{*2} values indicates that the crystallite shape differs from a spherical one. Besides, the (024) reflection shows higher deviation than other reflections and its broadening enlarged as the intensity of milling increased. There is also a systematic deviation between the line connecting the two orders of (012) and (024) reflections and the line connecting all

intensive reflections, the line concerning to the [012] direction lie above it. This may be understood by considering the anisotropy in the elastic properties of the single-crystal hematite, indicating that hematite crystal is 'soft' between the (024) and the others crystallographic directions. The similar results have been observed for Fe powder (Borner and Eckert, 1997; Vives et al., 2004) and ball-milled molybdenum powder (Lucks et al., 2004). This anisotropy character of line broadening attributed to the dislocation strain field anisotropy (Ungar and Borbely, 1996). It is beyond the scope of this paper to examine these anisotropic effects.

According to Figs. 11 and 12 for the same milling time and media surface, it can be further observed that the broadening for the samples milled with planetary mill is much larger than the broadening for the samples milled with vibratory and tumbling mills except the sample milled for 1 h. For evaluation, the strain and crystallite size of the samples were estimated from the slope and intercept of plots (Pourghahramani and Forssberg, in press). The concerning results are summarized in Table 3. Regarding the Williamson–Hall data as a sort of quantitative analysis, the values of strain and size make sense. With more damage, the particles receive more strain and reduction of the size of the defect-free subcrystals. The products of planetary mill, with a first approximation, yield smaller crystallite size and higher strain than other mill products. Prolonged grinding with higher media surface favors the generation of small crystallites and the induction of higher strain in hematite.

4.3.2. Size-strain in the [012] direction

As discussed, the Warren–Averbach analysis based on Fourier analysis provides detailed information regarding the crystallite size, lattice strain and their distributions. The results are discussed in next sections.

4.3.2.1. The microstrain distributions.
The strain distributions for samples ground in different mills and operational conditions are given in Fig. 13. A plot of $<\varepsilon_L^2>^{1/2}$ as a function of crystallite length, L, shows a decreasing curve for increasing L values. From this kind of plot, it is possible to appreciate the degree of disorder in samples from the observed trend in the $<\varepsilon_L^2>^{1/2}$ vs. L plot. The lattice disorder can be attributed to (1) paracrysttaline distortions, which arise due to fluctuations in the interplanar distance due to inhomogeneities in samples, and to (2) the presence of dislocations, which results in a Gaussian distribution of the microstrain (Jyung and Jenq, 1997). The high efficiency of the ball milling process on the domain size reduction and

ARTICLE IN PRESS

12   *P. Pourghahramani, E. Forssberg / Int. J. Miner. Process. xx (2006) xxx–xxx*

Fig. 11. Williamson–Hall plots, B_f^{*2} vs. d^{*2}, for samples milled in the tumbling, vibratory and planetary mills with lower media surface. The solid and dashed line refers to all intensive reflection peaks and direction [012], respectively.

strain increasing has been noticed whatever milling methods employed. The use of planetary mill brought about more reduction of domain size than vibratory and tumbling mills in the intensive grinding conditions.

4.3.2.2. The variations in the crystallite size and lattice strain. The crystallite size quantity and the root mean square strain $<\varepsilon_{L=10\ nm}^2>^{1/2}$ are given in Table 4. The results depict the nature of progressive evolution of the microstructure of the milling products vs. grinding conditions. Generally, the surface-weighted crystallite size shows decreasing and root mean square strain

$(<\varepsilon_{L=10\ nm}^2>^{1/2})$ increasing trend as both grinding time and media surface increase whatever mill used. In the earlier stages of milling, the crystallite size decreases rapidly to the nanometer range. Further refinement proceeds slowly and the final average grain size is in the order of 5–27 nm. Comparing the strain $(<\varepsilon_{L=10\ nm}^2>^{1/2})$ and crystallite size values for grinding up to 1 h indicates no clear pattern among the products of different mills. As the intensity of milling increases, the ground hematite in planetary mill yields more strain and smaller crystallites than that of ground in vibratory and tumbling mills. The planetary mill decreases the

ARTICLE IN PRESS

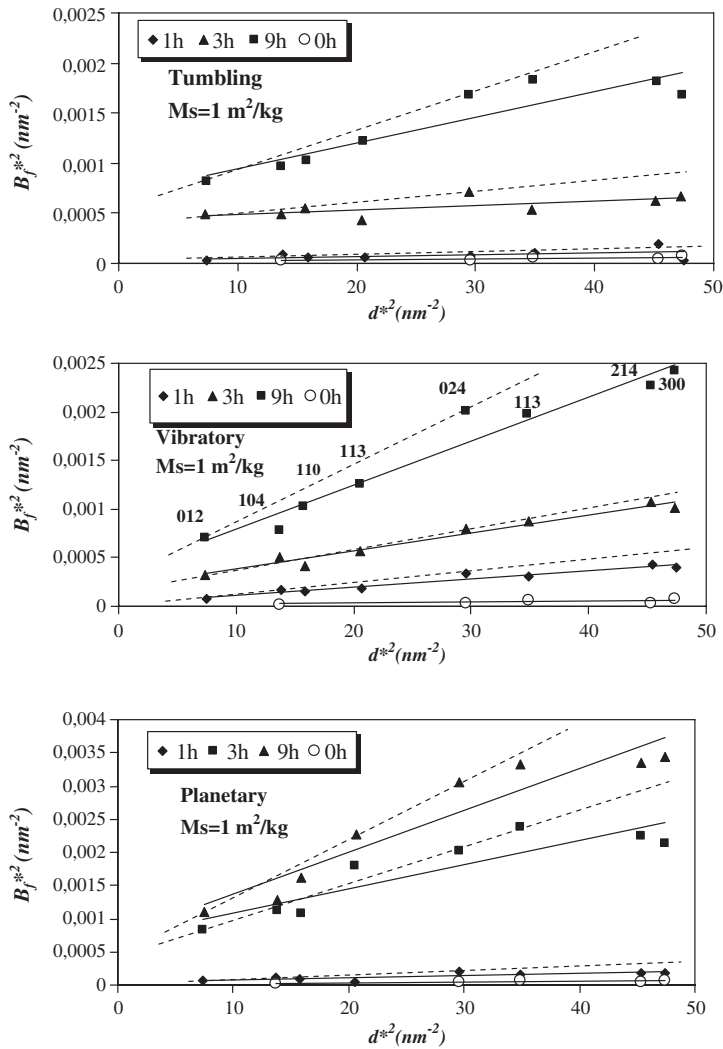*P. Pourghahramani, E. Forssberg / Int. J. Miner. Process. xx (2006) xxx–xxx*   13
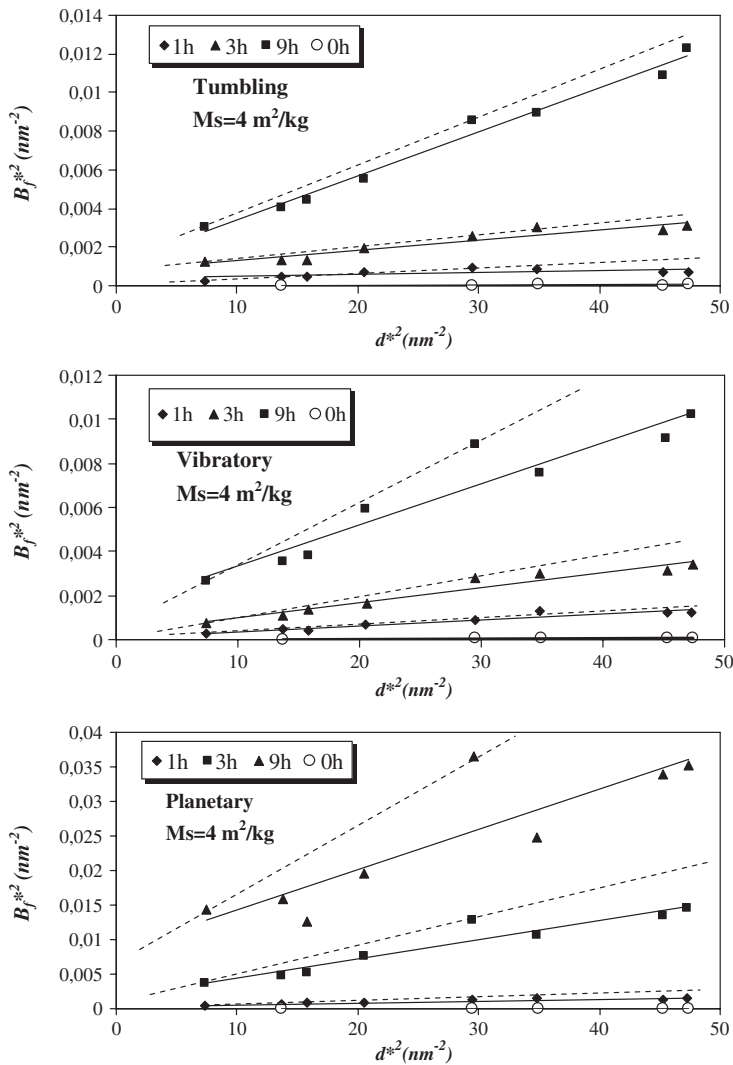
Fig. 12. Williamson–Hall plots, B_f^{*2} vs. d^{*2}, for samples milled in the tumbling, vibratory and planetary mills with higher media surface. The solid and dashed line refers to all intensive reflection peaks and direction [012], respectively.

crystallite size to a value of lower than 6 nm and increases strain to a value of higher than 5.3×10^{-3} by using higher media surface after 9 h of milling. This may be also attributed to the use of higher ball to powder weight ratio for milling in planetary mill (Table 1). The steady state was not observed for grinding conditions, suggesting that the production of small crystallites is possible with increasing the grinding intensity. Obviously, variations in the ball media surface have a more influence on the crystallite refinement.

The results concerning to tumbling and vibratory mills' products indicate some differences between size and strain components when the media surface changes in milling process. Obviously, grinding of hematite with lower media surface in vibratory mill resulted larger crystallite and higher strain than grinding in tumbling mill marginally as opposed with higher media surface case. This may be related to the changes in stressing manner of particles in milling process especially in vibratory mill. In non-rotary ball mills, the material is under the action of a combined stress and the

ARTICLE IN PRESS

14　　　　　　　　　　*P. Pourghahramani, E. Forssberg / Int. J. Miner. Process. xx (2006) xxx–xxx*

Table 3
Crystallite size (D_V) and lattice strain (ε) obtained using integral breadth method for different mills

Parameters		Ms=1 m²/kg		Ms=4 m²/kg	
Milling type	Time (h)	D_V (nm)	ε (×10^{-3})	D_V (nm)	ε (×10^{-3})
Tumbling mill	1	158.1±86 (223.6)	0.77±0.13 (0.7)	50±17.6 (–)	1.58±0.7 (2.73)
	3	50±16.3 (50)	1.12±0.4 (1.6)	35.3±10.6 (35.4)	3.54±0.6 (3.87)
	9	37.8±9.09 (44.7)	2.7±0.3 (3.2)	30.2±10.1 (28.9)	7.07±0.4 (7.1)
Vibratory mill	1	182.6±80 (–)	1.50±0.2 (1.6)	105.4±50 (141.4)	2.74±0.2 (2.7)
	3	70.7±22 (70.7)	2.2±0.3 (2.2)	57.7±27 (111.8)	4.18±0.5 (4.7)
	9	57.7±23 (57.7)	3.5±0.2 (3.9)	25.8±10.8 (40.8)	7.00±0.8 (8.7)
Planetary mill	1	141.4±55 (182.5)	0.89±0.2 (1.2)	57.7±19.8 (100)	2.73±0.3 (3.2)
	3	37.8±13 (50)	3.2±0.7 (3.5)	24.3±8.8 (37.8)	8.6±0.4 (10)
	9	37.8±14.1 (44.7)	3.9±0.4 (4.74)	10.9±4.5 (12.1)	12.2±0.4 (15.8)
Initial Hematite [a]	0	316.2±180 (–)	0.5±0.4 (–)	–	–

Confidence levels of data are given at 95%. The values corresponding to [012] direction are given in parentheses.

[a] Calculated using five reflection peaks.

predominant mode of stress varies depending upon the mode of mill performance (Tkacova, 1989). In our opinion, the use of low media surface supplies much material around grinding media and material stressing proceeds dominantly in compressive and impact mode. Consequently, this condition induces high strain in material being ground. Applying large media surface changes the dominant type of stress from compressive and impact to shear and/or attrition. These changes facilitate the size reduction and breakage in fine and ultrafine range.

4.3.2.3. The relative frequency of crystallite length distribution.

The relative frequency, a number which describes the proportion of observations (crystallite length) falling in a given category, of crystallite length as a function of milling operation is given in Fig. 14. At first glance, in the earlier stages of milling (low milling intensity), the two main crystallite groups were observed. With progress in milling in particular increasing the grinding periods, the size distribution curve represented mainly single crystallite group. Besides, the maximum relative frequency values for the crystallite length at the initial stages of milling are less than that of intensive milling. Approximately, the crystallites size (length) distributions at intensive milling follow the lognormal distribution behavior. This was reported previously for several minerals and materials; ball-milled molybdenum (Lucks et al., 2004) and milled iron powders (Vives et al., 2004).

Regarding the milling devices, the existence of the two main crystallite groups was extended for milling up to 3 h with low media surface in vibratory and tumbling mills. This stands only for grinding within 1 h with low media surface in planetary mill. In addition, the maximum relative frequency of the planetary mill's products is greater than other mill products for the same milling condition. There is no clear difference between the products of vibratory and tumbling mills. We can draw the conclusion that fragmentation of coarser particles results in the establishment of more uniform contact between the grinding media and particles being ground. The intensive grinding leads to uniform activation of hematite. In earlier stages of grinding especially with lower media surface, the coarse particles prevent the media from coming into contact with finer particles. Hence, hematite is activated non-uniformly. Having this in mind, the existence of two main crystallite size groups can be attributed either to the new phase formation or to the changes of the materials being ground. However, in our investigation we did not observe any phase transformation or new phase formation according to the XRD patterns. In our opinion, the non-uniform stressing of powders resulted in a non-uniform crystallite length distribution.

4.3.3. The variations in dislocation density

To estimate the dislocation density, ρ_D, ρ_ε and ρ, of the ball-milled hematite powders, the simple approach of Williamson and Smallman (1956) was followed, relating ρ to crystallite size D and strain $<\varepsilon_L^2>^{1/2}$:

$$\rho_D = \frac{3}{D^2}; \quad \rho_\varepsilon = \frac{k < \varepsilon_L^2 >}{b^2}; \quad \rho = (\rho_D \cdot \rho_\varepsilon)^{1/2} \qquad (1)$$

where ρ_D, ρ_ε and ρ correspond to the dislocation due to domain size, dislocation due to microstrain and real dislocation density respectively. The coefficient k depends on the mechanical properties of the crystal, its microstructure and on the type of distribution of displacement in it (its value are usually between 2 and 25) and b is the Burger's vector, which determines the

ARTICLE IN PRESS

P. Pourghahramani, E. Forssberg / Int. J. Miner. Process. xx (2006) xxx–xxx 15
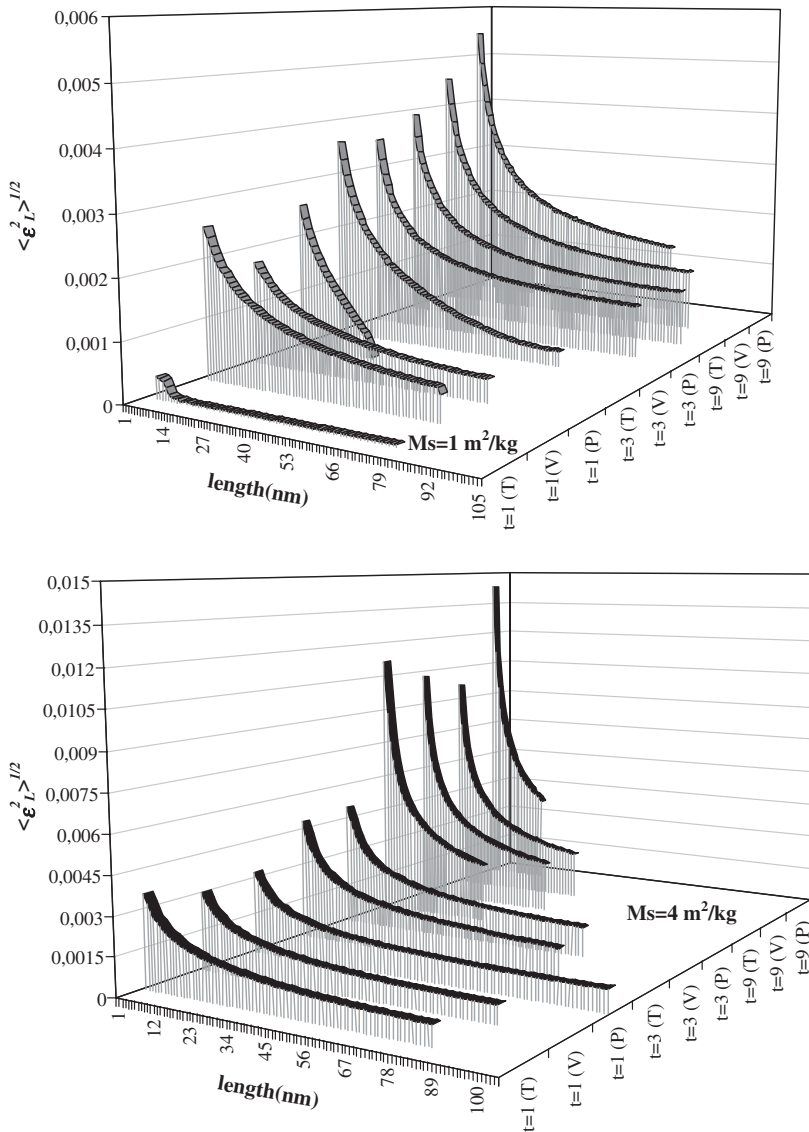
Fig. 13. The RMSS strain distribution as function of crystallite length with milling types and operational conditions. *t* refers to the activation time in h. V, T and P in parentheses correspond to the vibratory, tumbling and planetary mills, respectively.

distance and direction of displacement. We assumed that the Burger's vector direction of hematite is the same as for Corundum, in the [100] direction. Thus, the value of Burger vector for hematite in direction [100] was found about 5.03×10^{-10} m. Since the value of k for hematite was not found through literature; we assumed $k=2$. The results obtained by taking D_S and $<\varepsilon_{L=10 \text{ nm}}^2>^{1/2}$ from the Warren–Averbach analysis are given in Table 5. The dislocation density increases to a value of $\approx 46 \times 10^{14}$

after 9 h of milling with media surface of 4 m²/kg in the planetary mill. Regardless of milling machines, as hematite is imposed to intensive grinding, the dislocation density increases. The ground hematite in vibratory mill showed slightly higher dislocation than tumbling mill's products. The planetary mill induced much more dislocation in hematite, with the exception of the sample ground for 1 h with lower media surface. It seems that the hindering of grinding media because of a higher

Table 4
The microstructural characteristics in [012] direction using the Warren–Averbach method for activated Hematite in different environments

Parameters		Ms = 1 m²/kg		Ms = 4 m²/kg	
Milling type	Time (h)	D_S (nm)	$<\varepsilon^2_{L=10\ nm}>^{1/2} \times (10^{-3})$	D_S (nm)	$<\varepsilon^2_{L=10\ nm}>^{1/2} \times (10^{-3})$
Tumbling mill	1	54.16	0.062	44.4	2.236
	3	42.6	1.52	25.0	2.84
	9	27.3	2.25	17.3	4.44
Vibratory mill	1	73.5	1.75	36.4	1.84
	3	43.5	2.08	23.7	2.79
	9	29.6	2.58	12.2	3.95
Planetary mill	1	66.7	1.25	28.1	1.94
	3	20.5	2.03	11.6	4.44
	9	16.5	3.011	5.6	5.32
Initial Hematite [a]	0	199.1	n.d.(0)		

D_S and $<\varepsilon^2_{L=10\ nm}>$ indicate the surface weighted crystallite size and root mean square strain (RMSS) at $L = 10$ nm, respectively.
[a] Calculated using single peak method.

powder to ball weight ratio prevented the refinement of microstructure characters in the sample ground for 1 h with lower media surface in the planetary mill.

5. The contribution of long-lived defects to the energy state of activated hematite

For the interpretation of the mechanical activation process, the context between structures and energy content of the mechanically activated solids and consumed mechanical energy are of important and interest. As a result of previous investigations (Heegn, 1979; Heegn et al., 2003; Tkacova et al., 1993), the following defect structures of essential meaning for the energetic condition of the solids are: (1) dislocation concentration with the specific energy, (2) energy contributions of new surface formation, and (3) content of newly formed phases and amorphous fraction. The quantitative estimate of the increase in molar chemical free energy (increase in stored energy) due to dislocation concentration has been calculated by expression proposed by Tromans and Meech (2001). Besides, the energy fraction of amorphous phase and surface area are estimated using equations proposed by Heegn (1979). The estimation have been calculated with the material data for hematite of $\sigma_S = 1769$ erg/cm³ (specific interfacial energy) and $E_A = 90.99$ kJ/mol (molar amortization energy) (Heegn, 1987). Table 6 contains calculations of the energy parts and the sum of excess energy for activated hematite in different conditions and mills. From the data presented in Table 6, it follows that the contribution of amorphization energy to the energy change at activation amounted to 93–98.5%. Similar energy distributions were found for Quartz, Calcite, Magnesite, Kaolinite and Iron (Heegn, 1986a,b) and periclase (Tkacova et al., 1993). From Table 6, it is

apparent that energy contribution of new surface formation of activated hematite in vibratory mill accounted for the maximum values comparing to other mill products. Besides, the planetary mill products amounted to the greatest energy contribution of amorphization. These also include the largest part of energy due to dislocation density with exception of activation within 1 h.

6. The relationship between excess energy and grinding work

To compare the stored energy due to defect structures with grinding energy, the specific grinding work (stress energy) were calculated by expressions proposed by Heegn (1986b, 2000). The specific grinding work vs. stored energy is depicted in Fig. 15. It can be seen that the excess enthalpy content (stored energy) increases with growing the amount of grinding work. For a given stress energy, a higher stored energy was observed for tumbling mill products. For example, to achieve an excess energy in hematite by mechanical treatment about 60 kJ/mol, the required stress energy in tumbling, planetary vibratory milling is around 1300, 2800, 17,000 kJ/kg, respectively. In agreement with studies by Miyasaka and Senna (1985) and Tkacova et al. (1987) the excess enthalpy (ΔH) can be related to stress energy or grinding work (W) by the equation, where b and c are the constant values.

$$\Delta H_T = b\ \log_{10} W - c.$$

7. Conclusion

- The use of higher media surface and prolonged grinding lead to higher specific surface area, X-ray

ARTICLE IN PRESS

P. Pourghahramani, E. Forssberg / Int. J. Miner. Process. xx (2006) xxx–xxx 17
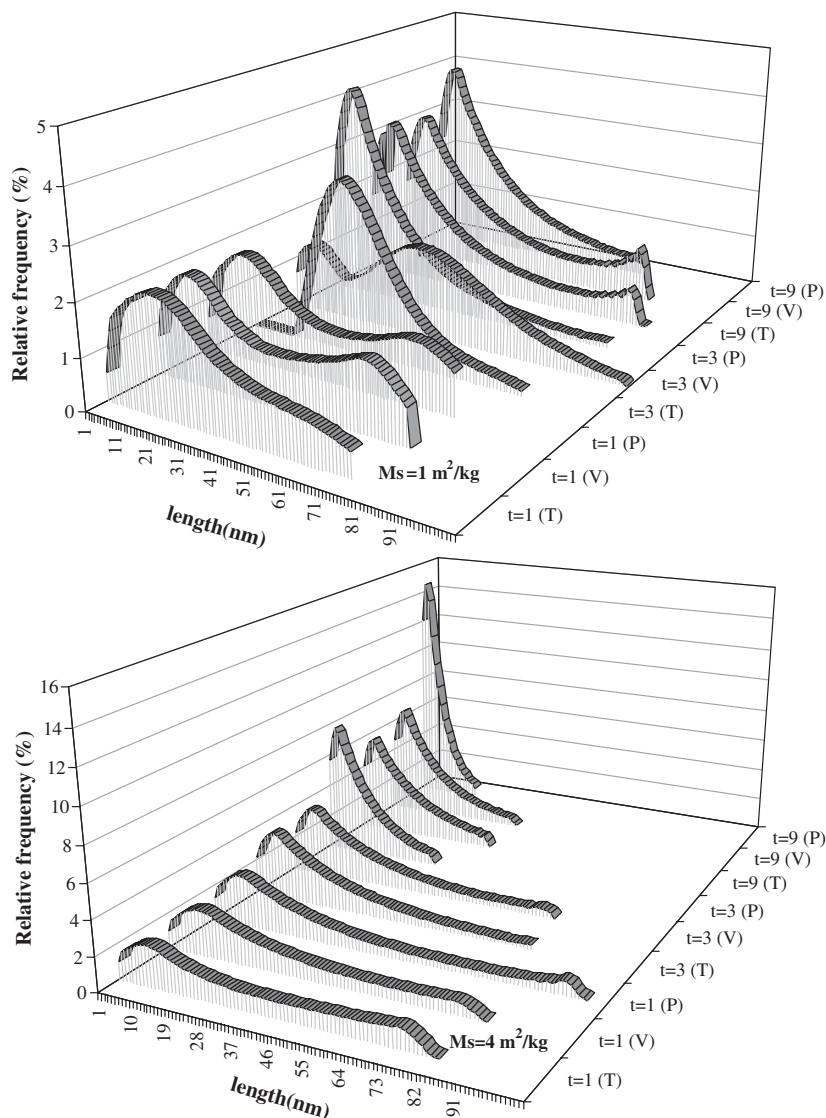
Fig. 14. The relative frequency of column length as a function of milling conditions. *t* indicates the activation time in h. V, T and P in parentheses correspond to the vibratory, tumbling and planetary mills, respectively.

amorphous material, physical broadening, micro-strain, dislocation density, stored energy and smaller crystallites whatever milling types were applied.

- The samples activated in the tumbling mill resulted the lowest specific surface area among the mills used, being between 1.41 m^2/g and 6.83 m^2/g depending on the grinding variables. The maximum specific surface area, 18.42 m^2/g, and amorphization degree, 85%, were achieved from the milling in the vibratory and planetary mills, respectively, with higher media

surface after 9 h of milling. The vibratory mill produced approximately the minimum X-ray amor-phization material compared to the other milling devices. Generally, the maximum and minimum line breadths of XRD diffraction were observed for the products of the planetary and tumbling mills respectively.

- From the Williamson–Hall plots, it was concluded that the hematite crystal is 'soft' between (024) direction and other crystallographic directions. The

ARTICLE IN PRESS

18   *P. Pourghahramani, E. Forssberg / Int. J. Miner. Process. xx (2006) xxx–xxx*

Table 5
The dislocation density, $\rho \times 10^{14}$ (m/m^3), for activated Hematite in different grinding mills and operational conditions

Grinding variables		Mill types		
Grinding time (h)	Media surface (m^2/kg)	Tumbling mill	Vibratory mill	Planetary mill
1	1	0.6	1.2	0.9
3	1	1.7	2.3	4.8
9	1	4.0	4.2	8.9
1	4	2.4	2.5	3.4
3	4	5.5	5.7	18.6
9	4	12.5	15.8	46.3

Warren–Averbach method suggested that the planetary mill products have smaller crystallites and higher microstrain than the products of tumbling and vibratory mills with the exception for the samples activated for 1 h with low media surface. The final products contain crystallites between 73.5 and 5.6 nm and the lattice strain (RMSS) at $L=10$ nm, $<\varepsilon^2_{L=10\ nm}>^{1/2}$, varies from 0.06×10^{-3} up to 5.32×10^{-3} depending on the milling performance.

▪ The energy contribution of amorphization is much more than the energy contribution of dislocation density and surface area changes, accounting for 93–98.5% of overall enthalpy or stored energy. The enthalpy contents in the activated material increased to the values between 21.5 and 81.32 kJ/mol of hematite. The planetary and vibratory mills need much more energy to reach the same effect as tumbling mill.

▪ The results suggest that the precise characterization of microstructures, make possible to distinguish differences among the used mills. The results indicated that for a given stress energy the products of tumbling mill have higher reactivity potential. However, experimental reactivity tests are needed to explore the real effect and availability of structural changes. Therefore, further study is needed to answer the remaining question.

Nomenclature

A	Peak area
b	Burger's vector
D_S	Surface-weighted crystallite size
D_V	Volume-weighted crystallite size
d	Interplanar spacing
FWHM	Full width at half-maximum of profile
(hkl)	Miller indices
I_{max}	Maximum intensity
RMSS	Root mean square strain
β	Integral breadth
β_f	The integral breadth of the physically broadened profile
β^*	$\beta\cos\theta/\lambda$, Integral breadth in the units of d^* (nm^{-1})
$<\varepsilon^2_L>$	Mean square strain, orthogonal to diffracting planes, averaged over the distance L

Table 6
Energy contributions of new surface formation, ΔH_S, dislocation density, ΔH_d, and amorphization, ΔH_A, to the overall change in enthalpy, $\sum \Delta H$, of Hematite with three types of mills in different condition

Mill types	Ms (m^2/kg)	Time (h)	ΔH_S		ΔH_d		ΔH_A		$\sum \Delta H$
			kJ/mol	%	kJ/mol	%	kJ/mol	%	kJ/mol
Tumbling mill	1	1	0.40	1.44	0.019	0.07	27.3	98.49	27.72
	1	3	0.73	1.53	0.054	0.11	46.9	98.36	47.68
	1	9	1.30	2.20	0.115	0.19	57.8	97.61	59.22
	4	1	1.17	2.11	0.074	0.13	54.1	97.75	55.34
	4	3	1.51	2.20	0.154	0.22	66.9	97.57	68.56
	4	9	1.93	2.56	0.320	0.42	73.1	97.01	75.35
Vibratory mill	1	1	0.53	2.46	0.037	0.17	21.0	97.37	21.57
	1	3	1.13	2.90	0.070	0.18	37.7	96.92	38.90
	1	9	1.47	2.69	0.121	0.22	53.0	97.09	54.59
	4	1	1.24	2.39	0.074	0.14	50.6	97.46	51.91
	4	3	2.13	3.57	0.159	0.27	57.3	96.16	59.59
	4	9	5.21	6.51	0.394	0.49	74.4	93.00	80.00
Planetary mill	1	1	0.6	1.68	0.03	0.08	35.1	98.24	35.73
	1	3	0.95	1.95	0.136	0.28	47.7	97.77	48.79
	1	9	1.25	1.87	0.236	0.35	65.2	97.77	66.72
	4	1	1.45	2.69	0.098	0.13	52.4	97.13	53.95
	4	3	2.26	3.13	0.456	0.63	69.5	96.24	72.22
	4	9	2.50	3.07	1.020	1.25	77.8	95.67	81.32
Initial Hematite	–	–	0.17	–	–	–	–	–	–

ARTICLE IN PRESS

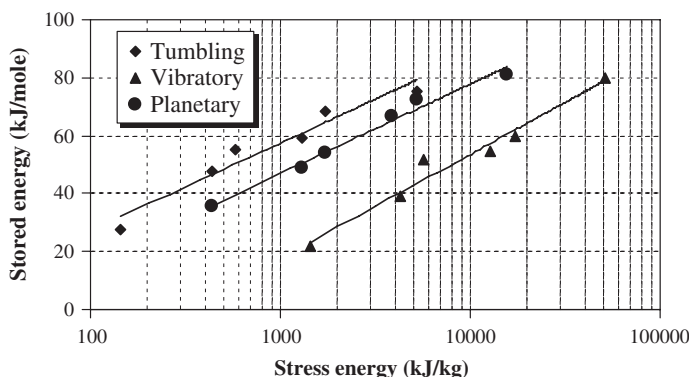*P. Pourghahramani, E. Forssberg / Int. J. Miner. Process. xx (2006) xxx–xxx* 19

Fig. 15. The comparison of relationship between the specific grinding work (stress energy) and stored energy in activated Hematite with various mills.

θ	Bragg angle
λ	X-ray wavelength
ρ	The real dislocation density
ρ_D	the dislocation due to domain size
ρ_ε	dislocation due to microstain
Å	Angstrom unit (10^{-11} m)
LPA	Line profile analysis
Ms	Grinding media surface level (m^2/kg) of milled sample)
W	Specific grinding work (kJ/kg)

References

Balaz, P., 2000. Extractive Metallurgy of Activated Minerals, first ed. Elsevier, Amsterdam.

Balaz, P., Huhn, H.J., Tkacova, K., Heegn, H., 1988. Laugungsverhalten und physico-chemische Eigenschaften von in unterschiedlichen Mullen vorbehandeltem chalkopyrite. Erzmetall 41, 325–331.

Balaz, P., Ficeriova, J., Sepelak, V., Kammel, R., 1996. Thiourea leaching of silver from mechanically activated tetrahedrite. Hydrometallurgy 43, 367–377.

Bernhardt, C., Heegn, H., 1978. Mechanische Aktivierung von Ton in einer diskontinuierlich und kontinuierlich arbeitenden Schwingmühle. Silikattechnik, Berlin 29 (12), 373–376.

Boldyrev, V.V., Pavlov, S.V., Goldberg, E.L., 1996. Interrelation between fine grinding and mechanical activation. Int. J. Miner. Process. 44–45, 181–185.

Borner, I., Eckert, J., 1997. Nanostructure formation and steady-state grain size of ball-milled iron powders. Mater. Sci. Eng., A Struct. Mater.: Prop. Microstruct. Process. 226–228, 541–545.

Cruz Sanchez, E., Torres, M.E., Diaz, C., Saito, F., 2004. Effects of grinding of the feldspar in the sintering using a planetary ball mill. J. Mater. Process. Technol. 152, 284–290.

Halder, N.C., Wagner, C.N.J., 1966. Separation of particle size and lattice strain in integral breath measurements. Acta Cryst. 20, 312–313.

Heegn, H., 1979. Effect of fine grinding on structure and energy content of solids. Proc. of 6th POWTECH, Birmingham, pp. 61–69.

Heegn, H., 1986a. Changes in the properties of solids during mechanical activation and fine grinding. Sc.D. Thesis, Research Institute of Mineral Processing of the Academy of the GDR, Freiberg (in German).

Heegn, H., 1986b. Concerning some fundamentals of fine grinding. In: Leschonski, K. (Ed.), Proc. 1st World Congress on Particle Technology: Part II. Comminution. Nürnberger Messe und Austellungsgesellschaft, Nürnberg, pp. 63–67.

Heegn, H., 1987. Model describing the resistance against structural changes and the hardness of crystalline solids. Cryst. Res. Technol. 22 (9), 1193–1203.

Heegn, H., 2000. Mechanical induced changes in structure and properties of solids. Proceedings of the XXI International Mineral Processing Congress: Part A4. Comminution, Classification and agglomeration, Rome, Italy, pp. 52–59.

Heegn, H., Birkeneder, F., Kamptner, A., 2003. Mechanical activation of precursors for nanocrystalline materials. Cryst. Res. Technol. 38 (1), 7–20.

Holland, T.J.B., Redfern, S.A.T., 1997. Unit cell refinement from powder diffraction data; the use of regression diagnostics. Mineral. Mag. 61, 65–77.

Jyung, D.L., Jenq, G.D., 1997. The use of X-ray line profile analysis to investigate crystallite size and microstrain for zirconia powders. J. Mater. Sci. 32, 5779–5790.

Kaczmarek, W.A., Ninham, B.W., 1994. Preparation of Fe_3O_4 and γ-Fe_2O_3 powders by magnetomechanical activation of hematite. IEEE Trans. Magn. 30 (2), 732–734.

Karagedov, G.R., Lyakhov, N.Z., 2003. Mechanochemical grinding of inorganic oxides. Kona 21, 76–86.

Kosmac, T., Courtney, T.H., 1992. Milling and mechanical alloying of inorganic nonmetallics. J. Mater. Res. 17 (6), 1519–1525.

Lucks, I., Lamparter, P., Mittemeijer, E.J., 2004. An evaluation of methods of diffraction-line broadening analysis applied to ball-milled molybdenum. J. App. Cryst. 37, 300–311.

Mineral database, 2005. http://webmineral.com/data/Hematite.shtml.

Miyasaka, K., Senna, M., 1985. Calorimetric and thermoanalytical assessment of mechanically activated $PbCO_3$. Thermochim. Acta 83 (2), 225–233.

ARTICLE IN PRESS

20   *P. Pourghahramani, E. Forssberg / Int. J. Miner. Process. xx (2006) xxx–xxx*

Ohlberg, S.M., Strickler, D.W., 1962. Determination of percent crystallinity of partly devitrified glass by X-ray diffraction. J. Am. Ceram. Soc. 45, 170–171.

Pourghahramani, P., Forssberg, E., in press. Microstructure characterization of mechanically activated hematite concentrate using XRD line broadening analysis. Int. J. Miner. Process.

Senna, M., 1983. Criteria of activation of powdery materials by a preliminary mechanical treatment. Kona 1, 48–52.

Stewart, S.J., Borzi, R.A., Cabanillas, E.D., Punte, G., Mercader, R.C., 2003. Effects of milling-induced disorder on the lattice parameters and magnetic properties of hematite. J. Magn. Magn. Mater. 260, 447–454.

Tkacova, K., 1989. Mechanical Activation of Minerals, first ed. Elsevier, Amesterdam.

Tkacova, K., Balaz, P., 1996. Reactivity of mechanically activated chalcopyrite. Int. J. Miner. Process. 44–45, 197–208.

Tkacova, K., Heegn, H., Stevulova, N., 1987. Changes in structure and enthalpy of carbonates and quartz accompanying grinding in air and aqueous environments. Powder Technol. 52, 161–166.

Tkacova, K., Heegn, H., Stevulova, N., 1993. Energy transfer and conversation during comminution and mechanical activation. Int. J. Miner. Process. 40, 17–31.

Tromans, D., Meech, J.A., 2001. Enhanced dissolution of minerals: stored energy, amorphism and mechanical activation. Miner. Eng. 14 (11), 1359–1377.

Ungar, T., Borbely, A., 1996. The effect of dislocation contrast on X-ray line broadening: a new approach to the line profile analysis. Appl. Phys. Lett. 69, 3173–3175.

Vives, S., Gaffet, E., Meunier, C., 2004. X-ray diffraction line profile analysis of iron ball milled powders. Mater. Sci. Eng., A Struct. Mater.: Prop. Microstruct. Process. 366, 229–238.

Welham, N.J., 2001. Enhanced dissolution of tantalite/columbite following milling. Int. J. Miner. Process. 61 (3), 145–154.

Welham, N.J., Llewellyn, D.J., 1998. Mechanical enhancement of the dissolution of ilmenite. Miner. Eng. 11 (9), 827–841.

Williamson, G.K., Smallman, R.E., 1956. Dislocation densities in some annealed and cold-worked metals from measurements on the X-ray Debye–Scherrer spectrum. Philos. Mag. 1, 34–45.

Zdujic, M., Jovalekic, C., Karanovic, Lj., Mitric, M., Poleti, D., Skala, D., 1998. Mechanochemical treatment of α-Fe_2O_3 powder in air and atmosphere. Mater. Sci. Eng., A Struct. Mater.: Prop. Microstruct. Process. 245, 109–117.

Zhang, Q., Kasai, E., Saito, F., 1996. Mechanochemical changes in gypsum when dry ground with hydrated minerals. Powder Technol. 87, 67–71.

Zoltan Juhasz, A., 1998. Aspects of mechanochemical activation in terms of comminution theory. Colloids Surf., A Physicochem. Eng. Asp. 141, 449–462.

Paper III

Changes in the Structure of Hematite by Extended Dry Grinding in Relation to Imposed Stress Energy

Parviz Pourghahramani and Eric Forssberg

Changes in the Structure of Hematite by Extended Dry Grinding in Relation to Imposed Stress Energy

Parviz Pourghahramani[*] and Eric Forssberg

Division of Mineral Processing, Luleå University of Technology, Luleå, Sweden

Abstract

The effect of extended dry milling in different mills on the structural changes of hematite concentrate has been investigated using a combination analysis of XRD line broadening, BET and particle size measurements. Structural changes were followed by XRD line broadening analysis using integral breadth method and Warren-Averbach approach. For analysis, the stress energy was estimated by considering different grinding variables in different mills and changes in the structure discussed in terms of stress energy.

Within comparable range of stress energy, lower BET surface area was produced by grinding in the vibratory mill. The maximum surface area increased to 18.4 m^2/g in the vibratory mill after releasing 51300 kJ/kg energy. The conversion of the 80% of initial hematite to amorphous phase during extended dry grinding by tumbling, planetary and vibratory mills, needs 4000, 8500 and 50000 kJ/kg energy respectively. It was understood that vibratory mill introduces the minimum lattice strain and gives the largest crystallites when applying the same level of stress energy. The smallest crystallites with grinding in tumbling, vibratory and planetary mills were obtained about 17.3, 13.5 and 5.6 nm after releasing 5230, 51300 and 15600 kJ/kg respectively. For these levels of stress energy, in turn, the microstrain $< \varepsilon_{L=10nm}^2 >^{1/2}$ exceeds $4.4 \times 10^{-3}, 3.9 \times 10^{-3}$ and 5.3×10^{-3}.

It was further revealed that higher concentrations of defects (Amorphization and excess energy) per unit surface area were induced by grinding in the planetary and tumbling mills. A theoretical calculation of the energy contribution to the long-lived defects indicated that products from tumbling and planetary mills have higher excess energy compared to the products from vibratory mill for the same stress energy. The maximum theoretical excess energy was estimated about 75.4, 80.0 and 81.3 kJ per mole of the ground hematite with tumbling, vibratory and planetary mills after releasing 5230, 51300 and 15600 kJ/kg of stress energy respectively. Grinding in vibratory mill needs much more energy to reach the same effect as the other used mills. A comparison of specific energy input and stress energy among the used mills points out that for generation of the same levels of stress energy, the planetary mill consumes more energy than the other used mills.

Keywords: Dry grinding, stress energy, structural changes, mechanical activation, hematite, Grinding methods

---

[*] Corresponding author: Tel:+46 920 491313; fax:+46 92097364
E-mail address: Parviz.Pourghahramani@ltu.se

1. Introduction

The production and properties of ultrafine iron oxides continue to attract considerable interest and attention because of their importance in various technologies. Part of this interest arises from the fact that ball milling is a novel technique for the preparation of new materials and phases and it can be used successfully for changing structures and improving properties of materials.

The application of high energy mills (such as planetary mill, vibratory mill, and tumbling mill or jet mill) allows a dramatic change of the structure and surface properties of solids to be induced [1,2]. Mechanical treatment in a high energy mill generates a stress field within solids. Stress relaxation can occur via several channels: (1) heat release, (2) development of surface area as a result of brittle fracture of the particles, (3) generation of various sorts of structural defects and (4) stimulation of chemical reaction within solids. All relaxation channels cause changes in the reactivity of the solid substance under treatment, which is why the resulting action is called mechanical activation [3]. The concentration of the mechanically induced defects and their spatial distribution depend upon the condition of the energy transfer in the mill. The concentration and distribution of the mechanically induced defects can be also influenced by varying the external conditions of stress. The creation of defects enhances the stored energy (enthalpy) in the solids and consequently causes a decrease of activation barrier for the process and/or subsequent processes [4].

A large number of studies have been devoted to the understanding of the influence of the grinding variables and conditions on the structural changes of mechanically-activated material. Structural changes of inorganic oxides have been shown to be intensified with increasing grinding media density, acceleration and duration of milling in a planetary mill [5]. It has been further reported that the crystallite size decreased exponentially with increasing milling time and the strain increased by extending activation time during mechanical activation of ilmenite [6]. A comparative study of the influence of Attritor, Ball and vibratory mills on the reactivity of sulphide minerals was carried out by Balaz et al. [7]. $\gamma - Fe_2o_3$ samples ground with smaller amplitude in a vibratory mill showed higher reactivity [8]. Among the various factors controlling defect development, the mill power and the efficiency of the energy transfer in the mill are the most important. On the other hand, grinding variables and conditions diverge widely through literatures; and therefore the direct comparison of mills and their efficiency are complicated tasks. Even comparing structural changes data on the same material obtained using different equipment or mill parameters is difficult. For example, the production of BET surface area around 3 m^2/g took about three hours using a planetary mill and less than one hour with a vibratory mill [9]. The question is how to compare the different mill effects on structure changes and at the same time consider most of the grinding variables. Direct comparison of mills will be possible, if the efficiency and ability of mills in transferring energy to the particles being ground are known.

However, the measurement of the efficiency of mills in energy transfer is really a complicated task; because the energy transfer in the course of grinding of particulate system takes place in three stages:

(1) The conversion of kinetic energy of drive to the grinding medium characterized by the effectiveness of a mill itself as the energy transformer.

(2) Transferring of the mechanical action to the particles being ground and the effect of grinding intensity on the efficiency of energy transferring from grinding medium to treated

solids. If the energy input is too high, the energy utilization decreases with increasing of grinding intensity.

(3) Transferring of energy taken up by a treated substance into the actual result of treatment [2, 10].

On the other hand, the efficiency of mills in energy transferring and evaluation of grinding intensity have not been adequately established as far as we know. In this case, some generalized factors are proposed by Heegn [11, 12] to characterize kinetic energy of grinding as a method for comparison of different mills. Although these considerations are based on a very simple model, they will be helpful for a better understanding of the influence of different mills and operating parameters on mechanical activation results and we used those generalized factors in this paper for comparison of mills.

The aim of this study is to investigate mechanically-induced changes in the hematite structure during extended dry milling using different mills. This is another way of comparing of different mills with respect to stress energy in various mills. Several microstructural characteristics like lattice strain, amorphization, crystallite size and integral breadths of XRD diffraction lines etc obtained using line profile analysis (LPA). The obtained parameters are correlated with stress energy to distinguish and interpret the differences among the used mills with considering grinding variables simultaneously instead of individual variables to gain insight into mill efficiency.

2. Experimental

In this section, the grinding condition and characterization methods are described.

2.1. Grinding

Dry grinding tests were carried out using three mills, vibratory, tumbling and planetary mills, in air atmosphere. Steel media was used as grinding bodies with dimensions between 22.2 mm and 6 mm with bulk density of $4.875\, g/cm^3$. The grinding tests were performed in closed condition, i.e., the lids of the mills were kept bolted during the grinding. The media surface was determined from the number and dimension of the grinding media. The media surface levels were set to 1 and 4 m^2 per kg of hematite and the related ball to powder weight ratio was recorded. The grinding tests were extended up to 9 hours. Among the used mills, only the vibratory mill had plastic liner. The grinding experimental conditions are given in Table 1.

Table 1. *Experimental milling conditions and mill types.*

Milling conditions	Tumbling	Vibratory	Planetary
Media filling *(%)*	38.9	70	23.4
Weight of grinding bodies *(kg)*	24.375	33.160	1.031
Ball to powder weight ratio	16.77:1 67:1	16.92:1 67.68:1	19.1:1 76.34:1
Media surface (m^2/kg)	1 4	1 4	1 4
Milling time *(h)*	1 3 9	1 3 9	1 3 9
Number of revolutions *(min⁻¹)*	60	1000	100 (axle) 200 (drum)
Amplitude *(mm)*	--	8	--
L×D *(mm× mm)*	275×245	320×185	87×115
Stress rate (m/s)	2.2	1.67	1.95
Material temperature ($°C$)	24-38	48-105	39-68

The specific energy input consumed by the mills was measured after finishing each run of grinding tests by an electrical meter called Micro VIP (Elcontrol Co., Italy). The frequency and amplitude in vibratory grinding and the drum and axle (sun wheel) speed in planetary mill were maintained constant during the experiments. The temperature of the activated hematite in the mill chamber was measured immediately after stopping mill by a thermometer. Each grinding test was performed continuously and independently. To obtain an impression about the intensity of the mechanical stress and to correlate the changes in structure with mechanical stress, the stress energy was calculated using expressions, proposed by Heegn [12], on the basis of the energy or intensity of single impact stressing factor and stressing energy for the sum of impacts:

$$E_{th} = \frac{1}{2}\left(\frac{m_1}{m_2}\right)ntV^2 \qquad (1)$$

where m_1, m_2, n, t and V refer to mass of grinding media, mass of material charge, speed, grinding time and stress rate in the mills respectively. The rate of stress was estimated for planetary and tumbling milling from the gravitational acceleration (tumbling mill b/g=1; planetary mill b/g=1.67) and mill diameter. The rate of stress for vibratory mill determined from the frequency and amplitude (Table 1). The terms b and g denote the acceleration and gravitational acceleration respectively.

2.2. Characterization

Size distributions of the samples were obtained from Laser diffraction analysis using a *CILAS 1064* particle size analyser in liquid mode. From the Laser diffraction measurements, the granulometeric surface area was calculated. The BET specific surface area was measured using the N_2-adsorption technique and a *Flow Sorb II2300* (Micromeretics Co. Ltd., USA) volumetric gas adsorption analyser.

The activated and non-activated hematite was also characterized using X-ray powder diffraction (XRD). The XRD analysis was performed using a *Siemens D5000* powder diffractometer with Bragg-Brentano geometry equipped with a curved graphite monochromator in the diffracted beam arm and using Cu Kα ($\lambda = 0.1546\,nm$) radiation (Siemens, Germany). The XRD patterns of samples were recorded in the range $2\theta = 10 - 90°$ using a step size of $0.02°$ and a counting time of 5 s per step. The same procedure was made for standard reference sample LaB$_6$, a standard proposed by the National Institute of Standards and Technology of USA (NIST), to remove the instrumental effect from the observed profile broadening.

The eight most intensive reflection peaks of hematite were considered for further characterization using the line profile analysis (LPA), known as line broadening technique. The Profile software [13] was used in profile fitting procedure to extract the line broadening characteristics. For this purpose, the Pseudo-Voigt line shape function, a linear combination of Cauchy and Gaussian line shape function, was fitted to the resulted XRD diffraction patterns. For each adjusted line profile, the following parameters were obtained:

(1) The maximum height of the peak (I_{max})

(2) The integral breadth of line profile ($\beta = A/I_0$ where A is the peak area)

(3) The full-width at half of maximum (FWHM)

(4) The mixing factor (η) of Lorentzian and Gaussian functions in the adjusted Pseudo-Voigt function for measured XRD patterns.

(5) The peaks position (2θ)

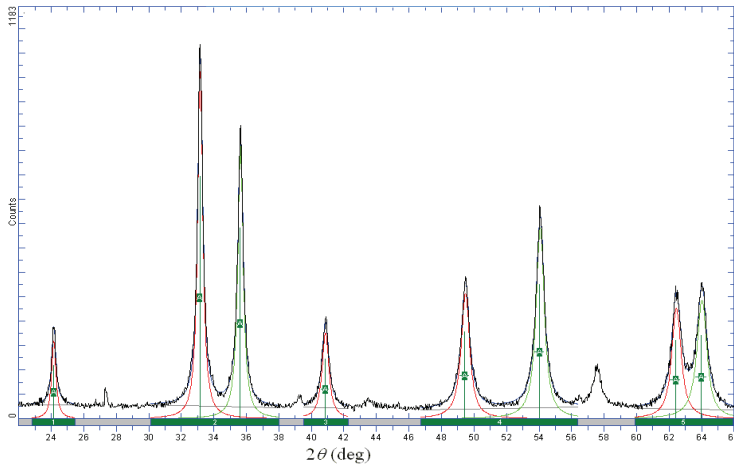An example of profile fitting is given in Fig. 1.

Fig. 1. *An example of profile fitting in which the Pseudo-Voigt function fitted to the XRD pattern of hematite ground after releasing 51300 kJ/kg stress energy in the vibratory mill.*

The physically-broadened lines and integral breadths of the XRD diffraction patterns were obtained after removing the instrumental broadening from XRD line breadths by the standard sample, LaB_6, according to the Halder-Wagner [14] approximation. The degree of amorphization of the samples was determined from X-ray diffraction patterns. For this proposes, the degree of crystallinity was defined as:

$$X = \frac{U_0}{I_0} \times \frac{I_x}{U_X} \times 100 \qquad (2)$$

where U_0 and U_x refer to the background of non-activated sample and activated sample, while I_0 and I_x are integral intensities of diffraction lines of non-activated sample and activated sample. The degree of amorphization (content of X-ray amorphous phase) is defined by equation [15]:

$$A = 100 - X \qquad (3)$$

5

For the deconvolution of the strain and crystallite contributions, the Warren-Averbach approach [16] was used in the [012] direction. Consequently, the lattice stain and crystallite size (surface weighted) were calculated. The total stored energy (enthalpy) in mechanically-activated hematite concentrate was obtained by adding up the three sources of energy contributing to defect structures. The expressions and more information regarding the line broadening analysis were given in previous works [17].

3. Material

High purity of natural hematite concentrate from LKAB (Luossavaara Kiirunavaara Aktiebolag) company in Sweden was used in this study. The particle size analysis of hematite concentrate indicated a particle size distribution of 90% $<110\,\mu m$, 50 %$< 46\,\mu m$ and a 10% $<2.5\,\mu m$. The chemical analysis showed that initial hematite powder contained 97.91% Fe_2O_3, 0.73% Al_2O_3, 0.73% SiO_2, 0.26% TiO_2, 0.20% MgO, 0.022% MnO, and 0.088% P_2O_5. The BET measurements gave a specific surface area of $0.59\,m^2/g$. The density of the starting material was calculated about $5240\,kg/m^3$ using a Pycnometer (Micromeretics Co. Ltd., USA). The XRD patterns showed only the hematite reflections.

4. Results and discussion

4.1. Surface area changes by milling

The mechanical activation of materials is accompanied by disintegration and generation of fresh previously-unexposed surfaces. The size distribution and the specific surface area also depend on the secondary processes like aggregation and agglomeration [18]. Fig. 2 shows how the BET surface area and granulometric surface area change with stress energy in different mills.

It is obvious that the rate of new surface formation depends on both applied stress energy and the types of mills. The BET surface area shows an increasing trend, especially at lower levels of stress energy. The BET surface area continues to increase during the intensive grinding stages when hematite is subjected to the milling in tumbling and vibratory mills. On the other hand, the BET surface area of the ground samples in the vibratory mill increases sharply at higher level of stress energy. With growing stress energy, the products of planetary mill produce marginally higher specific surface area than the products of tumbling mill as opposed to the initial stage of milling bearing lower intensity. However, the specific surface area in planetary doesn't follow a clear trend with stress energy. As discussed in previous work [9], the agglomeration of particles in planetary mill occurred in two stages including under lower media surface and higher media surface after three and one hours of milling respectively. Thus, the agglomeration at different stages disturbs the trend of BET surface area changes in terms of stress energy. It can be also concluded from the changes in the granulometric surface area as shown in Fig. 2b. The granulometric surface area increases at lower levels of stress energy in tumbling and vibratory milling operations. As the grinding progresses, the granulometric surface area tends to decrease, indicating the formation of agglomerates among particles. The agglomerates productions take place after releasing energy of 1740 and 12800 kJ/kg in the tumbling and vibratory mills respectively. It can be further concluded that the BET surface area increases in spite of the agglomeration of particles. Therefore, the agglomeration with available pores (soft agglomerates) occurred in tumbling and vibratory mill at intensive grinding condition. The agglomeration of the particles during extended dry

grinding was reported for sulphide minerals [1], oxide minerals [2], and olivine [19]. This behavior is common for dry grinding and is usually explained by agglomeration of the structurally modified particles following the initial reduction of particle size. This is because of the tendency of the activated material to reduce their surface free energy.
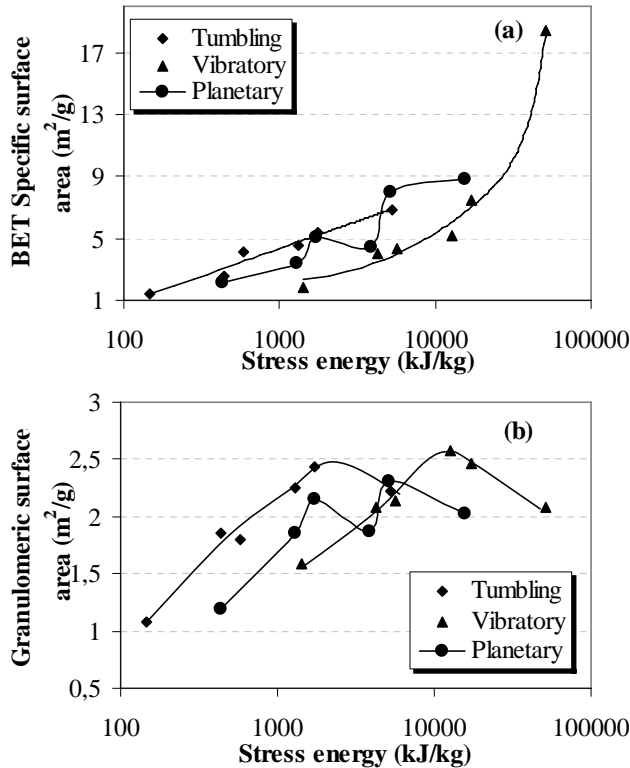

Fig. 2. *Change in specific surface area (a) and granulometric surface area (b) in different mills as a function of stress energy.*

In addition, the vibratory mill products that obtained at certain stress energy produce smaller specific surface area than the other mills. As a result, the tumbling and planetary mills show roughly higher efficiency in the production of a specific surface area than vibratory mill at certain stress energy levels. The maximum specific surface area was attained about 18.4 m^2/g for the ground sample in the vibratory mill after energy releasing around 51300 kJ/kg. The maximum BET surface area in the products of the planetary and tumbling mills were ranged with the values of 8.8 and 6.8 m^2/g after releasing 15600 and 5230 kJ/kg energy respectively. It can be further understood that that the production of unit surface area in the vibratory mill needs to release more energy than other mills.

4.2. XRD diffraction

The structural changes and the characterization of the microstructure characters were investigated using XRD analysis. The X-ray diffraction patterns were collected for all activated and non-activated samples. An example of the XRD patterns is given in Fig. 3 for comparison.
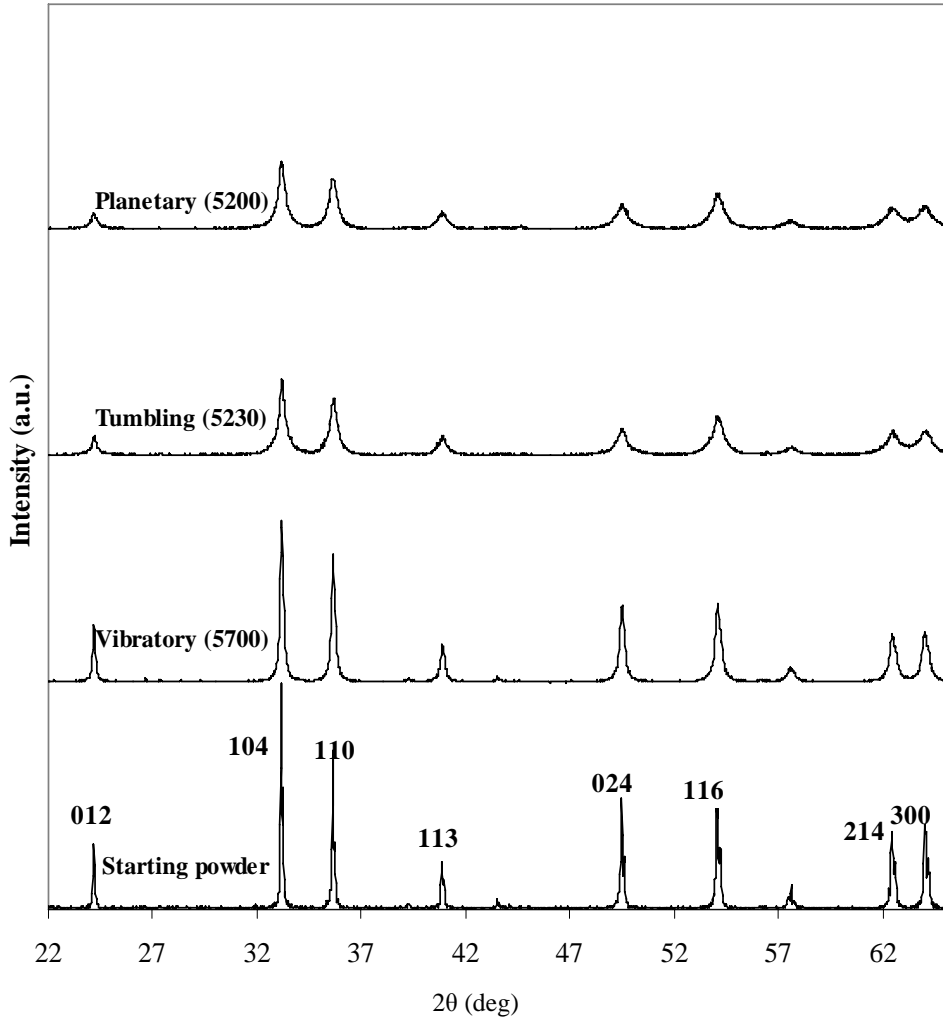

Fig. 3. *The XRD patterns of the starting and milled samples in different grinding devices. The values in parentheses correspond to the stress energy.*

The diffraction peaks for mechanically-activated samples are lower and broader than of those for non-activated samples, mainly due to a disordering process of hematite crystal structure by intensive grinding. The reduction of diffraction peaks intensities implies the formation of amorphous material. The decrease of X-ray diffraction intensities is accompanied by a general broadening of the XRD patterns. The increase of the XRD line breadths is due to the plastic deformation and disintegration of hematite. The XRD patterns showed only the

hematite reflections, indicating that hematite did not undergo significant reaction and phase changes. The presence of small, but remarkable, reflection peaks after intensive grinding in the grinding mills can be taken as a further indication of the high milling resistance and mechanical strength of the submicron hematite crystallites. Regarding the effect of different mills, it can be observed that planetary and tumbling mills bring about weaker and broader peaks than vibratory mill despite the release of larger stress energy in the vibratory mill.

4.3. The effect of grinding on the physical XRD line breadths

For quantitative comparison of the influence of the grinding mills on the alteration of the hematite structure, further investigations were followed by profile fitting technique. After adjusting a proper line shape (Pseudo-Voigt) for XRD diffraction profiles, the physical integral breadths of the reflection peaks were calculated. The physical integral breadth for (104) reflection and the average physical line breadths obtained from the eight most intensive reflection peaks of hematite were considered for comparison. The obtained results are exemplified in Fig. 4 in relation to applied stress energy.
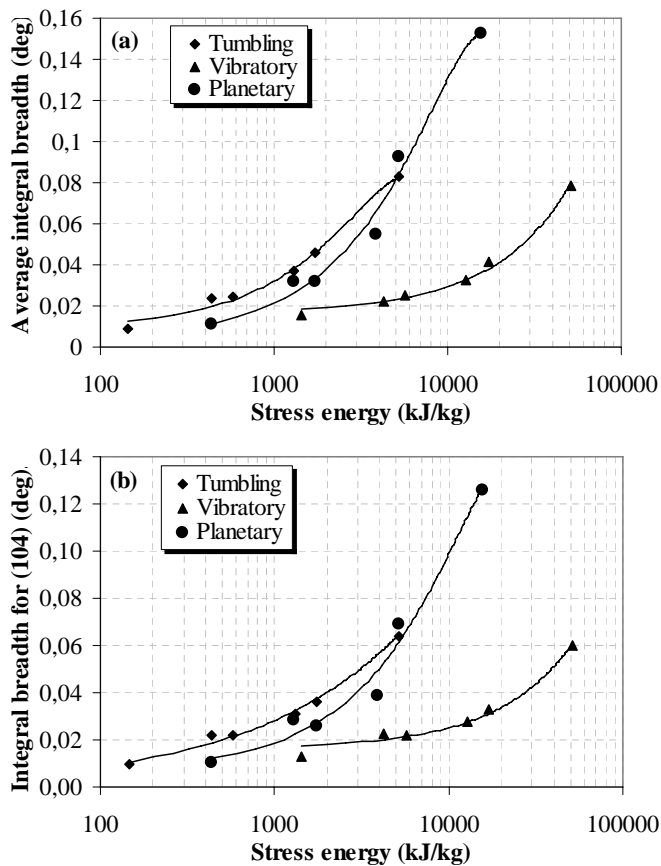

Fig. 4. *The comparison of the physical integral breadth for the ground hematite in different mills for the (104) reflection (a) and the average integral breadth (b).*

It should be reminded that both lattice strain and crystallites size components are contributing to the line breadths which will be resolved later for obtaining the microstructure characters. The plots for the reflection (014) and average physical integral breadths displayed similar trends. This also stands for other reflections, implying that all eight studied lattice faces are disordered during mechanical stressing of hematite. After releasing 5230, 51300 and 15600 kJ/kg energy in the tumbling, vibratory and planetary mills, the broadening of the (014) reflection increased to 0.0639, 0. 0598 and 0.1260 degree respectively.

The development of the integral breadth vs. stress energy in various milling methods can be observed in Fig. 4. The broadening of the diffraction lines at lower levels of the stress energy develops steadily and continues to increase sharply with growing stress energy whatever milling machines used. The curve trends give evidence to more plastic deformation and disordering of the hematite lattice in the intensive grinding conditions. The influence of the mills is also reflected on the plots as well. The tumbling mill brings about approximately more plastic deformation and/or structural changes at the initial stages of milling. As the milling intensity increases, the broadening resulted from the planetary milling exceeds the broadening obtained from the tumbling milling. For a given stress energy, the vibratory mill caused far less broadening in the XRD diffraction patterns. The difference of both tumbling and planetary mills with the vibratory mill becomes more distinguished as the stress energy increases. This may be related to the fact that most of grinding energy in intensive grinding stages are used for establishment and development of plastic deformation rather than grinding energy in the initial stages of milling in which a part of energy is consumed for size reduction process. In other words, when grinding proceeds into ultrafine grinding range at intensive grinding, the stress energy is used mainly for creating structure defects not size reduction. The reduction of XRD diffraction intensities and the broadening of different peaks appear to be the common X-ray diffraction characteristics of the dry milled hematite. The minimum average broadening about 0.0087 was attained in the tumbling mill with 145 kJ/kg stress energy. The maximum average broadening was obtained from planetary milling around 0.1522 degree applying 15600 kJ/kg energy.

4.4. The degree of amorphization

In this section, the average relative intensity of the reflection peaks obtained from the eight most intensive reflection peaks of the ground hematite and the amorphization degree of hematite are studied. As discussed, the intensity of XRD patterns reduces during mechanical treatment of hematite because of the formation of the amorphous material. The obtained results are depicted in Fig. 5. The diffraction peaks show a progressive reduction in intensity when comparing with the starting powder diffractions. The tumbling and planetary mills bring about much more reduction in the intensity of the X-ray diffraction peaks than the vibratory mill with certain stress energy. The reduction of XRD diffraction intensities is intensified with increasing of the grinding intensity.
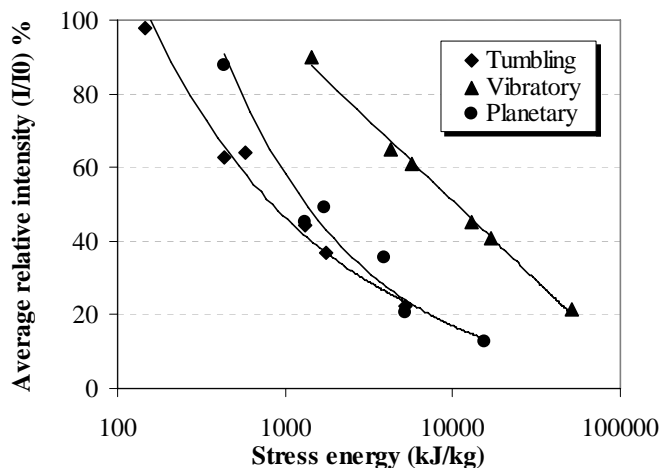
Fig. 5. *The effect of grinding mills on the intensity reduction of the reflection peaks. Terms I and I_0 refer to the peak intensity of the milled and starting samples respectively.*

From the intensity of the reflection peaks and their background, the degree of X-ray amorphization is estimated according to equation (3) and the results are depicted in Fig. 6.
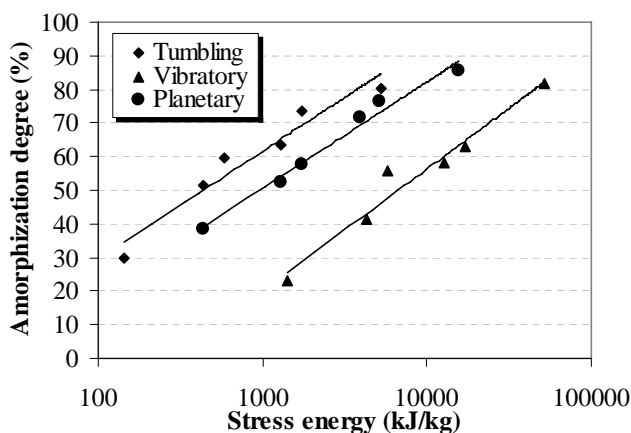

Fig. 6. *The content of X-ray amorphous phase in different milling environment as a function of stress energy.*

The content of X-ray amorphous phase in hematite depends on both grinding mill and stress energy field. The portion of X-ray amorphous phase in the ground hematite with tumbling mill is even higher than of that ground hematite in the planetary mill for a given stress energy. The fraction of the X-ray amorphization increases steadily with growing amount of grinding work despite the particle size reduction in mills and the BET surface area values during the grinding in the planetary mill. These results are in line with relative intensity reduction as well. The amorphization degree increased to 80, 82 and 86% by grinding in the tumbling, vibratory and planetary mills respectively, after releasing 5230, 51300 and 15600 kJ/kg of energy. These results show that more energy is needed in the vibratory and planetary mills

than tumbling mill to produce the same amorphization degree. The increase of X-ray amorphous phase due to intensive milling was reported for calcite, quartz and magnesite [20, 21] and sulphide minerals [2]. The amorphization is in fact a highly distorted periodicity of lattice elements, and it is often characterized as a short range order in contrast to the long order of a fully crystalline structure.

4.5. Microstructural characteristics

To obtain the microstructural characteristics, the Warren-Averbach method based on Fourier analysis, which can precisely determine microstructure characters [22], was used for direction [012]. In this method, the experimentally observed broadening of the line profile was corrected for instrumental effects using Stokes deconvolution [23] and Warren-Averbach method. From the Warren-Averbach method, We calculated the root mean square strain (RMSS), $< \varepsilon_L^2 >^{1/2}$, and surface weighted crystallite. The surface weighted crystallite size of the ground samples in the mills are compared in Fig. 7.
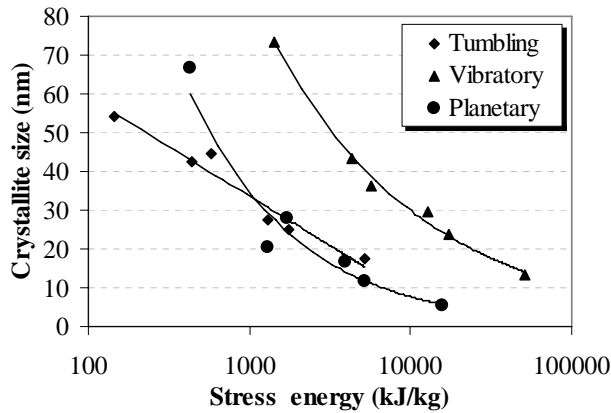

Fig. 7. *Variations of the surface weighted crystallite size in [012] direction with milling in different mills as a function of stress energy.*

A large difference exists between the obtained crystallite sizes from vibratory mill and other mills used. It is evident that the ground samples in the vibratory mill have larger crystallites than the ground samples both in the tumbling and planetary mills within comparable range of stress energy. It can be observed from Fig.7 that the planetary mill products yield marginally smaller crystallite than tumbling mill when hematite is subjected to intensive grinding in contrary to less intensive milling stage. The planetary mill gives larger crystallites than tumbling mill in the initial stages of milling. It seems that the hindering of grinding media because of higher powder to ball weight ratio prevent the refinement of microstructure characters in the sample ground in the initial stages of milling in the planetary mill. We can draw a conclusion that the largest crystallites are resulted from the milling in the vibratory mill at the same stress energy level. With the planetary, tumbling and vibratory mills, the hematite crystallites refined up to the values of 5.6, 17.3 and 13.5 nm, respectively; after receiving the stress energy levels to the values of 15600, 5230 and 51300 kJ/kg during grinding in mills.

The root mean square strain values $< \varepsilon^2_{L=10nm} >^{1/2}$ for activated hematite in mills are displayed in Fig. 8.

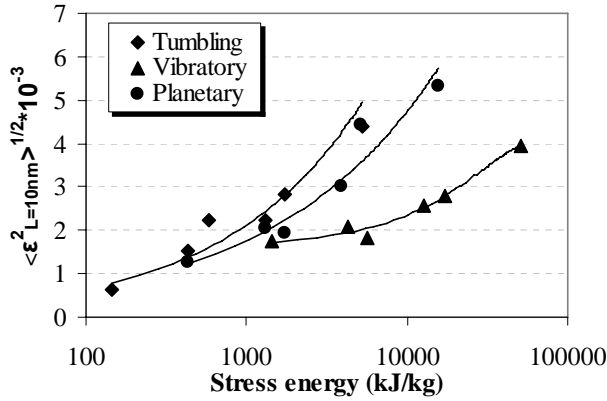**Fig. 8.** *Variations of the lattice strain ($< \varepsilon^2_{L=10nm} >^{1/2}$) values in different grinding machines vs. stress energy.*

At lower levels of stress energy, there is minor difference among the mills in deformation of hematite lattice; while with growing the grinding intensity the difference becomes greater. With a first approximation, distinguished difference among mills starts above 1700 kJ/kg of energy and the magnitude of differences maintains to increase as the stress energy intensifies. Changes in the microstructural characteristics, integral breadth, microstrain and crystallite size reveals that in the initial stages of milling, the particles tend to grind easily. With the progress of milling, the particle size falls into the ductile range and they undergo mainly plastic deformation and consequently the long-lived defects accumulate in the particles being ground. Interestingly, the trend of crystallite size and strain components contributed to the line breadth appears to change in the tumbling and planetary mills as a function of grinding intensity.

The dislocation lines, as line defects, inducted in the case of mechanically-activated material, is another energy carrier in the stressed materials [24, 25] in addition to the generation of fresh new surfaces and phase transformation. The dislocation density summarizes the effects of microstructure characters (crystallite size and strain) of mechanically-stressed material altogether. The minimum dislocation density was determined according to Williamson and Smallman expression [26]. Our results are presented in Fig. 9 as a function of stress energy for ground hematite in various milling devices. Since the dislocation density includes both characters of the lattice strain and crystallite size, the difference among the mills can be easily detected. The lower efficiency of the vibratory mill is pronounced here once again. In other words, to achieve the same effect in vibratory mill, much more energy is needed. These results confirm the previous results. The tumbling mill induced marginally more damage and dislocation defects to hematite lattice than planetary mill at lower levels of stress energy.
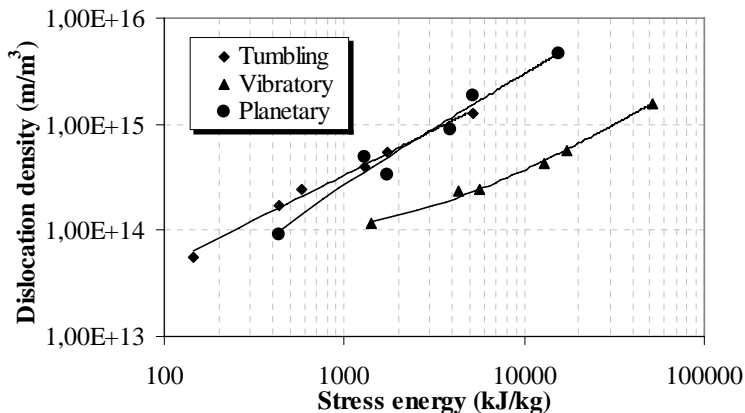
Fig. 9. *Change in dislocation density with the stress energy for mechanically stressed hematite by various mills.*

4.6. The relationship between defect characteristics

Figure 10 shows the variation of amorphization degree and excess energy versus the BET specific surface area in different mills. Generally, a distinguished difference can be observed between tumbling and vibratory mills. According to Fig. 10, it can be seen that the formation of unit surface area in tumbling is associated slightly with a sharper increase in the amorphization degree. The difference between tumbling and planetary mills is negligible. The concentration of defects in the ground hematite with vibratory mill appears to be slightly less than of those in tumbling and planetary mills. Besides, with regard to the rate of stress in mills, structural defects that are vital for mechanical activation are accumulated in the near surface layer for ground hematite in mills.
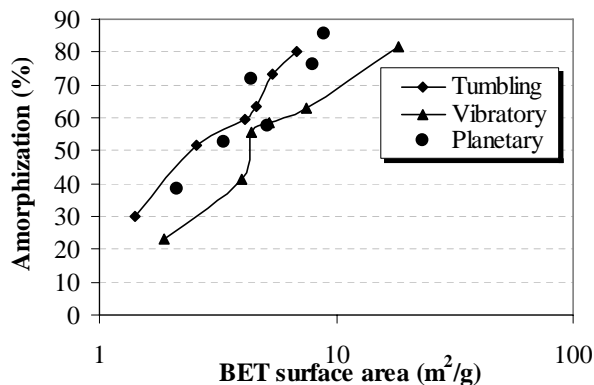

Fig. 10. *X-ray amorphous phase versus specific surface area of hematite samples ground in various mills.*

According to Tkacova [2], the long-lived defects are being equally distributed throughout the bulk of particles when the material is subjected to grinding in mills bearing higher stress rate such as jet mills and high-speed disintegrator. If the material is subjected to the grinding in mills producing lower rate of stress like tumbling and planetary mills, the long-lived defects accumulate preferentially in the near surface layer. This can be assumed as a consequence of

a quasiadiabatic energy accumulation at the mechanical action of shorter duration than the time required for the formation of the critical crack ($t<t_{crit}$). At higher number of loading cycles and substantially slower rates of stress in the three used mills, the defects are accumulated near the surface layer due to the mechanism of cyclic micro plastic deformation. This agrees with the rate of stress in different mills in which the rate of stress set to a comparable range during experiments, varying between 1.7 and 2.2 m/s (table.1).Their differences are at of least important.

4.7. The stored energy contributions to the long-lived defects

For the interpretation of the mechanical activation process, the context between structures and energy–content of the mechanically activated solids and consumed mechanical energy are of important and interest.

Real solids and in particular, nanodisperse or mechanically activated solids, must be calculated with different types and concentrations of defects in meta-stable condition. As a result of previous investigations [24, 25], the defect structures of essential meaning for the energetic condition of the solids are dislocation concentrations with the specific energy ΔH_d, energy contributions of new surface formation ΔH_S and content of newly-formed phases and amorphous fraction ΔH_A. The quantitative estimate of the increase in molar chemical free energy (increase in stored energy or enthalpy) due to dislocation defects has been calculated by expression proposed by Tromans and Meech [27]. Energy fraction of newly-formed phases (our experiments suggested only amorphization, not the formation of other new phases) and specific surface area as a measure for the grain boundary to the surrounding medium were evaluated by equations expressed by Heegn [24]. The stored energy (excess enthalpy) on basis of long-lived defects is compared for various mills as a function of stress energy in Fig.11.
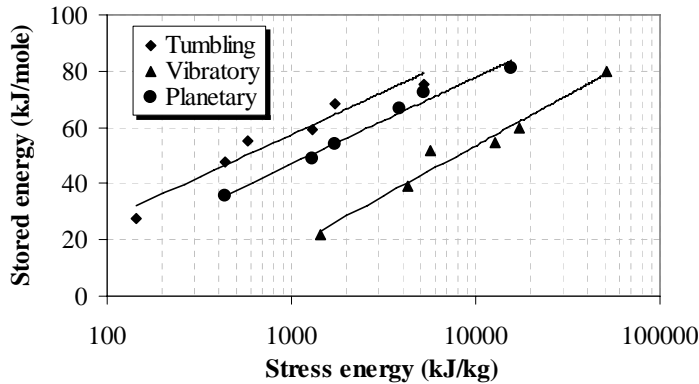

Fig. 11. *The relationship between the stress energy and excess energy of the mechanically activated hematite by different mills.*

Obviously, there is a direct relationship between excess energy and stress energy, i.e. the higher grinding work (stress energy), the more excess energy is stored in hematite. According to Fig. 11, distinguished differences can be observed between vibratory mill and the other two used mills. In other words, for a given stress energy, the activated hematite in the tumbling mill contains higher excess enthalpy (stored energy) and in the vibratory mill has lower

excess energy. For example, to achieve an excess energy in hematite by mechanical treatment of about 60 kJ/mole, the required stress energy in tumbling, planetary and vibratory milling is around 1300, 2800 and 17000 kJ/kg respectively. It is worthwhile to mention that the energy contribution from amorphization or quasi-amorphization to the energy changes at activation amounted to 92-98 % of overall stored energy [9] and subsequently these curves have similar trend as of Fig. 6. These results are in line with the results obtained for quartz, calcite, magnesite, kaolinite and iron [20, 21] and periclase [25]. In agreement with the study by Miyasaka and Senna [28] and Tkacova et al. [29], the excess enthalpy (ΔH_T) can be related to stress energy (W) by the equation:

$$\Delta H_T = bLnW - c \tag{4}$$

where b and c are the constant values. The corresponding equations for different mills are:

$$\Delta H_T = 13.15LnW - 33.38 \qquad\qquad \text{Tumbling mill} \tag{5}$$

$$\Delta H_T = 13.37LnW - 45.38 \qquad\qquad \text{Planetary mill} \tag{6}$$

$$\Delta H_T = 15.58LnW - 89.95 \qquad\qquad \text{Vibratory mill} \tag{7}$$

The correlation coefficients exceed 0.96, suggesting excellent model.

A comparison of mills based on input and stress energy can be seen in Fig. 12. There is a direct relationship between stress energy and specific energy input for mills. This suggests that only a part of specific energy input affects the particles being ground. The planetary mill needs more specific energy input than the other mills to achieve identical stress energy energy. In this sense, the vibratory mill consumes minimum specific energy input to release the same stress energy as the vibratory and planetary mills.
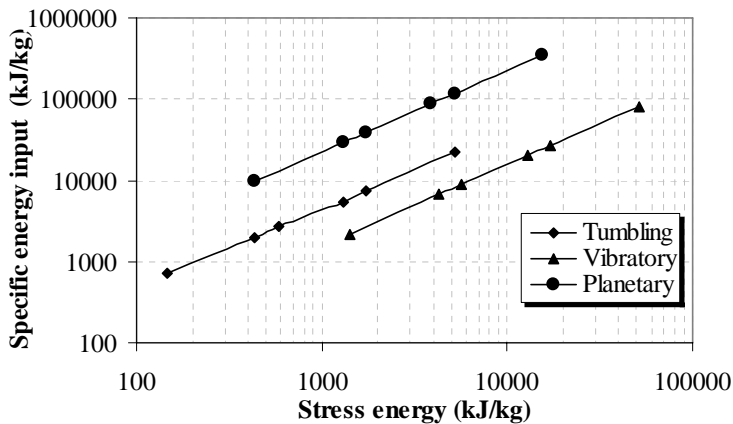

Fig. 12. *The comparison of the specific energy input and stress energy for mills.*

Although these considerations are based on a very simple model, they will be useful for a better understanding of the influence of different mills and operating parameters on grinding results, mechanical activation and induction of microstructure characters in hematite crystal. Another aspect that should be also kept in mind is the potentiality of upscaling of the milling process for application and commercialization. The results suggest that the mechanically-activated hematite in tumbling mill and planetary mill have theoretically higher reactivity than the activated hematite in the vibratory mill. The further study is needed to study the availability of the stored energy in an actual reaction which is addressed by many authors [30-33].

5. Conclusions

It is shown that structural changes characters in different mills can be correlated with stress energy (grinding work), which addresses roughly the grinding intensity. This correlation enables a general understanding of the extended dry grinding behavior of different mills on the induction of structural changes. The grinding in vibratory mill needs much more stress energy to reach the same effect as both tumbling and planetary mills. It was revealed that the planetary mill consumes more specific energy input to reach the same level of stress energy as vibratory and/or tumbling mills. This is related to the scale and capacity of the used mills and is of another aspect that has to be considered in practical applications. The obtained results show that tumbling and planetary mills favor the induction of structural changes and subsequently the enhancement of reactivity irrespective to capacity and specific energy input and stress energy. Comparing the tumbling and planetary mills in terms of specific energy input and capacity, the tumbling mill seems promising device for activation. In other words, tumbling mill shows higher efficiency than the other used mills with regard to grinding intensity. It should be noted that the planetary mill used in this study had less intensity than the others often used in the literature.

Experiments for measuring the actual reactivity of the mechanically-activated hematite in mills are recommended for verifying and correlating with structural changes as the parameters studied so far. Feasibility studies after actual reactivity tests are essential to evaluate accurately their applicability.

Acknowledgments

References

[1] P. Balaz, Extractive Metallurgy of Activated minerals, Elsevier (2000), Amesterdam.
[2] K. Tkacova, Mechanical Activation of Minerals, Elsevier (1989), Amesterdam.
[3] V.V. Boldyrev, K. Tkacova, Mechanochemistry of solids: Past, Present, and Prospects, Journal of Material synthesis and Processing 8 (Nos.3/4) (2000) 121-132.
[4] U. Steinike, K. Tkacova, Mechanochemistry of solids-Real structure and Reactivity, Journal of Material synthesis and Processing 8 (Nos.3/4) (2000) 197-203.
[5] G.R. Karagedov, N.Z. Lyakhov, Mechanochemical grinding of inorganic oxides, Kona 21 (2003) 76-86.

[6] N.J. Welham, D.J. Llewellyn, Mechanical enhancement of the dissolution of ilmenite, Mineral Engineering 11 (9) (1998) 827-841.

[7] P. Balaz, H.J. Huhn, K. Tkacova, H. Heegn, Laugungsverhalten und physico-chemische Eigenschaften von in unterschiedlichen Mullen vorbehandeltem chalkopyrite, Erzmetall 41(1988) 325-331.

[8] M. Senna., Criteria of activation of powdery materials by a Preliminary mechanical treatment, Kona 1(1983) 48-52.

[9] P. Pourghahramani, E. Forssberg, Comparative Study of Microstructural Characteristics and Stored Energy of Mechanically Activated Hematite in Different Grinding Environments, International Journal of Mineral Processing, in press.

[10] A.S. Kheifets, I.J, Lin, Energy transformations in a planetary grinding mill Part1; General treatment and model design, International Journal of Mineral Processing 47(1996) 1-19.

[11] H. Heegn, Stressing of Solids by Fine Grinding and Mechanical Activation, Proceedings of 1st International Conference on Mechanochemistry, Kosice, Slovakia (1993), pp. 127-133.

[12] H. Heegn, Mechanical induced changes in structure and properties of solids, Proceedings of the XXI International Mineral Processing Congress, Part A4, Comminution , Classification and Agglomeration, Rome, Italy (2000), pp.52-59.

[13] Siemens AG, Diffrac plus profile fitting manual program (1996), pp. 23-26.

[14] N.C. Halder, C.N.J. Wagner, Separation of particle size and lattice strain in integral breadth measurements, Acta Crystallography 20 (1966) 312-313.

[15] S.M. Ohlberg, D.W. Strickler, Determination of Percent Crystallinity of Partly Devitrified Glass by X-Ray Diffraction, Journal of the American Ceramic Society 45 (1962) 170-171.

[16] B.E. Warren, X-ray diffraction, Addison-Wesley (1969), New York

[17] P. Pourghahramani, E. Forssberg, Microstructure Characterization of Mechanically Activated Hematite using XRD Line Broadening, International Journal of Mineral Processing, in press.

[18] A.Z. Juhasz, Mechanochemical activation of silicate minerals by dry fine grinding, *Aufbereitungs-Technik* 10 (1974) 558–562.

[19] R.A. Kleiv, M. Thornhill, Mechanical activation of olivine, Minerals Engineering, 2005, forthcoming

[20] H. Heegn, Changes in the properties of solids during mechanical activation and fine grinding. In: *Sc.D. Thesis*, Research Institute of Mineral Processing of the Academy of the GDR, Freiberg (in German) (1986).

[21] H. Heegn, Concerning some fundamentals of fine grinding. In: Leschonski, K., Editor, 1986. *Proc. 1st World Congress on Particle Technology, Part II. Comminution*, Nürnberger Messe und Austellungsgesellschaft, Nürnberg (1986), pp. 63–67.

[22] D. Balzar, Voigt-Function Model in Diffraction Line-Broadening Analysis, in *Defect and Microstructure Analysis from Diffraction*, edited by R.L. Snyder, H.J., Oxford university (1999), New York, pp. 94-126.

[23] A.R. Stokes, A numerical Fourier-analysis method for the correction of widths and shapes of lines on X-ray powder photographs, Proceedings of the physical society 61 (1948), London, pp. 382-391.

[24] H. Heegn, Effect of fine grinding on structure and energy content of solids, in: Proc.of 6th POWRECH (1979), Birmingham, pp. 61-69.

[25] K. Tkacova, H. Heegn, N. Stevulova., Energy transfer and conversation during comminution and mechanical activation, International journal of mineral processing 40 (1993) 17-31.

[26] G.K. Williamson, R.E. Smallman, Dislocation densities in some annealed and cold-worked metals from measurements on the X-ray Debye-Scherrer spectrum, Philosophical Magazine 1 (1956) 34-45.

[27] D. Tromans, J.A. Meech, Enhanced dissolution of minerals: stored energy, amorphism and mechanical activation, Mineral Engineering 14(11) (2001) 1359-1377.

[28] K. Miyasaka, M. Senna, Calorimetric and thermoanalytical assessment of mechanically activated $PbCO_3$, Thermochemica Acta 83 (1985) 225-233.

[29] K. Tkacova, H. Heegn. N. Stevulova., Changes in structure and enthalpy of Carbonates and Quartz accompanying grinding in air and aqueous Environments, Powder Technology 52 (1987) 161-166.

[30] M. Senna, The evaluation of activity and reactivity of mechanically treated fine powdered materials, Kona 5 (1987) 76-81.

[31] M. Senna, Determination of effective surface area for the chemical reaction of fine particulate materials, Particle and Particle Systems Characterization 6(1989) 163-167.

[32] K. Tkacova, P. Balaz, Structural and temperature sensitivity of leaching of chalcopyrite with Iron (III) sulphate, Hydrometallurgy 21 (1988) 103-112.

[33] P. Balaz, A. Alacova, M. Achimovicova, J. Ficeriova, E. Godocikova, Mechanochemistry in hydrometallurgy of sulphide minerals Hydrometallurgy 77 (1-2) (2005) 9-17.

Paper IV

Review of applied particle shape descriptors and produced particle shapes in grinding environments. Part I: particle shape descriptors

Parviz Pourghahramani and Eric Forssberg

Taylor & Francis
Taylor & Francis Group

REVIEW OF APPLIED PARTICLE SHAPE DESCRIPTORS AND PRODUCED PARTICLE SHAPES IN GRINDING ENVIRONMENTS. PART I: PARTICLE SHAPE DESCRIPTORS

PARVIZ POURGHAHRAMANI and Eric Forssberg

Division of Mineral Processing, Luleå University of Technology, Luleå, Sweden

The various types of particle shape, morphology, texture, and particle angularity descriptors that are applicable and useful in different grinding methods with respect to various geometric measures existing in image analysis software are presented and reviewed. In addition, some disadvantages of such descriptors are discussed.

Keywords: grinding, conventional particle shape descriptors, morphology

The importance of particle shape and its influence on physical and behavioral properties including packing and fluid interaction (Allen 1990; Zou and Yu 1996), angle of internal friction (Chan and Page 1997), powder flow rate, apparent and tap densities (Carnavas and Page 1994; Hausner 1973), and deformation behavior in the determining of bulk powder properties (Ting et al. 1995), in the use of particles as abrasive and in applications involving the packing in powder compacts, slurry rheology, and flowability and coal particle behavior in combustion (Kaye et al. 2002), have been well known. The shape of particles produced by a different process of wear has been used to assist in identifying the wear

mechanism behind their generation (Raadnui and Roylance 1995; Stachowiak 1998, 2000) and some attempts were made to identify the breakage mechanism during grinding by using shape parameters (Frances et al. 2001; Lecop et al. 1999). One common method of producing particles is by comminution and milling. While it is generally recognized that comminution can lead to changes in particle shape and morphology, relatively few attempts have been made to quantify, correlate, and characterize ground minerals and ores as they relate to comminution processes. In most of the articles included in this survey, the shape and morphology of the ground particles were reported only as a secondary topic. In addition, there is some disagreement on the characterization and evaluation of particle shape in the grinding process because of the lack of widely accepted measures of shape.

Qualitative characterization of particle shape is a relatively easy matter. Visual inspection of particles by comparison with a reference sample shape or standard particles can be performed. However, this kind of characterization does not give much information about particulate behavior. Consequently, quantitative descriptors are necessary.

Although particle shape is inherently a three-dimensional (3-D) attribute, many characterization techniques utilize two-dimensional (2-D) data. Often, this is in the form of a projected or sectional image of the particle under study or a 2-D section of the field of radiation scattered by the particle (German 1984; Ghadiri et al. 1991; Hentschel and Page 2003; Kaye 1998; Stachowiak and Podsiadlo 2001). Shape characterization by analysis of 3-D images is possible, although the collection of accurate data and its reduction to meaningful parameters is considered to be problematic (Hentschel and Page 2003; Stachowiak and Podsiadlo 2001).

Since the characterizations of the ground particle, especially in the case of minerals and ores, need the appropriate shape descriptors and characterization method, in this article, some of shape descriptors with regard to their feature and applicable in the image analysis systems in the present time are reviewed and presented.

GEOMETRICAL PARTICLE FEATURES

Three basic categories of geometric measures exist in particle shape and morphology characterization: particle volume, surface area, and linear distances between particle features. Some examples of geometric

measures and their definition are listed in Table 1. One of the most common geometric measures used frequently in particle shape characterization is Feret diameter, the distance between two parallel tangents. Because of the diameter variations according to different angles of the convex hull of the silhouette, the set of various Feret diameters in image analysis is used with regard to various orientations.

Another well-known geometric measure is the equivalent diameter, the diameter of a sphere or circle with the same physical properties as the irregular particle. Different physical measuring techniques result in the different values of equivalent diameter (Table 1 and Figure 1).

PARTICLE SHAPE DESCRIPTORS

Shape descriptors can describe the shape at different levels of complexity, but they should be invariant from the point of view of object size and position in the image. There are several macroscopical descriptors, of general use for a simple characterization, which are available in most image-analysis packages: elongation, circularity, etc. In addition, some mesoshape descriptors and mathematical methods have been investigated and reported for particle shape characterization. However, mathematical methods such as fractal analysis and Fourier analysis are beyond the scope of this article.

Macro Shape Descriptors

Particle shape often is habitually described by subjective descriptors such as spherical, triangular, cubical, flake-like, fibrous, dendritic, etc. However, such descriptors are often very ambiguous and more robust methods, such as those employing mathematical equations, have to be used in order to describe the particle morphology more precisely (Greg 2001).

Some of the most commonly used shape factors evaluate the deviation of a particle-projected area from that of a sphere or ellipse, as a reference shape, and others with regard to the convexity and concavity of silhouette are presented in Table 2. The elongation (L/B) ratios may be the simplest shape factors derived from microscopic measurements. Elongation grows for the ellipses with an increase in the ratio of the major and secondary axes (Figure 2) (Greg 2001; Mikli et al. 2001). However, since such factors are derived from particles viewed in two dimensions, it is not an adequate descriptor of 3-D particle shape.

Table 1. Some examples of some geometric measures applied in particle shape and morphological characterisation (Greg 2001; Hentschel and Page 2003; Mikli et al. 2001; Muller et al. 2001)

| Geometric measures	Definitions and measurement methods
Feret diameter;	
Vertical, $d_{F,\text{ver}}$	Distance between bottom and top-most image pixels
Horizontal, $d_{F,\text{horiz}}$	Distance between right-and left-most image pixels
Maximum, L ($d_{F,\text{max}}$), F_{max}	Maximum Feret measured for all orientations
Orthogonal to maximum, $L_{90°}$	Feret diameter 90° to maximum Feret
minimum* ($d_{F,\text{min}}$), F_{min}	Minimum Feret measured for all particle orientations
Orthogonal to minimum, $B_{90°}$	Feret diameter 90° to minimum Feret
Mean, D_m ($d_{F,\text{mean}}$)	Mean of Feret diameters for all orientations
Median, F_{med}($d_{F,\text{median}}$)	median of Feret diameters for all orientations
Minimum area bounding rectangle	
Length, A	Longest Feret diameter of the pair (d_F, $d_{F,90°}$), whose product is a maximum over all orientations
Breadth, B	Shortest Feret diameter of the pair (d_F, $d_{F,90°}$), whose product is a minimum over all orientations
Chord length;	
Vertical, $d_{c,\text{horiz}}$	Distance between boundary pixels that intersect a vertical line passing through the particle centroid
Horizontal, $d_{c,\text{horiz}}$	Distance between boundary pixels that intersect a horizontal line passing through the particle centroid
Maximum, c_{max}($d_{c,\text{max}}$)	Maximum chord length for all particle orientations
Orthogonal to Maximum, $C_{\text{max},90°}$ ($d_{C,\text{max},90°}$)	Length of chord 90° to the maximum
Minimum,C_{min}($d_{C,\text{min}}$)	Minimum chord length for all particle orientations
Orthogonal to Minimum,$C_{\text{min},90°}$ ($d_{C,\text{min},90°}$)	Length of chord 90° to the minimum
mean,C_{av} ($d_{C,\text{mean}}$)	Mean of chord length for all orientations
Median, C_{med} ($d_{C,\text{median}}$)	Median of chord length for all orientations
Martin's diameter, MD	Length of the chord that most closely bisects the particle area
Equivalent diameters by comparing to sphere; D_S, D_A, D_V, D_W, and D_{SL}	Equivalent diameter of a sphere with the same surface area, projection area (in a fixed position), volume, settling velocity, and light-scattering intensity, respectively.
Circular equivalent diameter, D_{eq}	Equivalent diameter of a circle with the same area
Perimeter, P	Sum of the distance between successive boundary pixels
Area, S	Total number of pixels in the particle image
Thickness, T	Distance between two planes parallel to the plane of greatest stability and tangential to the surface of the particle
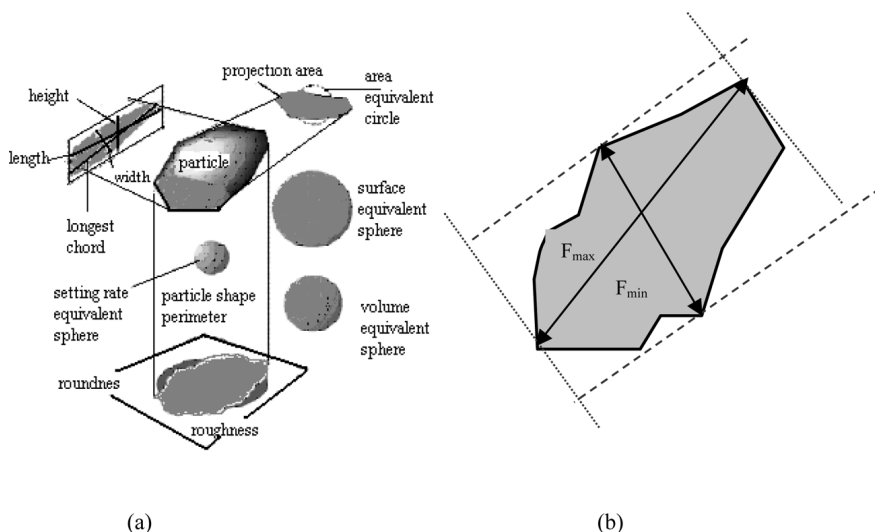
Figure 1. (a) Equivalent diameter and particle shape (Muller et al. 2001) and (b) Feret diameter.

The aspect ratio, sometimes also termed roundness, is a factor dependent upon the orientation of a particle. It follows that a sphere will have an aspect ratio of 1 whatever the orientation and particles of other shapes will exhibit aspect ratios of either <1 or >1. Both low and high values of the aspect ratio indicate an irregularity of a particle shape. Circularity is a factor combining both geometric shape and surface smoothness. A sphere with surface asperities below the level of detection of the employed method of measurement will have a circularity value of 1. A sphere with rough surfaces and particles of any other shapes will possess circularity values >1. The higher the circularity value, the more irregular the shape of the particle. Sphericity, also termed rugosity (Carstensen 1980; Greg 2001), has been used to assess the surface smoothness of lactose particles (Kassem 1990; Greg 2001). However, sphericity also is a combination of particle geometric shape and surface smoothness. A sphere with negligible surface asperities will have a sphericity value of 1, but a sphere with detectable surface asperities and particles of any other shapes could also have sphericity values >1. Particles of the same geometric shape but with different surface smoothness will have different sphericity values and particles with the same surface smoothness but of different geometric shapes will also possess different

Table 2. The most commonly used macroshape descriptors (Carstensen 1980; Frances 2001; Greg 2001; Heywood et al.1970; Kassem 1990; Kulu et al. 1998; Mikli et al. 2001; Otsuka et al. 1988; Pons et al. 1997, 1999; Sasov and Sokolov 1984; Singh 1976; Vivier et al. 1994)

Macro Shape Descriptors		
Shape factor	Formula	Comments
Form factor	$F = P^2/4\pi S$ or $4\pi S/p^2$ or $FR = P/d_A$	Compares the surface of the object S to the surface of the disc of same perimeter p.
Roundness	$RN = 4S/\pi F_{max}^2$ $= D_{eq}/F_{max}$ or $4S/\pi L^2$	Compares the surface of the object S to the surface of the disc of diameter F_{max}
Aspect ratio	$AR = F_{max}/F_{min}$ or L/B	Often used in terms of elongation
Elongation	$EL = L_G/E$	Aspect ratio substitute for a very elongated particle (fiber)
Curl	$Cur = F_{max}/L_G$	Suitable for very elongated objects, suitable
Convexity	$CI = P/P_C$	P_C is the perimeter of the convex bounding polygon
Solidity	$SI = S/S_C$	S_C is the surface of the convex bounding polygon
Compactness	$CO = \sqrt{Roundness}$	Compares the roundness
Extent	$EX = S/(F_{max}F_{min})$	Compares the ratio of surface to multiplication of maximum and minimum Fevet diameters
Relative width	$RW = B/L$ or F_{min}/F_{max}	Higher value indicates less elongated particles
Flatness	$FL = B/T$ or F_{min}/T	Its value is always more than 1 and higher value indicates flatter particles

(*Continued*)

Table 2. Continued

Macro Shape Descriptors		
Shape factor	Formula	Comments
Circularity	$\mathrm{Cir} = P/P_{\mathrm{cir}}$	>1 for any shape except sphere (because sphere is unit)
Sphericity	$\mathrm{Sph} = S/S_{\mathrm{sph}}$	>1 for any shape except sphere (for sphere is unit)
Simplified shape factor	$e_R = \frac{P_{cir}}{P} - \sqrt{1 - \left(\frac{\text{breadth}}{\text{length}}\right)^2}$	Its value may vary between −1 and 1. The smaller the value, the greater the shape irregularity
Shape coefficient	$K_a = Sd_{\mathrm{sph}}/V_p$	Measurement of three-dimensional particle shape and also is a combination of geometric and surface textures
Dispersion	$DP = \log_2(\pi\, ab)$	Dispersion of an ellipse is zero and it grows with the increase of the object' roughness
Irregularity parameter	$IP = D/d$	IP can be applied both to elongated and irregular particles, but it does not allow us to decide whether the particle is elongated or irregular

sphericity values. Thus, sphericity can be used to compare particle surface smoothness only when the particles considered have the same geometric shape (Greg 2001).

The shape coefficient is another common parameter used to determine particle shape (Greg 2001; Singh 1976). This factor is a measurement of 3-D particle shape and also is a combination of geometric shape and surface texture. At a constant volume, any means of increasing surface area, including change in shape and surface smoothness, will
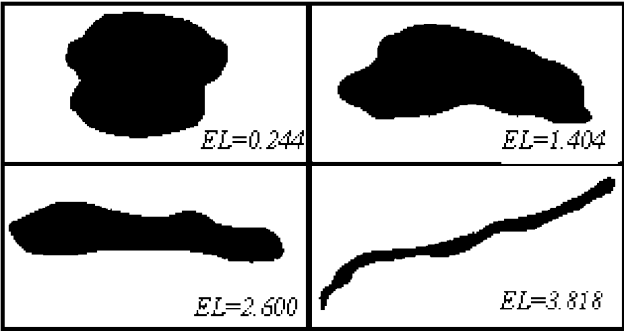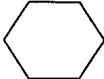
Figure 2. Samples with different values of the elongation *EL* (Mikli et al. 2001).

increase the value of the shape coefficient. If particles have smooth surfaces, the values of shape coefficient will increase from 6 for spherical particles to more than 100 for very thin flakes (Greg 2001; Heywood et al. 1970); the higher the value of the shape coefficient, the more irregular the shape or the rougher the surfaces of the particle.

The form factor, as defined and calculated for various shape in Table 2 and 3, is a 2-D representation of particle shape. It is the shape parameter on which many image analysis techniques are based and, once again, it is a combination of geometric shape and surface smoothness. The value of the shape factor for a perfectly smooth sphere is 1 and the value for any other shape will be less than 1, depending on the geometric shape and surface rugosity of the particle. The lower the value of the shape factor, the more irregular the particle. However, values of the shape factor only vary between 0 and 1 and a large difference in particle morphology will be required to produce a marked change in its absolute value. This may particularly be the case when the particle morphology

Table 3. Shape factors of particles of different form (Mikli 2001)

Shape factor	Configuration				
	◯	⬡	⬡	▢	△
F	1.0	1.055	1.103	1.273	1.654
FR	1.0	1.027	1.050	1.128	1.286
IP	1.0	1.082	1.155	1.414	2.0

deviates distinguishably from a perfect sphere. Thus, the reciprocal of the value, i.e., $P^2/4\pi S$, may be a more appropriate factor to express particle shape since its values can vary from 1 to infinity (Greg 2001).

Apart from the aforementioned shape factors, other factors have also been generated to measure particle shape under specific conditions. For example, the ratio of the diameter of the internal contact sphere to that of the external contact sphere has been used to determine the shape of granules. Wojnar (1999) and Mikli et al. (2001) called this the irregularity parameter (IP) and defined it as $IP = D/d$ (Figure 3a). This factor is able to distinguish between spherical and nonspherical particles, but its application has been limited in the characterization of particles that have small numbers of extremely deep gaps. According to its definition, it is a factor similar to the reciprocal of the elongation ratio. Yet another shape factor has been generated by dividing the actual projected area of a particle by the area of a circle having a diameter equivalent to the maximum projected length (Figure 3b). Such a factor has been employed to determine both geometric shape and surface smoothness of some powder systems (Greg 2001; Otsuka et al. 1988). A well-known descriptor used to characterize particle irregularity is Form factor (called Roundness factor by el Mikli) object. Form factor is defined as (Kulu et al. 1998; Mikli et al. 2001; Sasov and Sokolov 1984)

$$F = P^2/4\pi S. \tag{1}$$

The Form factor of a circle is equal to one. If the object's shape approaches a line segment, it approaches infinity. To characterize the Form factor, sometimes shape factor $FR = 1/F$ is used. The shape factor
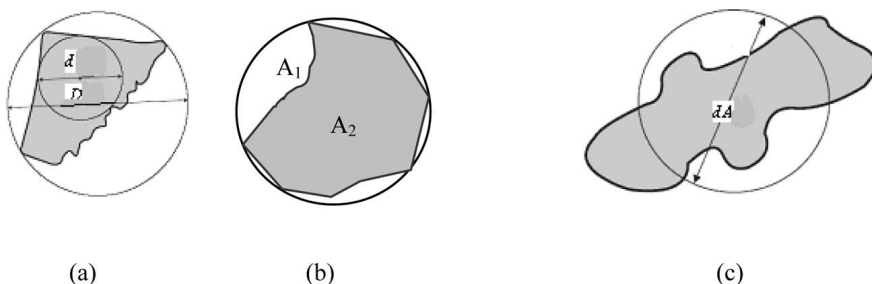

(a) (b) (c)

Figure 3. (a) Morphology study based on the maximum inscribed and minimum circumscribed circles, (b) circle having a diameter equivalent to the maximum projected length, and (c) circle with the same area as the particle (c) (Mikli et al. 2001).

was proposed by Kulu et al. (1998) and Mikli et al. (2001). *FR* was defined by

$$FR = P/d_A \qquad (2)$$

where d_A is the diameter of the circle with the same area as the particle (Figure 3c).

A simplified shape factor, e_R, was devised to estimate the combination of surface asperities and deviation of shape from a circle (Greg 2001; Kulu et al. 1998). This descriptor takes into account both the deviation from circularity and the variation in surface roughness. It can give a value ranging from -1 to 1 and the smaller the value, the greater the shape irregularity.

None of the single shape factors mentioned before can distinguish between geometric shape and surface smoothness. Thus, a combination of these factors has to be employed to differentiate between these two phenomena. Depending on the purpose of measurement, different strategies may be employed. For example, the contribution of geometric shape to the overall sphericity value has to be eliminated when this factor is used to compare surface smoothness of different particles.

Mikli et al. (2001) tried to find new shape descriptors for the characterization of particles.To characterizes particle shape, different shape factors were calculated. Ellipticity parameters were used. Ellipticity can be effectively measured and calculated. To characterize ellipticity, aspect *AS* was used

$$AS = a/b \qquad (3)$$

where a and b are the axes of the Legendre ellipse (Figure 4a). The Legendre ellipse is an ellipse with the center in the object's centroid and with the same geometrical moments up to the second order as the
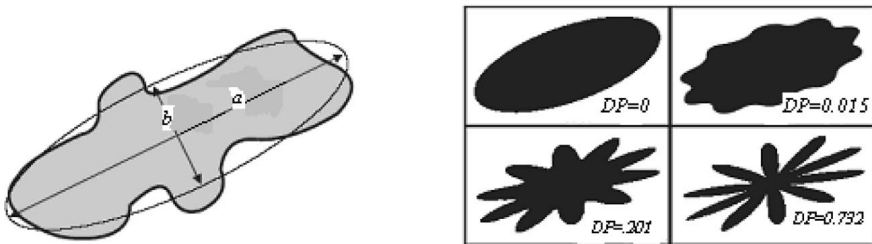

Figure 4. (a) Morphology study based on the Legendre ellipse and (b) Samples with different values of the dispersion *DP* (Mikli et al. 2001).

original object area. The Legendre ellipse is often used instead of the original object (Greg 2001; Kulu et al.1998). The shape factor elongation based on Legendre ellipse *EL*is defined as

$$EL = \log_2(a/b) \tag{4}$$

and dispersion *DP* as

$$DP = \log_2(\pi ab). \tag{5}$$

The relationship *EL* and *AS* can be expressed as

$$EL = \log_2(a/b) = \log_2 AS = \log AS / \log 2 \Rightarrow AS = 2^{EL}. \tag{6}$$

Dispersion is a measure that allows one to evaluate differences in smoothness. It makes it possible to compare the smoothness of the evaluated object with the ideal ellipse; dispersion of an ellipse is zero and it grows with the increase of the object's roughness (Figure 4b).

The comparison to a reference shape, such as the convex bounding polygon, can give a more detailed appreciation of the shape. Some shape descriptors have been defined using morphological mathematics by Vivier et al. (1994) and Pons et al. (1997, 1999). The ratio of the perimeter and the surface of the convex bounding polygon to the silhouette perimeter and surface is defined as convexity and solidity descriptors, respectively (Table 2 and Figure 5).

Particle Shape Angularity Descriptors

Another character of particle shape is its angularity. Kaya and et al. (2002) used an image-analysis system to provide digitized particle profiles from optical microscopy (or from scanning electron micrographs) by means of a procedure developed by Dumm and Hogg (1990) and modified by Kumar (1996) and Kaya (1996). In this algorithm, a series of straight-line segments was fitted to the set of *N* points representing the complete profile as illustrated in Figure 6. The intersections of these linear segments define a reduced set of *n* perimeter points ($n < N$) and describe an *n*-sided polygon that represents the essential features of the original profile. Designating the *x-y* coordinates of the original perimeter points as (x_i, y_i), the cross-sectional area of the particle was determined from

$$A = \frac{1}{2} \sum_{i=1}^{N} (x_{i+1} - x_i)(y_{i+1} + y_i) \tag{7}$$
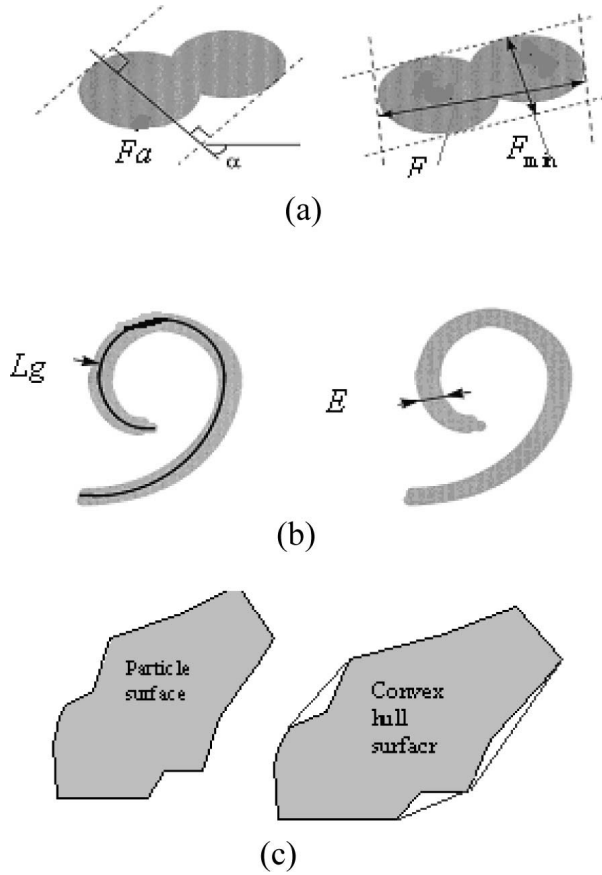
(a)

(b)

(c)

Figure 5. (a) Primary parameters for a rather convex particle from Pons (1999), (b) for an elongated concave particle, and (C) convex and concave bounding.

where the point at (x_{N+1}, y_{N+1}) represents the return to the initial starting point $(i = 1)$. The coordinates $\bar{x}$, $\bar{y}$ of the centroid of the image can be obtained from

$$\bar{x} = \frac{\sum_{i=1}^{N} (x_{i+1}^2 - x_i^2)(y_{i+1} + y_i)}{2 \sum_{i=1}^{N} (x_{i+1} - x_i)(y_{i+1} + y_i)} \tag{8}$$

$$\bar{y} = \frac{\sum_{i=1}^{N} (y_{i+1}^2 - y_i^2)(x_{i+1} + x_i)}{2 \sum_{i=1}^{N} (y_{i+1} - y_i)(x_{i+1} + x_i)}. \tag{9}$$

The equivalent-circle mean radius of the particle and the radial vectors R_i from the centroid to each of the n perimeter points on the
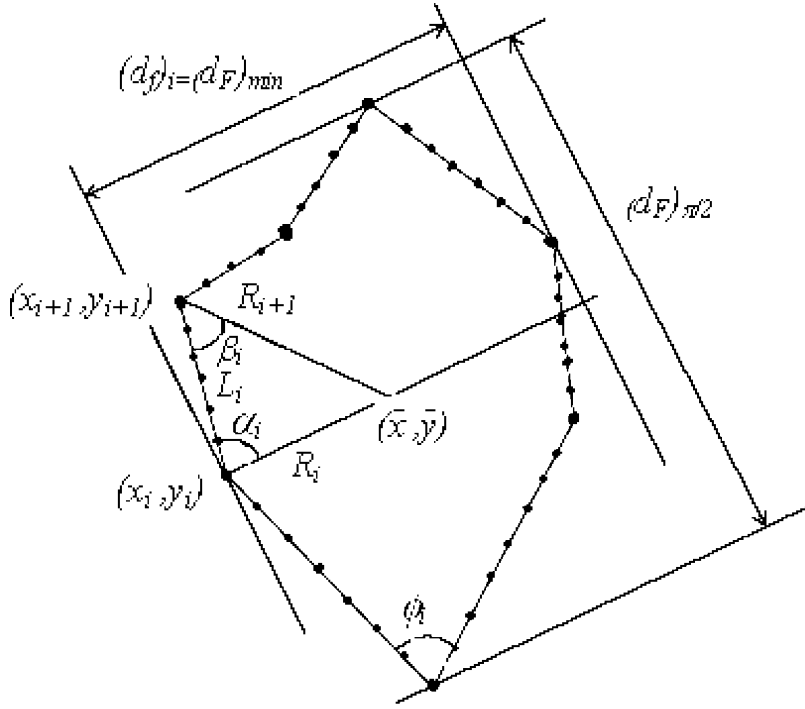
Figure 6. Representation of a particle profile consisting of N perimeter points ($N = 40$ in this example) by a fitted polygon defined by a set of n reduced perimeter points ($n = 7$ in this case) (Kaye et al. 2002). A polygon is fitted on the particle outline and measurement marks are placed on the polygon.

reduced profile can be calculated by using the following equations, respectively:

$$R_O = \sqrt{A/\pi} \tag{10}$$

$$R_i = \sqrt{(x_i - \bar{x})^2 + (y_i - \bar{y})^2}. \tag{11}$$

For the edges intersecting at the perimeter point (x_i, y_i), the angle α_i and β_i can be obtained from the following equations, respectively:

$$\cos \alpha_i = \frac{R_i^2 + L_i^2 - R_{i+1}^2}{2R_i L_i} \qquad (12)$$

$$\cos \beta_i = \frac{R_{i+1}^2 + L_i^2 - R_i^2}{2R_{i+1} L_i} \qquad (13)$$

where L_i is the length of the edge connecting points (x_i, y_i) and (x_{i+1}, y_{i+1}). The angle ϕ_i is simply the sum $\alpha_i + \beta_i$. The following shape descriptors were defined to represent specific geometric features of the profile.

1. The elongation E was defined using the ratio of the minimum Feret's diameter to that at right angles to it. Thus

$$E = \left[(d_F)_{\pi/2} / (d_F)_{\min} \right] - 1 \qquad (14)$$

where $(d_F)_{\min}$ is the minimum of the set of measured Feret's diameters and $(d_F)_{\pi/2}$ is the Feret's diameter measured perpendicular to $(d_F)_{\min}$. As defined, the elongation is zero for a circular profile.

2. The angular variability V_ϕ was defined to represent the variation in the angles ϕ_i between adjacent edges on the reduced profile. Specifically, for ϕ_i expressed in radians

$$V_\phi = \sum_{i=1}^{n} \left(1 - \frac{\phi_i}{\pi} \right)^3 . \qquad (15)$$

The third term was used in order to emphasize the role of the smaller angles, which are considered to contribute the most to the "angularity" of a particle. A many-sided polygon fitted to a circle gives a set of angles close to π with a corresponding angular variability close to zero.

3. The radial variability VR was used to describe the departure of the profile from a circle. The particular definition used was

$$V_R = \sum_{i=1}^{n} \left| \frac{R_i}{R_o} - 1 \right| . \qquad (16)$$

Mesoscopic Descriptors

Mesoscopic shape descriptors have been defined using morphological mathematics. Let ω_1 and ω_2 be, respectively, the number of erosions, probing asilhouette by a pixel, necessary to completely eliminate the silhouette and its residual set with respect to the reference shape (often

the convex bounding polygon or circumscribed circle centerd on the object barycenter; (Figure 7a). After normalization with respect to S, the robustness factor is defined as

$$\Omega_1 = 2\omega_1/\sqrt{S} \qquad (17)$$

and the reduced size of the largest concavity is defined as

$$\Omega_2 = 2\omega_2/\sqrt{S}. \qquad (18)$$

Another descriptor with respect the shape and size Ω_i' which combines the effect of shape and size, is defined as
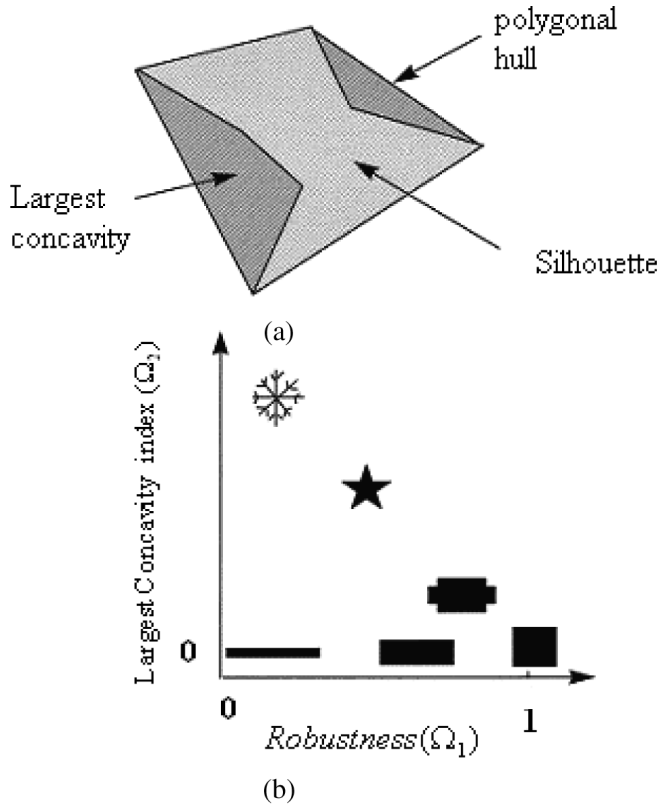
$$\Omega_i' = \Omega_i.D_{eq}. \qquad (19)$$

Figure 7. (a) Polygonal convex hull and Ω_2 vs. Ω_1 plot (b) (Pons et al.1999).

Robustness can be seen as an elongation descriptor for the object, while F_{max}/F_{min} refers to the elongation of the convex hull. The Ω_2 vs. Ω_1 plot is used for a rapid screening of the shapes (Figure 7b; Belaroui et al. 1999; Faria et al. 2002; Pons et al. 1997, 1998, 1999; Vivier et al. 1994; Vucak et al. 1998).

Texture Analysis of Faceted Materials

Direct analysis of the texture descriptors is generally difficult. The descriptors enable us to compare one structure to another, but do not give an absolute grading to the texture. Principal component analysis has been found to be useful in that domain to summarize the information.

A novel technique has been proposed for the rapid characterization of facetted materials based on mathematical morphology applied to binary images (Pons et al. 1998, 1999). It stems from the idea that the visual texture of particles related to the complexity of particles. To characterize, two steps are necessary: obtaining the facet images and characterizing the facet network. Obtaining the facet images carried out by a series of logical operation on binary images such as enhancement sharp gray-level variations on an image, thresholding, filling of the object, image cleaning and debris removal, logical inversion and logical subtraction (Figure 8). To characterize the facet network, they used the notion of Apollonian packing of squares developed by Brachotte et al. (1995) to describe the complexity of corrosion images. The set of squares cover completely the object zones of binary image. They also used

(a)   (b)   (c)   (d)
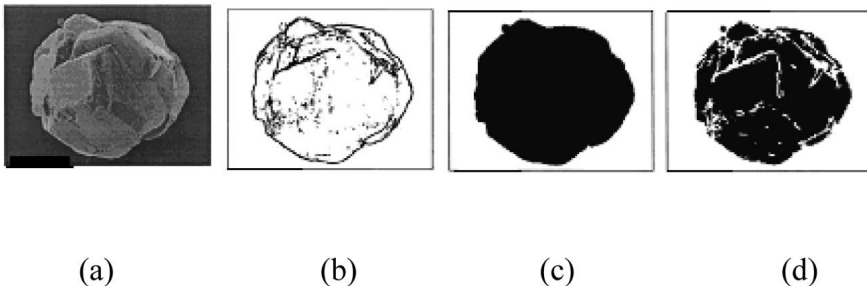
Figure 8. Main steps in the procedure to obtain the silhouette image (A) (by convention for printing of binary images $0 =$ white and $1 =$ black). (a) Initial gray-level image, (b) binary image with particle and facet edges (c), silhouette image (binary image), (d) and facet image (binary image) (Pons et al. 1998 and 1999).
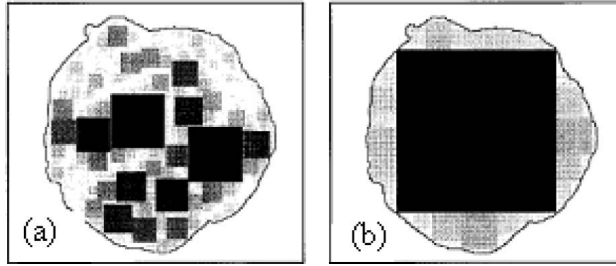
Figure 9. Packing of squares corresponding to (a) the facet image (b) and the silhouette image. The particle borderline has been added to facilitate the visualization. Background and facet edges are printed in white. Decreasing gray-level corresponds to decreasing square size (Pons et al. 1998, 1999).

the Euclidian distance map (EDM) of the binary image method for obtaining the square sets (Figure 9). The shortest distance of each pixel to an edge and detection of the local maxima corresponding to the centers of facets are estimated using the EDM map. On the facet images, the simplicity (ξ) of the facet network and the size (X_{max}) of the largest visible facet of the particles were offered as morphological descriptors (Frances et al. 2001; Pons et al. 1999). Abrasion will decrease the sharpness of the edges and, therefore, the complexity of the network. The calculation of the simplicity is based on the division of the facet zones into squares of the increasing size, so that the total available area is covered. This procedure can be applied on the facet and silhouette of the particles and results in the distribution of squares of side length x, aligned with the image grid. A distribution in number $f(x)$ of square of size x results in

$$F_{\mathrm{facet}}(u) = \int f_{\mathrm{facet}} du \, F_{\mathrm{silhouette}}(u) = \int f_{\mathrm{silhouette}} du \qquad (20)$$

where u is the normalized side length $u = x/\sqrt{s}$. A size and quasi-position invariant simplicity index ξ is computed as

$$\xi = \frac{\int (1 - F_{\mathrm{facet}}) du}{\int (1 - F_{\mathrm{silhouette}}) du}. \qquad (21)$$

SUMMARY

Particle shape analysis is one of the most difficult problems in powder technology; to date, there is no general shape factor available that clearly

differentiates all possible kinds of shapes. Because of some complexity in the nature of shape and its measurement, the numerous shape descriptors have been applied by many authors. Most conventional shape factors are obtained by comprising with a reference shape such as circle or sphere and/or formed mainly from a ratio of two particle size measurements. However, a significant limitation of using one of these shape factors is that its value is often not unique to a specific shape.

If two measures of particle size are available, an elementary descriptor of particle shape can be defined by combining them as a ratio. The value of this ratio relative to that of a reference shape indicates the degree to which the particle under study differs from the reference shape. However, given that particle size can be defined in many different ways, correspondingly a large number of conventional shape descriptors are also possible. Each descriptor will be most sensitive to a specific attribute of shape, depending on the size measures selected. If more than two measures of a size is available, the question then arises as to which combination provides the best description of the shape. In other words, which size measures are most appropriate to use when defining certain descriptors? For example, is the average Feret diameter or maximum Feret diameter more appropriate in the definition of roundness? A case could be conceivably applied for either, but the resulting values obtained will depend on the choice.

In addition, another problem arises from the practical issue relevant to characterization techniques incorporating particle perimeter. For many particles, the measured perimeter (length) is dependent on the length scale at which it is investigated (resolution), i.e., perimeter is not an absolute measurement. In spite of this, shape descriptors incorporating the perimeter may still be useful so long as the particles being compared are all of similar size and are imaged on the same scale (magnification), as comparative perimeter length will still be indicative of gross particle shape.

Therefore, use of the several shape descriptors may be a means to tackle this problem, but the particle size can be defined in a large number of ways and resulted in the numerous particle shape descriptors. Using both 3-D and 2-D shape descriptors as well as qualitative and quantitative descriptors gives more detail information about particle shape and morphology if it could conceivably be applied for a case study. Consequently, the selection of descriptors and their statistical analysis by using fractal analysis, cluster analysis, neural net, and or self-organizing map methods

for particle shape characterization would be useful and important. In addition, from a statistical view point, in order to obtain confident and appropriate results, depending on the differences and similarities among particle shapes and those size distributions at each investigation case, an adequate number of particles must be analyzed.

NOMENCLATURE

A	Length of the smallest possible rectangle that bounds the particle of the projected particle image
a, b	Axes of the Legender ellipse
B	Breadth of the smallest possible rectangle that bounds the particle
B_{90}	Length of the Feret diameter $90°$ to B
C	Concentration of suspension
C_{av}	Mean chord of length
C_{max}	Maximum (longest) chord length
$C_{max,90}$	Length of the chord $90°$ to C_{max}
C_{med}	Median chord length
C_{min}	Minimum (shortest) chord length
$C_{min,90}$	Length of the chord $90°$ to C_{min}
d	Diameter of the external contact sphere
D	Diameter of the internal contact sphere
D_{eq}	Equivalent circular diameter
D_m	Mean Feret diameter
DP	Dispersion
D_{SL}	Equivalent velocity settling diameter
d_{sph}	Diameter of a sphere having the same projected area of particles
D_v	Equivalent volume diameter
D_W	Equivalent high scattering intensity diameter
E	Thickness measured by EDM
e_R	Simplified shape factor
F_{facet}	Frequency distribution of squares on facet image
F_{max}	Maximal Feret diameter
F_{min}	Minimal Feret diameter
$F_{silhouette}$	Frequency distribution of squares on silhouette image
IP	Irregularity factor

K_a	Shape coefficient
L	Length (maximum Feret diameter)
L_{90}	Length of the Feret diameter $90°$ to L
L_g	Geodesic length
MD	Martin's diameter
P	Perimeter of the projected particle image
P_c	Perimeter of the convex bounding polygon
P_{cir}	Perimeter of a circle with the same area as the particle projected image
S	Silhouette surface
S_c	Surface of the convex bounding polygon
S_M	Specific surface area per mass unit
S_{sph}	Sphere having the same volume of surface areas of the measured particles
V_p	Particle volume
W	Thickness
x	Square side length
ξ	Simplicity
d_A	Diameter of the circle having the same projected area of particles
ω_i	Number of erosions
Ω_1	Robustness
Ω_2	Large concavity index

REFERENCES

Allen, T. 1990 *Particle Size Measurement*, London: Chapman and Hall, pp. 125–191.

Belaroui, K., Pons, M. N., Vivier, H., and Meijer, M. 1999 Wet grinding of gibbsite in a bead mill. *Powder Technol.*, 105, pp. 396–405.

Brachotte, D. C. and Roques carmes, C. 1995 On the use of complementary set fractal dimension in image analysis. Acta Sterol, 142, pp. 129–139.

Carnavas, P. C. and Page, N. W. 1994 Particle shape factors and their relationship to flow and packing of bulk materials. *Int. Mech. Eng. Cong., Perth WA, Preprints of Papers*, The Institution of Engineers, Australia, 2, pp. 241–246.

Carstensen, J. T. (Ed.), 1980 *Solid Pharmaceutics: Mechanical Properties and Rate Phenomena*. London: Academic, pp. 34–36.

Chan, L. C. Y. and Page, N. W. 1997 Particle fractal and load effects on internal friction in powders. *Powder Technol.*, 90, pp. 259–266.

Dumm, T. F. and Hogg, R. 1990 Characterization of particle shape. *Proc. Int. Symp. Respirable Dust in the Mineral Industries*, SME, Littleton, CO, pp. 283–288.

Faria, N., Pons, M. N., Feyo, S., De Azevedo, Rochs, F. A., and Vivier, H. 2002 Quantification by image analysis, of effect of operational conditions on size and shape of precipitated barium sulphate. *Chem. Eng. J.*, 87, pp. 135–147.

Frances, C., Bloay, N. Le., Belaroui, K. B., and Pons, M. N. 2001 Particle morphology of ground gibbsite in different grinding environments. *Int. J. Mineral Process.*, 61, pp. 41–56.

German, R. M. 1984 *Powder Metallurgy Science*, Metal Powder Industries Federation, NJ.

Ghadiri, M., Farhadpour, F. A., Clift, R., and Seville, J. P. K. 1991 Particle characterization: Size and morphology. In *Powder Metallurgy: An Overview* (I. Jenkins and J. V. Wood, Eds.), London: The Institute of Metals, pp. 56–75.

Greg, M. G. 2001 *Interaction in Dry Powder Formulation for Inhalation*, London: Taylor & Francis. pp. 220–234.

Hausner, H. H. 1973 *Handbook of Powder Metallurgy*, New York: Chemical Publishing.

Hentschel, M. L. and Page, N. W. 2003 Selection of descriptors for particle shape characterization, *Part. Syst. Charact.*, 20, pp. 25–83.

Heywood, H., Everett, D. H., and Ottewill, R. H. (Eds), 1970 *Pro. Int. Symp. Surface Area Determination*, London: Butterworths.

Kassem, N. M. 1990 Generation of deeply inspirable dry powders, *PhD Thesis*, Univ. London.

Kaya, E. 1996 Control of particle characteristics in the production of fine powder by grinding, *Ph.D. Thesis*, Pennsylvania State Univ.

Kaye, B. H. 1998 Characterization of powders and aerosols. *Part. Syst. Charact.*, 15, pp. 281–298.

Kaye, E., Hogg, H., and Kumar, S. R. 2002 Particle shape modification in comminution. *Kona*, 20, pp. 188–195.

Kaya, E., Hogg, R., and Kummar, S. R. 2002. Particle shape modifications in comminution. *Kona*. 20, pp. 188–195.

Kulu, P., Tumanok, A., Mili, V., Kaerdi, H., Kohutek. I., and Besterci, M. 1998 Possibilities of evaluation of powder particle granulometry and morphology by image analysis. *Proc. Estonian Acad. Sci. Eng.* 4, pp. 3–17.

Kumar, S. R. 1996 Characterization of particle shape, *M. S. Thesis*, Pennsylvania State Univ.

Lecop, O., Guigon, P., Pons, and M. N. 1999 A grindability test to study the influence of material processing on impact behaviour. *Powder Technol.*, 105, pp. 21–29.

Mikli,V., Kaerdi, H., Kulu, P., and Besterci, M. 2001 Characterization of powder particle morphology, *Proc. Estonian Acad. Sci. Eng.*, 7, pp. 22–34.

Muller, F., Polk, R., Schafer, M., and Scholz, N. 2001 Particle system characterization and modeling. *Part. Charact.*, 18, pp. 248–253.

Otsuka, A., Iida, K., Danjo, K., and Sunada, H. 1988 Measurement of the adhesive force between particles of powdered materials and a glass substrate by means of the impact separation method, III: Effect of particle shape and surface asperity. *Chem. Pharm. Bull.*, 36, pp. 741–749.

Pons, M. N., Vivier, H., Belaroui, K., Bernard-Michel, B., Cordier, F., Oulhana, D., and Dodds, J. A. 1999 Particle morphology: From visualization to measurement. *Powder Technol.*, 103, pp. 44–57.

Pons, M. N., Vivier, H., and Dodds, J. A. 1997 *Part. Syst. Charact*, 14. pp. 272–277.

Pons, M. N., Vivier, H., and Rolland, T. 1998 Psedo-3Dshape description for facetted materials. *Part. Syst. Charact.*, 15, pp. 100–107.

Raadnui, S. and Roylance, R. J. 1995 The classification of wear particle shape, *Lubrication Eng.*, 51, pp. 432–437.

Sasov, A. Y. and Sokolov, V. N. 1984 Numerical processing of REM images. *Izv. Acad. Nauk SSSR*, *Fiz*, 184, pp. 2389–2396 (in Russian).

Singh, K. S. W. 1976 In *Characterization of Powder Surface with Special Reference to Pigments and Fillers*. (G. D. Parfitt and K. S. W. Sing, Eds.) London: Academic. pp. 4–9.

Stachowiak, G. W. 1998 Numerical characterization of wear particles morphology and angularity of particles and surfaces. *Tribol. In.* 31, pp. 139–157.

Stachowiak, G. W. 2000 Particle angularity and its relationship to abrasive and erosive wear. *Wear*, 241, pp. 214–219.

Stachowiak, G. W. and Podsiadlo, P. 2001 Characterization and classification of wear particles and surfaces. *Wear*, 249, pp. 194–200.

Ting, J. M., Meachum, L., and Rowell, J. D. 1995 Effect of particle shape on the strength and deformation mechanisms of ellipse shaped granular assemblages. *Eng. Comput.*, 12, pp. 99–108.

Vivier, H., Marcant, B., and Pons, M. N. 1994 Morphological shape characterization: Application to oxalate crystals. *Part. Syst. Charact.*, 11, pp. 150–155.

Vucak, M., Pons, M. N., Peric, J., and Vivier, H. 1998 Effect of precipitation conditions on the morphology of calcium carbonat: Quantification of crystal shapes using image analysis. *Powder Technol.*, 97, pp. 1–5.

Wojnar, L. 1999 *Image Analysis Applications in Materials Engineering.*, Boca Raton, FL: CRC.

Zou, R. P. and Yu, A. B. 1996 Evaluation of the packing characteristics of monosized non-spherical particles. *Powder Technol.*, 88, pp. 71–79.

Paper V

Review of applied particle shape descriptors and produced particle shapes in grinding environments. Part II: the influence of comminution on the particle shape

Parviz Pourghahramani and Eric Forssberg

Taylor & Francis
Taylor & Francis Group

REVIEW OF APPLIED PARTICLE SHAPE DESCRIPTORS AND PRODUCED PARTICLE SHAPES IN GRINDING ENVIRONMENTS. PART II: THE INFLUENCE OF COMMINUTION ON THE PARTICLE SHAPE

PARVIZ POURGHAHRAMANI and Eric Forssberg

Division of Mineral processing, Luleå University of Technology, Luleå, Sweden

In this article the literature on the shape of particles produced by comminution methods and the grinding condition is reviewed and presented. Some agreement and disagreement among workers for the shapes that are produced by comminution are presented. In addition, the important factors affecting the shape of particles in different comminution methods are also described.

Keywords: grinding, particle shape, particle morphology, shape descriptor

The importance of particle shape in determining bulk powder properties is now recognized in a great variety of industries. It is known that the shape of pigment particles affects the flow and surface failure characteristics of paint and the way in which coal particles behave in combustion is strongly influenced by their shape (Holt 1981). Shape influences the way particles burn, compact, flow in fluids, sinter, dissolve in liquid, react with chemicals, and retain fluids and permit fluids to flow (Durney and Meloy 1986).

The importance of particle shape was not been completely known yet in the mineral-processing processes. The effect of particle shape on entrainment in flotation was investigated by Ata and Ahmed (1998). They concluded that the degree of entrainment was affected by the particle shape at pulp densities below 5%. Ferrara et al. (2000) studied the influence of particle shape on the dynamic dense medium separation of plastic. They reported that single particle sizes and shapes are separated with high sharpness in a Tri-Flo separator using salt solutions as a medium. Lileg and Schnizer (1989) reported the effect of particle shape on forces in magnetic separators. It seems that beneficiation processes such as flotation, electrostatic, gravity, and magnetic separation leaching behavior of minerals, and sorting, are all influenced by particle shape and morphology. However, to discover these influences, precise and extensive investigations must be undertaken.

The characterisations of the ground particle, especially in the case of minerals and ores, need the appropriate shape descriptors and characterization method. In our previous work (Pourghahramani and Forssberg 2004), some of the shape descriptors were described with regard to their feature and are applicable in the image-analysis systems at the present time. As one common method of producing particles is by comminution, the aim of this article is to review and summarize the produced ground particle shapes in various grinding environments and important factors affecting the shape of ground material in particular for minerals and ores.

INVESTIGATION EMPHASIS MAINLY ON GRINDING METHODS

An extensive investigation into the crushing and grinding of rocks, which included observations on the shape of products, was carried out by Gaudin (1926). It was found that the particle shape of ground quartz in different grinding methods depends on the particle size and concluded that the action of a jaw crusher is substantially the same as that of a roll crusher, because of some similarities in their produced particle shapes and other similarities between the two grinding machines. In addition, the size of the balls in a ball mill was found to be an important factor in determining the particle shape. The particle shapes produced in different grinding method are summarized in Table1.

The evaluation of the flakiness of ground ore using square-hole and rectangular screens was investigated by Coghill (1928). In the grinding of

Table 1. Common particle shape of quartz ground in various grinding methods (Gaudin 1926)

	Fine particles	Large particles
Roll mill	Elongated and acicular-angular	Fairly flat-angular
Rod mill	Elongated and acicular-angular	Equidimentional grains and some regular polyhedral
Ball mill	Sharp splinters	Equidimentional or polyhedral above critical ball size, but rounded grains bellow a critical ball size

chert and dolomite, roll mills were found to give a flakier product than ball mills. Charles (1956) observed that the shape of glass particles produced by a single fracture was dependent on the rate of application of stress. Durney and Meloy (1986) stated that material fed once through an impact mill gave a cubical product and a gyratory crusher produced sharp pieces. They also reported that the shape of particles depends on the type of mill used.

Grasse (1954) was awarded a patent for the design of a roll crusher producing cubical shaped fragments and Papacharalambous (1964) was also awarded a patent for the design of a cyclone with walls made of abrasive material that produced spherical particles.

Rose (1961) reported that angularity of the product increases with mill type in the following order: ball mill, ring roll mill hammer mill. Rose believes that while the properties of the material determine, to some extent, the particle shape after comminution, the mill type has an even more marked effect. Yigit et al. (1967) and Holt (1981) reported that an electrohydraulic crushing produces a clean aggregate of generally cubic shape from a wide range of quarry stones. They compared the flakiness, proportional of cubical grains remaining on the rectangular; hole screens to flaky grains passing through it; and elongation, the ratio of length to width, of particles produced in jaw crushers with those produced by electrohydraulic crushing. According to the Figures 1 and 2, it is clear that differences in elongation and flakiness factors between those crushers are significant. The produced particles of the jaw crusher were more elongated and flakier than those produced in the electrohydrulic crusher. These factors were also dependent on the rock type, but the crusher type was a much more important influence on particle shape.
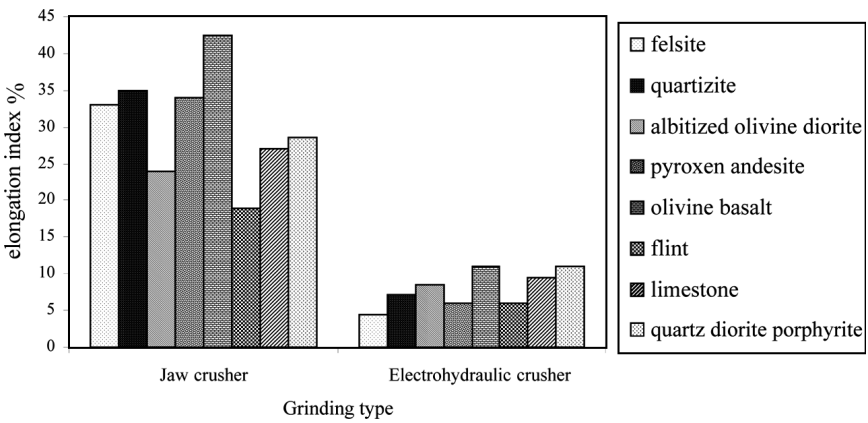
Figure 1. Comperative elongation of various rocks [data from Yigit (1967)].

Roll crushing of kaolin was determined to produce uniformly angular particles while the dry-panning produced more compact coarse particles (Holt 1981).

Gilvarry and Bergstrom (1961), in their work on the fractured glass spheres by compression between two diametrically opposed platens, found that the most probable fragment shape was a flat tetrahedron (sphenoid) with the ratio of maximum to minimum dimension less than 2, followed by columnar and then cubic forms and a fraction of the fragments, up to a limit of 10%, having an acicular shape in which
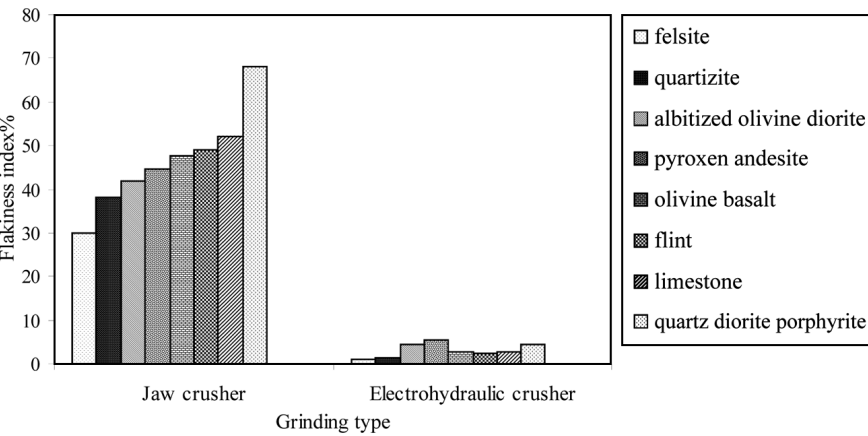

Figure 2. Comperative flakiness index of various rocks- [data from Yigit (1967)].

the ratio of the maximum to median exceeded 10. Arbiter et al. (1969), who fractured glass spheres by slow compression, reported that the areas in contact with the plates formed the base of a cone that was finely comminuted and the material of the central core along the axis if loading disintegrated into elongated prismoidal and sphenoidal particles.

It was investigated that autogenous grinding produced rounded particles with higher degrees of liberation and equiaxiality and lower roughness. These properties resulted in a higher grade concentrate and better recovery (Forssberg and Hongxin 1985).

Measurement and statistical analysis of sand particles comminuted by a screen mill were carried out by Kuga et al. (1985). The impact velocity of hammers was set at 32.3, 61.6, and 91.0 m/s, respectively. Sixteen kinds of shape factors were determined from each set of periphery data. These indices were reduced by factor analysis to four main shape characteristic factors: elongation, global roughness, surface roughness, and angularity, respectively. They contained about 85% of the information of the 16 shape indices and expressed the characteristics of comminuted particle shape well. Several small particles comminuted at low impact velocity (32.3 and 61.6) had large values of the first factor and high elongated shape. It was reported that, in other cases, no appropriate differences in shape as characterized by the four factors were observed between the original particles and the comminuted particles of size approximately 10–350 μm.

Kinetics and shape factors of ultrafine dry grinding in a laboratory tumbling ball mill was investigated by Austin, Leonard et al. (1990). Analysis of the shape of the particles in the 25×38 μm size range showed that particles of this size produced by roll crushing or by 8 min of grinding of a 425×600 μm feed were not different, but at long grinding times the particles were rounded. As a result, it was concluded that the breakage mechanism changes to give more chipping and abrasion and less disintegrative fracture.

Differences in the shape mix of glass particles crushed under open and choke flow conditions were demonstrated using Fourier analysis by Durney and Meloy (1986). Particles ground in open flow were more angular and have larger asperities and more complex shapes. Smaller particles were more elongate, complex, and angular. It was also found that smaller particles were more complex, irregular, and have higher aspect ratio than larger ones.

INVESTIGATIONS EMPHASIZING MATERIAL CHARACTERISTICS

Material type is one of the most important factors affecting particle shape. Bond (1954) considered that the character of material being broken has more influence on the shape of the product than the type of size-reduction machine used. Heywood (1961) presented the shape information and length, breath and thickness measured by hand of 142 crushed sandstones particles retained on a 1-in^2 aperture sieve. Heywood believes that the shape of particles produced on initial fracture is solely dependent upon the characteristics of the material. Holt (1981) reported that the same results of similar measurements on particles of crushed siliceous rocks and minerals with remarked cleavage were found to have a characteristic shape of particle. It was suggested that the character of material being broken has more influence on particle shape; for example, a laminated or bedded material always tends to produce slabs.

Meloy (1988) stated that there is a major difference between the appearance of particle shape of the glasses and the fine-grained rocks. In the glasses, the edges and points are far sharper than those in the fine-grained rocks. While the fine-grained rocks have very clear edges and points, these features are less sharp and appear feathery, making identification of the smaller traces difficult.

Coal samples were comminuted in a ball mill under controlled temperature, in helium. Microstructural analyses of the coal particles before ball milling and at various times during milling showed relationships between the microstructure and the size and shapes of the resulting particles. During milling, fracture lines tended to proceed through pores and cracks and organic-to-organic and mineral-to-organic interfaces; thus, these features greatly influenced the size and shapes of particles produced. In the early stages of milling, a porous component of lignite produced needle-like or plate-shaped particles that were later broken into blocky and rounded particles (Lytle et al. 1983).

INVESTIGATIONS EMPHASIS ON MULTI PARAMETERS

The mode of breakage, whether single-particle breakage or interparticle breakage, is claimed to play a role in generating particles of different shape. The comparison of mineral particle shape effects in the particle-bed breakage with conventional laboratory rod-mill grinding and piston-die press grinding of a chromite ore was investigated (Hosten and Ozbay 1998). The form factor is defined as $(4\pi \times \text{area})/(\text{perimeter})^2$

and is used for shape characterization of particles. Marginal shape differences were found between particles of different size fractions produced by rod-mill grinding. In particle-bed breakage, however, particles became more irregular (lower form factor values) as particle size decreased. Also, particle-bed breakage occurring in the piston-die press produced particles with more irregularity than the particles of rod mill product in the finer size (48×65, 65×100, and 100×150 mesh fractions) of the investigated size fractions. Increasing the applied pressure from 30 to 60 MPa in particle-bed breakage (Figure 3) showed little rises in the form factor values for 48×65 and 65×100 mesh sizes, offering breakage of more irregular particles to assume smoother profiles and a shift of shape differences to relatively finer sizes. Except for the 65×100 spectrum, the form factor value increased slightly from fine sizes to coarser fractions. In particular, it was concluded that the products of individual breakage events were typically angular and irregular in shape. Prolonged exposure to the grinding environment leads to rounding of the particles. Mill types employing high energy input gave particles including a high proportion of irregularity for a given product size distribution. Therefore, such mills favor the production of irregular particles. Grinding devices for which the energy input is relatively low, on the other hand, are based on repeated breakage action for size reduction and tend to produce more rounded particles.
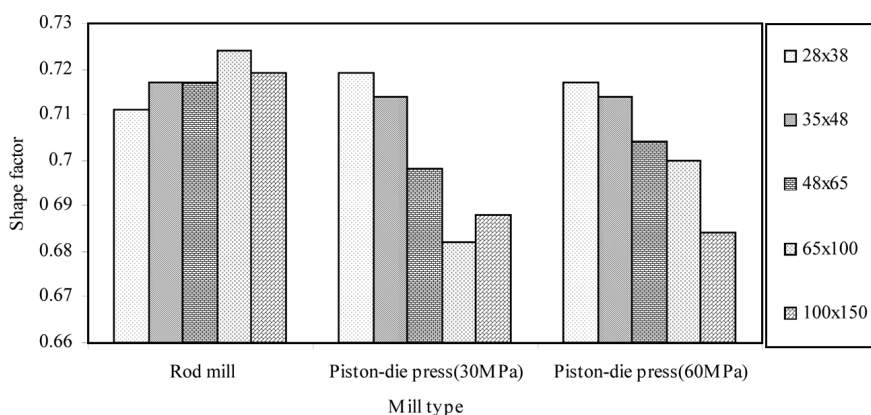

Figure 3. Shape factor values of fully liberated chromite grains in ground products [data from Hosten and Ozbay (1998)].

Particle shape of three milling products (ball mill, attrition bead, and jet mill) for three different minerals [limestone, Flue gas desulphurization (FGD) gypsum, and waste gypsum] was measured using image analysis by Oja and Nyström (1997) and Oja and Tuunila (2000). The product particles were characterized by size and six shape factors. The shape descriptors were

$$(\phi_1 = 4\pi S/C^2, \phi_2 = d_{min}/d_{max}, \phi_3 = d_F/d_{max}, \phi_4 = d_F/d_p, \phi_5 = d/d_F,$$
$$\phi_6 = d/d_{max}).$$

The typical feature of mineral product was extracted by self-organizing map (SOM) that gives spatial order the cluster. In this application a specific shape was not connected to a specific size; all size ranges had elongated and round particles as well as rough and smooth particles. When the ground waste gypsum particles of the attrition bead mill were clustered with the SOM net, most of small and large particles were placed in the units where the concavity shape values were larger than the mean value. These particles were called rounded particles. While the waste gypsum particles ground in the jet mill contained few rounded particles and many elongated and concave particles, the waste gypsum ground particles ground in the ball mill showed all particle shapes. The results also showed that, with limestone, the influence of the grinding method was significant, with the product of the jet mill being more concave particles. Both ball mill and bead mill produced the small and rounded particles. In the ball mill product, the concave particles were totally negligible. For the FGD gypsum, the differences in concavity shape factor values reported were very small and, therefore, the SOM surface for concavity shape factors was flat (Figure 4). It was also reported that feature-extraction methods based on the particle shape without size do not give technically relevant information about minerals and their behavior in a process. Different mill products were clustered differently, showing that the fraction of concave particles is a relevant shape feature for the grinding method. The obtained results showed that size reduction caused by impacts produces concave particles and size reduction caused by attrition produces rounded particles (Figure 4).

The effect of a grinding device on shape was analyzed for coal and quartz particles using the Bleuler ring-and-puck Pulverizer and the planetary ball mill; grinding times were set so as to give a similar extent of
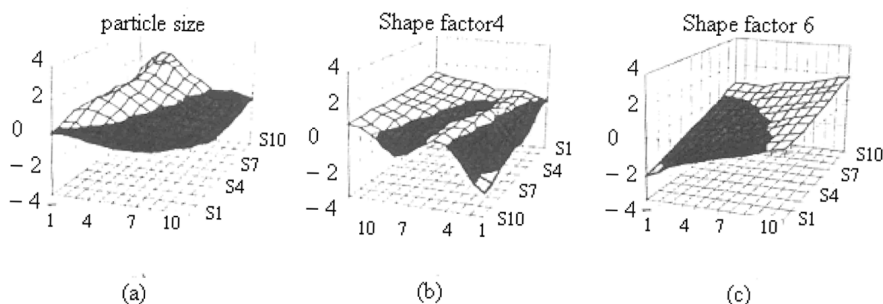
Figure 4. SOM—surface visualization of the SOM trained by 500 waste gypsum particles, x- and y-axis, and the codes for the SOM unit, and z-axis is the normalized value of the parameter. (a), SOM surface for particle size (b), SOM surface for the shape factor that characterizes concavities selectivity (c) and one of the elongation surfaces for waste gypsum (Oja and Tunnila 2000).

grinding for each mill (Kaye et al. 2002). Descriptors related to particle elongation, roundness, and angularity were evaluated. For the given descriptors, the distributions of measured values generally followed a constituent pattern (often roughly log normal) and it was concluded that prolonged grinding leads to rounding of the particles and that shape does not change substantially with grinding in a high-energy mill (Bleuler mill) (Figure 5). It was found that the effect of grinding type leads to small variation in differences in particle-shape descriptor value; however, the trends are consistent and similar for each of the descriptors. Further, large particles produced by single breakage events tend to be quite irregular in shape, while particles subject to repeated breakage or long exposure to the grinding environment usually are more rounded. They expressed that the shape of particles was controlled by the type and nature of material, the type of grinding method (device), and the grinding time.

Extensive investigations on ground mineral shape and morphology in various grinding environments in order to correlate them with wettability, hydrophobicity parameters of a mineral, characterization of surface roughness, etc., have been carried out (Hicyilmaz et al. 2004; Ulusoy et al. 2003a, 2003b; Yekeler et al. 2004a, 2004b). Various minerals ground in various grinding environment (ball mill, rod mill, and autogeneous mill). To characterize produced particle shape and morphology, they applied four shape descriptors including elongation (L/B), flatness $(P^2/4\pi S)$ Roundness $(4\pi S/P^2)$, and relative width
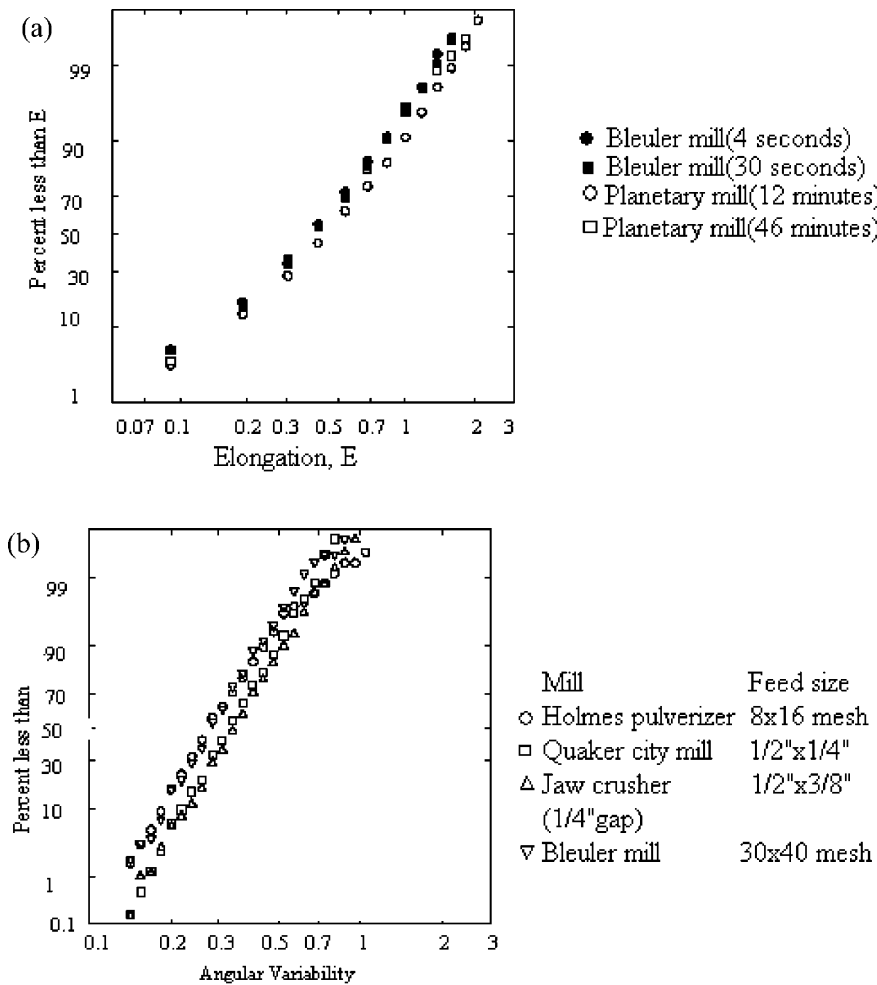
Figure 5. (a) Number distributions of elongation for coal particles $(200 \times 270$ U.S. mesh$)$ produced in both the Bleuler and planetary mills using different grinding times **(b) and** number distributions of angular variability for coal particles $(70 \times 100$ U.S. mesh$)$ produced by different comminution devices (Kaye et al. 2002).

(W/L). A and P are the particle area and perimeter, respectively, which were calculated from

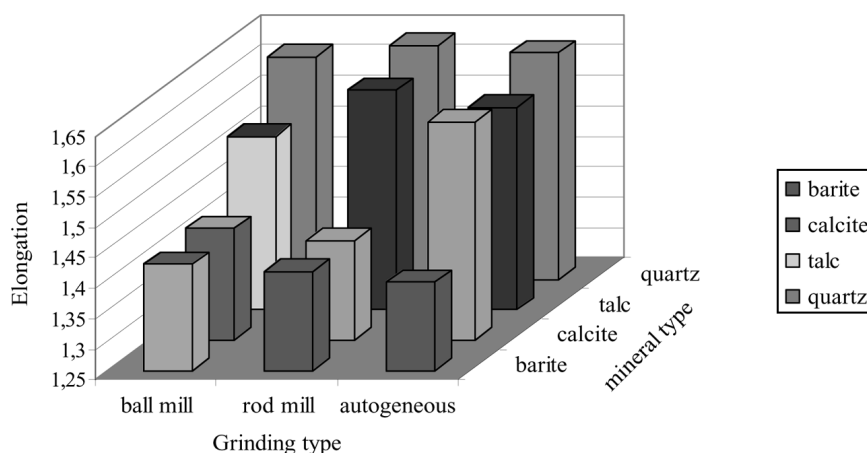$$A \approx (\pi LB)/4$$
$$P \approx (\pi/2)[1.5(L+B) - (LB)^{1/2}].$$

Figure 6. Comparison of the elongation calculated by SEM measurement of different minerals ground by different Mills (Hicyilmaz et al. 2004, data from Ulusoy et al. 2003a and 2003b, Yekeler et al. 2004a and 2004b).

Results obtained for minerals are summarized in Figures 6 and 7. From the figures, it can be concluded that the particle-shape properties of different minerals ground in different environment at the same condition showed some variations, as particles of talc and quartz minerals were ground in a ball mill showed higher roundness and relative width,
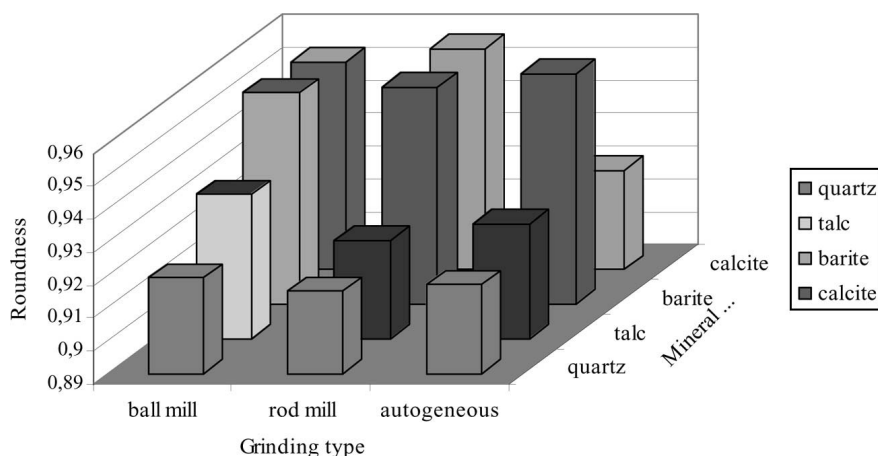

Figure 7. Comparison of the roundness calculated by SEM measurement of different minerals ground by different mills (Hicyilmaz et al. 2004, data from Ulusoy et al. 2003a and 2003b, Yekeler et al. 2004a and 2004b).

while a rod mill produced particles having higher elongation and flatness. In contrast, the ground particles of calcite represented higher elongation and flatness in autogeneous milling and higher roundness and relative width in rod milling. Grinding barite in a ball mill showed higher elongation and flatness, while the higher roundness and relative width was obtained from autogeneous milling. Despite the fact that the different grinding produced particles having differences in particle-shape properties, a significant difference was observed in the same shape property value in various grinding environments for different minerals at the same grinding conditions, suggesting the influence of mineral type on the particle-shape properties and probably shape, depending to size and size distribution.

Experimental investigations on the comminution of gibbsite in four different types of mills were carried out by Frances et al. (2001). Those included tests of dry grinding in a tumbling ball mill, a shaker ball mill, a shaker bead mill, and an air jet mill, as well as tests of wet grinding in a tumbling ball mill and in a stirred bead mill. A quantitative characterization of the size and shape of a ground product had been made in order to define the path in which fragmentation occurred. Several shape descriptors were measured: the ratio of maximal Feret diameter to minimal Feret diameter (F_{max}/F_{min}); robustness factor $\Omega_1 = 2\omega_1/\sqrt{S}$; the reduced size of the largest concavity $\Omega_2 = 2\omega_2/\sqrt{S}$; and circularity $C = P^2/4\pi$.

Where Ω_1, and Ω_2 are, respectively, the number of erosions necessary to completely eliminate the silhouette and its residual set with respect to the convex bounding polygon, S corresponds to particle surface and P denotes the silhouette perimeter.

Results obtained for particle-shape descriptors were reported as a function of the median size and it was observed that, with regard to imposed different grinding method and stress, the produced particle-shape morphology differs in different grinding environments. With regard to the initial shape of gibbsite and particle-shape descriptor changes during grinding, two fragmentation paths, including rupture of joints, chipping, and breakage, according to the nature of the main stress (impact or attrition), suggested comminution processes (Figure 8).

Particle shape produced by comminution in the Szego mill, a planetary ring roller mill, in different coal grinding operations was studied by Olev et al. (1995). It was observed that particle shape was dependent on the type of operation and was used to explain the breakage
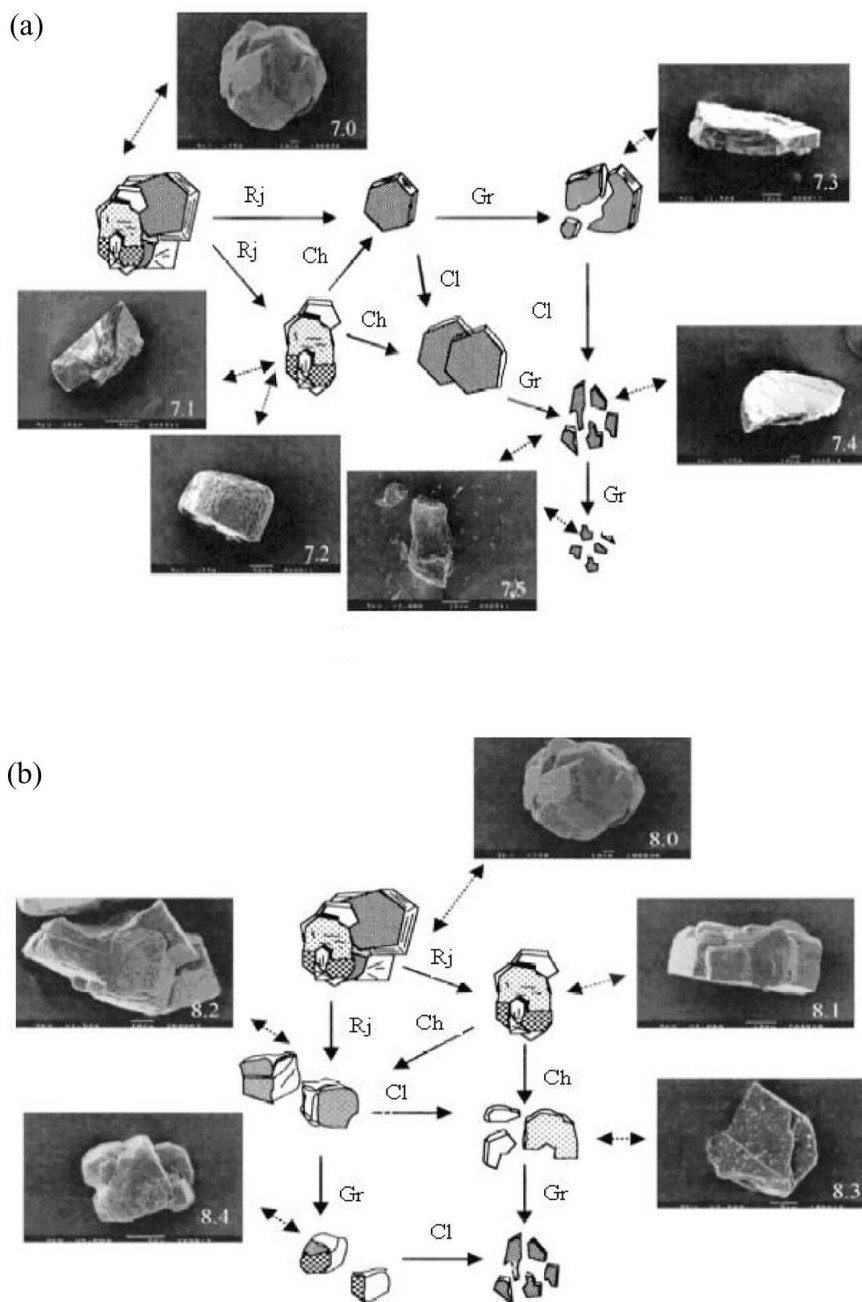
(a)

(b)

Figure 8. Fragmentation scheme for gibbsite ground in (a) media mills (b) and in jet mill. R_j, rupture of joints; C_h, chipping; C_l, cleavage; G_r, ultimate grinding (after 10 min. of grinding) (Frances 2001).

mechanism that grinding produces particles with a low aspect ratio due to interparticle attrition; significant briquetting of fine particles may occur. In wet grinding, flaky particles were produced, which were selected for breakage at rates lower than those for granular particles. Coil-oil-water grinding produced uniform particles with a low aspect ratio due to interparticle attrition within the agglomeration.

The effect of dry grinding on the particle size, structure, and shape was studied on talc from Puebla de Lillo by Sanchez Soto et al. (1997). The structural changes have been correlated with a particle's size, shape, and coefficient of texture. It is reported that, with prolonged grinding, the rate of size reduction decreases with time, but reduction continues up to about 30 min. At this stage, particle size was reduced to about 0.02 μm in diameter and 0.009 μm in thickness, with aspect ratio 2.6, producing an increased degree of amorphism and a decrease in surface area by aggregation of the ground powder (Table 2).

A topographical study of particle surface of sulphide ore (dry grinding and wet grinding with 66% and 90% solids content) was investigated as second topic for a flotation study by Feng and Aldrich (2000). The typical atomic force microscope (AFM) images are shown in Figure 9. According to the figures, it can be seen that the particle surfaces resulting from wet grinding were much smoother than those resulting from dry grinding. It was stated that two- and three-dimensional defects appeared in the particle surfaces by dry grinding. Higher stresses were induced in

Table 2. Surface area, particle sizes, and texture indexes for ground talc (Sanchez Soto et al. 1997)

Grinding time (min)	S_{BET} (m^2/g)	e.s.d (D) (μm)	Best mean (μm)	ε; Scherrer (μm)	a^a (μm)	Aspect ratio (aε)	Shape[b] factor (M)	Texture coefficient (g)
0[c]	3.2	0.727	0.025	0.040	2.243	56	0.21	0.55
5	11.4	0.204	0.022	0.032	0.372	11.6	0.19	0.3
10	24.6	0.095	0.017	0.027	0.129	4.8	0.19	0.3
20	47.7	0.049	0.012	0.016	0.062	3.9	0.12	0.0
30	109.7	0.021	0.009	0.009	0.023	2.6	0.12	0.0
60	28.7	–	–	–	–	–	–	–
210	2.8	–	–	–	–	–	–	–

e.s.d. = equivalent spherical diameter; $^a a^2 = [4/3\pi(D/2)^3]/\varepsilon$;   [b]calculated from the equation of Murtagh and Holland (1989) using peak height; [c]natural (not milled).

(a) Wet grinding with 66% solids

(b) Wet grinding with 90% solids
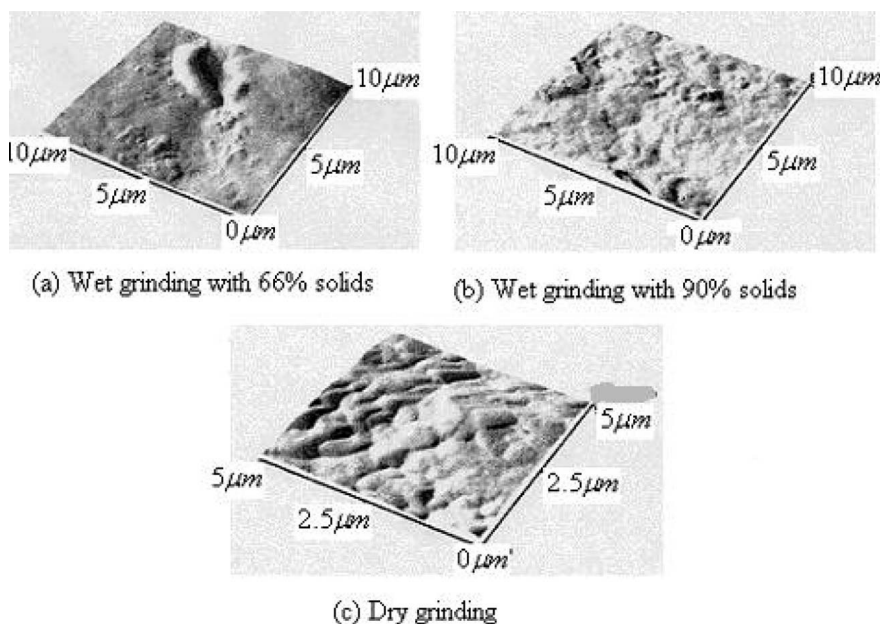
(c) Dry grinding

Figure 9. Topographies of the sulfide particle surfaces by AFM; (a) wet grinding with 66% solids, (b) wet grinding with 90% solids, and (c) dry grinding (Feng and Aldrich 2000).

the particles in the denser slurry (90% solids) and, as a consequence, some defects also appeared on these particle surfaces. Particles in dry grinding conserved more energy, some of which existed in the form of defects. These defects played an important role in subsequent particle dissolution and reagent adsorption.

Wet grinding of gibbsite in a bead mill in different operation conditions including the concentration of suspension, mass and diameter of grinding beads, and type of gibbsite ("radial" and "mosaic"), investigated by Belaroui et al. (1999). It was found that a large bead favors the initial breakage of "radial" gibbsite particles, while chipping is observed with small beads. Abrasion is clearly observed in the case of autogenous grinding. "Mosaic" gibbsites were found to be more prone to abrasion in the early moments of the grinding than "radial" gibbsite. Particle shape and morphology descriptors calculated and analyzed for different ground gibbsite in various grinding conditions. It was concluded that particle shape descriptors differ in different grinding conditions. The variations are presented in Figure 10 and Table 3.
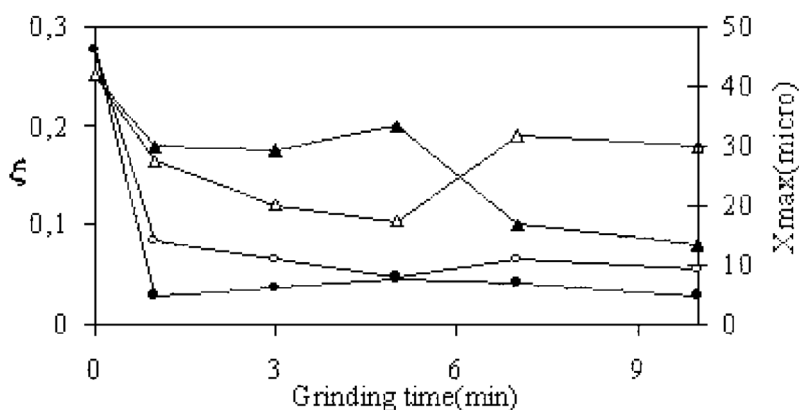
Figure 10. Variations of ξ ($\blacktriangle$, $\triangle$) and X_{max} ($\blacksquare$, $\square$) during grinding; ($\blacktriangle$, $\blacksquare$) $M_b = 250$ g and ($\triangle$, $\square$) $M_b = 500$ g (Belaroui et al. 1999).

SUMMARY

For particles produced by comminution, shape may be determined by material characteristics such as crystal cleavage and by the nature of the breakage process involved. While it is generally accepted that comminution leads to changes in the particle shape, there are some disagreement among workers due to difficulties in measuring the shape of particles. For instance, Bond (1954) stated that the character of material being broken has more influence on the shape of product than the type of reduction machine used. Similarly, Heywood (1961) claimed that the shape of particles produced on initial fracture were

Table 3. Comparison of shape descriptors with $D_b = 1.25 - 1.6$ mm, $M_b = 500$ g, $C = 23$, and 46% at time $= 5$ min, and initial values at $t = 0$. Standard deviations in parentheses, analysis on 80 particles for each sample (Belaroui et al. 1999)

Descriptor	C = 23%	C = 46%	Initial
D_{eq} (µm)	46 (15)	62 (30)	170 (20)
Circ	1.48 (0.17)	1.50 (0.29)	1.16 (0.08)
F_{max}/F_{min}	1.64 (0.45)	1.76 (0.51)	1.18 (0.11)
Ω_1	0.17 (0.07)	0.69 (0.08)	0.77 (0.04)
Ω_2	0.07 (0.03)	0.07 (0.03)	0.04 (0.02)
ξ	0.15 (0.10)	0.12 (0.12)	0.25 (0.15)
X_{max}	8.00 (5.3)	7.7 (6.9)	45.8 (22.2)

dependent upon the characteristics of the material. However, Rose (1961) and Oja and Tuunila (2000) suggested that the type of mill has the main effect on the particle shape, although the property of material is also a factor. Similarly, Charles (1956) stated that the shape of glass particles produced by a single fracture was dependent on the rate of application of stress. On the other hand, Kaya et al. (2002) observed that the shape of particles produced by size reduction for quartz and coal is controlled by three main factors, including: the type of comminution and breakage mechanism; the nature of the material being reduced; and grinding time. The investigations of Ulusoy et al. (2003a, 2003b), Yekeler et al. (2004a, 2004b), and Hicyilmaz et al. (2004) also confirmed the role of milling and mineral types on particle shape.

There is some agreement among workers as to the characteristic shapes that are produced by comminution machines. For example, it is generally agreed that roll crushers produce angular products, whereas the products, of ball mills tend to be equidimensional and rounded. In addition, the particular mode of breakage is likely to affect the shape of product particles. A massive fracture can be expected to produce highly irregular particles with sharp edges formed by the intersection of propagating cracks. Attrition of particles, by surface erosion or chipping at edges or corners, is more likely to cause rounding of particles, although the small fragments removed may be quite irregular in shape. It follows that grinding conditions that favor one breakage mode over another may be critical in determining product particle shape. The different types of mills can be classified with regard to the main stress that acts on the particles: compression, shear, attrition, impact, and internal forces. Of course, it is often difficult to discriminate these types of stress and combinations of at least two are obviously acting simultaneously in each machine. Moreover, three modes of fragmentation are usually defined (Frances et al. 2001). These modes take place simultaneously during a comminution process, but it might be useful to quantify the relative importance of each in order to improve the operation in existing mills or the design of new machines. The quantitative analysis of produced particle shape in different grinding methods seems to be promising for this purpose.

The reason for the neglect of this area of mineral processing is partly due to difficulties in measuring shape of particles and wide variation of grinding processes, and minerals. However, with the development of

image analysis systems, it has become technically feasible to investigate produced particle shape and their effects on beneficiation processes, as well as provide shape descriptors that are sufficient for the characterization of a particle population.

REFERENCES

Arbiter, N., Harris, C. C., and Stamboltzis, G. A. 1969 Single fracture of brittle spheres. *Trans. Amer. Inst. Min. Metall. Pet. Eng.*, 244, pp. 118.

Ata, S. and Ahmed, N. 1998 Particle shape effects on entrainment in flotation. *Proc. 26th Australasian Chemical Engineering Conf.* (Chemeca '98), Port Douglas, Australia.

Austin, leonard G., Yekeler, M., Dumm Timonthy, F., and Hogg, R. 1990 Kinetics and shape factors of ultrafine dry grinding in a laboratory tumbling ball mill. *Part. Syst. Charact.*, 7, 4, pp. 242–247.

Belaroui, K., Pons, M. N., Vivier, H., Meijer, M. 1999. Wet grinding of gibbsite in a bead-mill. *Powder Technology*, 105, pp. 396–405.

Bond, F. C. 1954, Control particle shape and size. *Chem. Eng.*, 61, pp. 195–198.

Charles, R.J. 1956, High velocity impact in comminution. *Mining Eng.*, pp. 1028–1032.

Coghill, W. H., Holmes, O. W., and Campbell, A. B. 1928 Determination of flakiness of ores. *U.S. Bur. Mines Rep. 2899*, 1.

Durney, T. E. and Meloy, T. P. 1986 Particle shape effects due to crushing method and size. *Int. J. Mineral Process.*, 16, pp. 109–123.

Feng, D. and Aldrich, C. 2000 A comparison of the flotation of ore from the Merensky Reff after wet and dry grinding. *Int. J. Mineral Process.*, 60, pp. 115–129.

Ferrara, G., Bevilacqua, P., Lorenzi, L. D., and Zanin, M. 2000 The influence of particle shape on the dynamic dense medium separation of plastics. *Int. J. Mineral Process.*, 59, pp. 225–235.

Forssberg, E. and Hongxin, Z. 1985 Shape and surface properties of the particles librated by autogenous grinding. *Scand. J. Metallurgy*, 14, 1, pp. 25–32.

Frances, C., Bloay, N. Le., Belaroui, K. B., and Pons, M. N. 2001 Particle morphology of ground gibbsite in different grinding environments. *Int. J. Mineral Proc.*, 61, pp. 41–56.

Gaudin, A. M. 1926 An investigation of crushing phenomena. *Trans. AIME*, 73, pp. 253–317.

Gilvarry, J. J. and Bergstrom, B. H. 1961 Fracture of brittle solids II: Distribution function for fragment size in single fracture (experimental). *J. Appl. phys.*, 32, pp. 400–410.

Grasse, A. M. Roll crusher for producing cubical shaped fragments. U.S. Patent 2696 949, 1954.

Heywood, H. 1961 Powders in industry. *Soc. Chem. Ind.*, pp. 25–26.

Hicyilmaz, C., Ulusoy, U., and Yekeler, M. 2004. Effects of the shape properties of talc and quartz particles on the wettability based separation process. *Appl. Surf. Sci.*, 233, pp. 204–212.

Holt, C. B. 1981 The shape of particles produced by comminution. *Powder Technol.*, 28, pp. 59–63.

Hosten, C. and Ozbay, C. 1998 A comparison of particle bed breakage and rod mill grinding with regard to mineral liberation and particle shape effects. *Mineral Eng.*, 11, 9, pp. 871–874.

Kaya, E., Glogg, R., Kumar, S. R. 2002. Particle shape modification comminution. *Kona.*, 20, pp. 185–195.

Kuga, Y., Ma, X., Koga, J., Endoh, S., and Inoue, I. 1985 Measurement and statistical analysis of shape of particles comminuted by a screen mill. *Powder Technol.*, 44, 3, pp. 281–290.

Lecop, O., Guigon, P., and Pons, M. N. 1999 A grindability test to study the influence of material processing on impact behaviour. *Powder Technology*, 105, pp. 21–29.

Lileg, K. and Schnizer, B. 1989 Influence of particle shape on forces in magnetic separators. *IEEE Trans. Magnetics*, 25, 5, pp. 4292–4297.

Lytle, M. J., Daniel, J. L., and Prisbrey, K. A. 1983 Effect of microstructure on the size and shape of coal particles during comminution. *Fuel*, 62, 11, pp. 1304–1309.

Meloy, T. P. 1988 Geometry for characterizing fractured particle shape. *Powder Technology*, 55, pp. 285–291.

Murtagh, M. J. and Holland, H. J. 1989 The effect of talc particle morphology and size on the variability of its specific surface area. Presented at the 9th Int. Clay Conf., Strasbourg, Abstr. Proc. pp. 273.

Oja, M. and Tunnila, R. 2000 The influence of comminution method to particle shape. *Proc. XXI Int. Mineral Processing Congress, Rome, Italy*, C4, pp. 63–70.

Oja, M. and Nyström, L. 1997 The use of self-organizing maps in particle shape quantification. *Proc. XX Int. Mineral Processing Congress*, GDMB, Aachen, Germany, pp. 141–150.

Olev, T., Ramesh, K. V., and George, P. 1995 Particle shape produced by comminution in the Szego Mill. *Part. Par. Par. syst. charac.*, 12, 3, pp. 158–165.

Papacharalambous, H. G. 1964 Method of producing spherical particles. U.S. Patent 3, 160, 997.

Pourghahramani, P. and Forssberg, E. 2005. Review of applied particle shape descriptors and produced particle shapes in grinding environments, Part I:

Particle shape descriptors. *Mineral Process. Extractive Metallurgy Review*, 26, pp. 145–166.

Rose, H. E. 1961 Particle shape and surface area. *Powders in Industry, Soc. Chem. Ind.*, pp. 130–149.

Sanchez Soto, P. J., Wiewiora, A., Aviles, M. A., Justo, A., Perez Maqueda, L. A., Perez-Rodriguez, J. L., and Bylina, P. Talc from Puebla de Lillo, Spain, 1997, II. Effect of dry grinding on particle size and shape. *Appl. Clay Sci.*, 12, pp. 297–312.

Ulusoy, U., Hicyilmaz, C., and Yekeler, M. 2003a Role of shape properties of calcite and barite particles on apparent hydrophobicity. *Chem. Eng. Process.*, 43, pp. 1047–1053.

Ulusoy, U., Yekeler. M., and Hicyilmaz, C. 2003b Determination of the shape, morphological and wettability properties of quartz and their correlations. *Mineral Eng.*, 16, pp. 951–964.

Yekeler, M., Ulusoy, U., and Hicyilmaz, C. 2004a Effect of particle shape and roughness of talc mineral ground by different mills on the wettability and floatability. *Powder Technol.*, 140, pp. 68–78.

Yekeler, M. and Ulusoy, U. 2004b Characterization of surface roughness and wettability of salt type minerals: Calcite and barite. Unpublished.

Yigit, E., Johnston, H. A., and Maroudas, N. G. 1967 *Quarry Managers J.*, 12, pp. 467.